2008

Computational model of MST neuron receptive field and interaction effect for the perception of self-motion

Chen-Ping Yu

Computational model of MST neuron receptive field and interaction effect for the perception of self-motion

A Thesis Submitted in Partial Fulfillment of the Requirements for the Degree of Master of Science in Computer Science

by

Chen-Ping Yu

cpu1982@gmail.com

Submitted to the Department of Computer Science

Rochester Institute of Technology

July 21, 2008

Approved by Committee Members:

Dr. Roger Gaborski, RIT
Chairman

Drs. Charles Duffy, U. of Rochester
Reader

Dr. William Page, U. of Rochester
Observer

Abstract

Biologically plausible approach is an alternative to conventional engineering approaches when developing algorithms for intelligent systems. It is apparent that biologically inspired algorithms may yield more expensive calculations when comparing its run time to the more commonly used engineering algorithms. However, biologically inspired approaches have great potential in generating better and more accurate outputs as healthy human brains. Therefore more and more new and exciting researches are being experimented everyday in hope to develop better models of our brain that can be utilized by the machines.

This thesis work is an effort to design and implement a computational model of neurons from the visual cortex's MST area (medial superior temporal area). MST's primary responsibility is detecting self-motion from optic flow stimulus that are segmented from the visual input. The computational models are to be built with dual Gaussian functions and genetic algorithm as its principle training method, from the data collected through lab monkey's MST neurons. The resulting computational models can be used in further researches as part of motion detection mechanism by machine vision applications, which may prove to be an effective alternative motion detection algorithm in contrast to the conventional computer vision algorithms such as frame differencing. This thesis work will also explore the interaction effect that has been discovered from the newly gathered data, provided by University of Rochester Medical Center, Neurology Department.

Table of Contents

1. Introduction

The human brain excels in just about every aspect of function as an intelligent system. Therefore, biologically inspired systems attempt to base its designs from the organization and the functionalities of the human brain. This thesis work is an effort to design and implement a computational model of neurons from the visual cortex's MST area (medial superior temporal area), with dual Gaussian receptive field functions derived by a GA as its principle training method My goal is to fit the data collected in awake monkey neurophysiological studies of MST neurons, and to better understand the receptive field mechanisms of their role in the visual motion processing of optic flow stimuli.

The results of the computational models of this thesis will bring us closer to developing a better biologically feasible computer vision system. However, due to the fundamental differences between the computational algorithms and the brain's neuronal format, it is difficult to implement biologically feasible algorithms and systems with many computational approaches. Another obstacle is that we do not currently have enough understanding of how the brain process visual information. As we make progress toward understanding the brain in greater detail, we will be able to develop better and more accurate models for specific parts of the brain. These new understandings can then be utilized onto machine algorithms that are more biologically plausible.

The criterion of biologically plausibility is an alternative to conventional engineering approaches when developing algorithms for intelligent systems. It is apparent that biologically inspired algorithms may yield more expensive calculations when comparing its run time to the more commonly used engineering algorithms. However, biologically inspired approaches have great potential in generating better and more accurate outputs that mimic the functioning of the

healthy human brain. Therefore more and more new and exciting research is being developed in hope of creating the foundation for better models of our brain that can be implemented in machines.

Computer vision, being a branch of the field of artificial intelligence, is one of the areas that may benefit greatly from new understandings of biological vision. Approaches include Gaussian derivative models for motion related detections that are based on the receptive fields of visual cortex neurons and are able to sense the movement of objects across multiple display frames [22]. Dr. Young has done extensive research in regards to biologically plausible models of the visual cortex. His models of Gaussian derivatives mimic the center-surround receptive field organization of visual cortical neurons. By taking more derivatives of Gaussian curves, it is possible to create various different models that contain different lobes, phase, directions, and frequencies. Using these Gaussian derivatives he was able to create models that detect basic moving edges, as well as cars moving on the highway. The Gaussian derivative models also has great potential to be used in many different motion sensing applications such as surveillance cameras and object tracking systems.

There is also modeling effort done in the higher level of the visual cortex. VisNet is one such example [18]. VisNet focuses on the modeling of connections between neurons within visual cortex, rather than single neuron's receptive field representations. VistNet is a network of nodes interconnected in a hierarchical format. The nodes are initially generated with random connections, and it is a supervised network which is trained with its training set, with Bayesian probabilistic learning rules that either keep or cut off connections between nodes. The trained VisNet model can be used as pattern recognition systems, or object recognition applications.

Computational neuroscience models that are related to the visual cortex can also

contribute as biologically inspired models that can be used in machine vision systems. Gaussian derivative models [22] are included in this category since their development was based on the neuron's center-surround receptive field organization [14]. There are also models developed based on the MT (medial temporal) area of the visual cortex that is analyzed to understand how the MT neurons can sense motion of visual pattern [19].

Thus, computational neuroscience models includes single neuron models, sensory processing models, neuron organization models such as VisNet [18], and models of higher cognitive function, learning, and consciousness. This thesis work focuses on single neuron contributions of visual motion sensory processing. The work may be used in future machine vision applications that are related to motion processing as biologically inspired computer vision systems. Specifically, this thesis work is aimed at developing receptive field models of MST neurons with discovered interaction effects that may account for flow selectivity in some neurons [24]. The interaction dependent changes in selectivity can be as dramatic as reversing the direction of visual motion preferences. To model these effects, recorded firing rates from neurophysiological studies of interactions between local motion stimuli will be trained into the MST receptive field models. The interaction effects will be tested to determine whether they allow the models to mimic the neurons optic flow selectivity by shifting local motion selectivity according to specific combinations of local-motion across a neuron’s receptive field.

Understanding the pathway of visual information processing enables future research efforts related to biologically inspired machine vision systems. At the highest level, we all accept that the eyes receive light that is reflected from the objects around us. The retina transduces that light to create a neuronal signal that it relays through the optic nerve, then the thalamic lateral geniculate nucleus (LGN), and then the primary visual cortex, also known as area V1 (Figure 1).

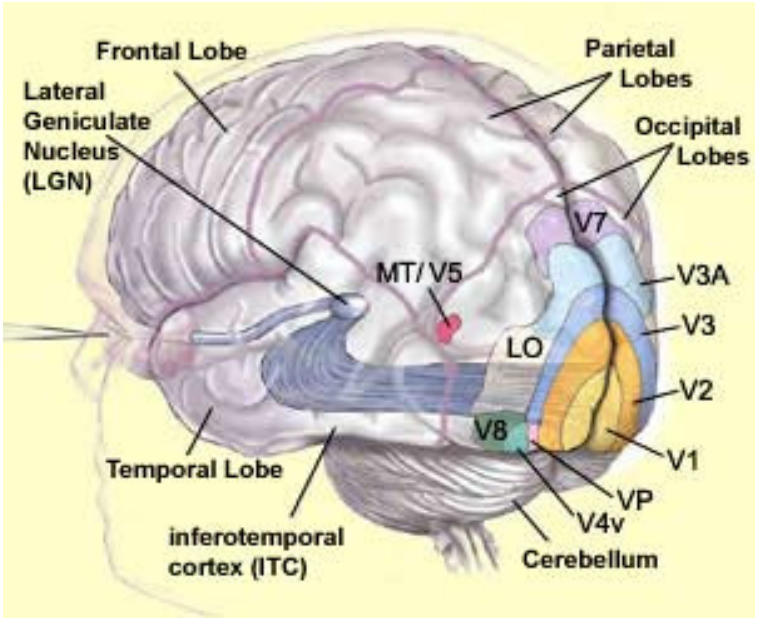

Figure 1 **from McGill U. Website, Canada**

From V1, visual information splits into two parallel steams of processing: the ventral stream, also known as the *what* pathway, and the dorsal stream, also known as the *where* pathway (Figure 2). The ventral stream goes from V1 to V2, V4, then IT (inferior temporal area). This pathway is called the *what* pathway because it mainly detects and recognizes objects from the visual information. The dorsal stream goes from V1 to V2, MT (medial temporal area), then MST. This pathway is called the *where* pathway due to its ability to process object's motion in the scene, as well as self-motion. The combination of these two information processing steams in parallel results in the precise understanding of what we see.

Some further details of each area and each process pathway will be explained in the next section. In addition, basic receptive field properties and features of the optic flow that is seen during self-motion will also be discussed in greater length in the next section as they are the focus of this computational modeling effort.

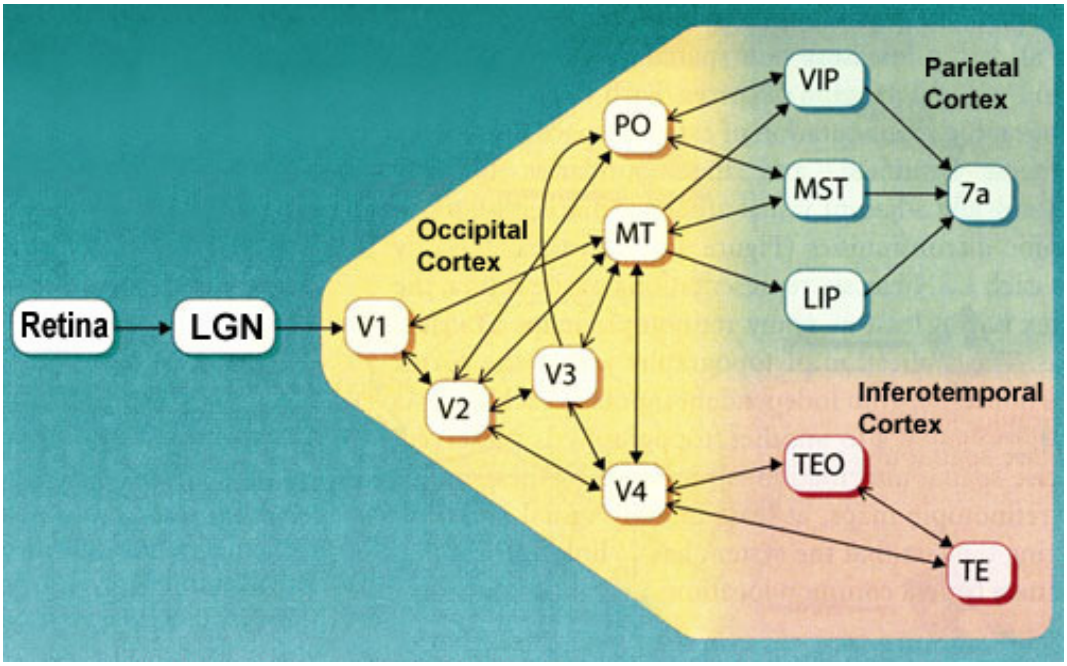

Figure 2 **The Visual Pathway, from McGill University Website, Canada**

2. Background

Before the details of any neuronal modeling effort can be understood, it is essential to have some agreed upon description of the basic architecture of the brain systems to be considered. Since this research is on modeling the receptive field properties of MST neurons, and interactions between segments of MST neuronal receptive fields, it is important to be aware of how the human brain processes the visual input received from the eyes.

2.1. Retina

The retina is at the back of the eye and contains several layers of cells that allow us to process color and light intensities [11]. The retina includes layers of ganglion cells, bipolar cells, horizontal cell, rods, and cones (Figure 3).

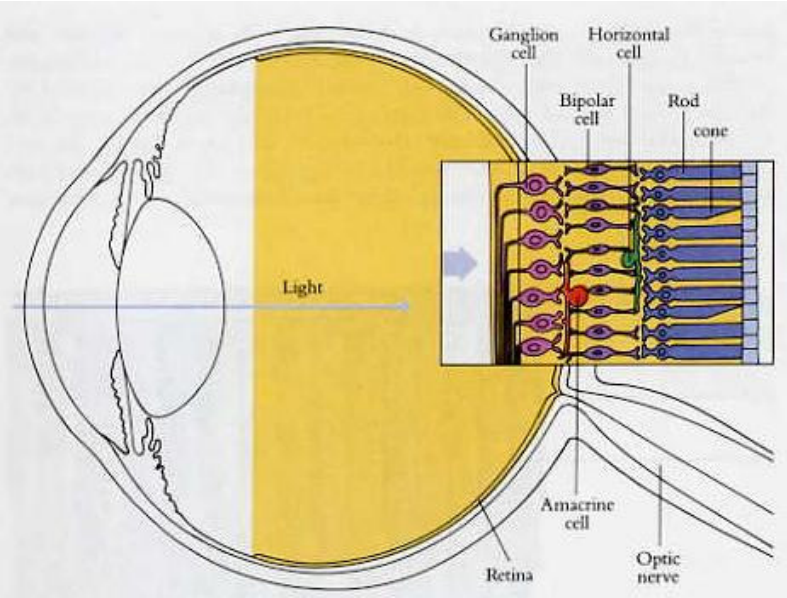

Figure 3 from Hubel, "Eye, Brain, and Vision." 1995.

Although the ganglion cells are closest to the iris, the light that passes through the cornea would pass through all the layers of ganglion cells and bipolar cells, and be received by the rods and cones first, then the input information is propagated to bipolar cells, ganglion cells, then along the optic nerve to the visual cortex at the back of the brain [11].

The rods are responsible in processing input information in low ambient light intensity conditions; the cones process color input at higher light intensity conditions [11]. Rods are also in a much larger numbers compared to the cones in the retina, there are approximately 100 million rods as comparing to just 5 million cones in our retina. However, our fovea, which is where we see the most detail with our central vision, contains mostly cones.

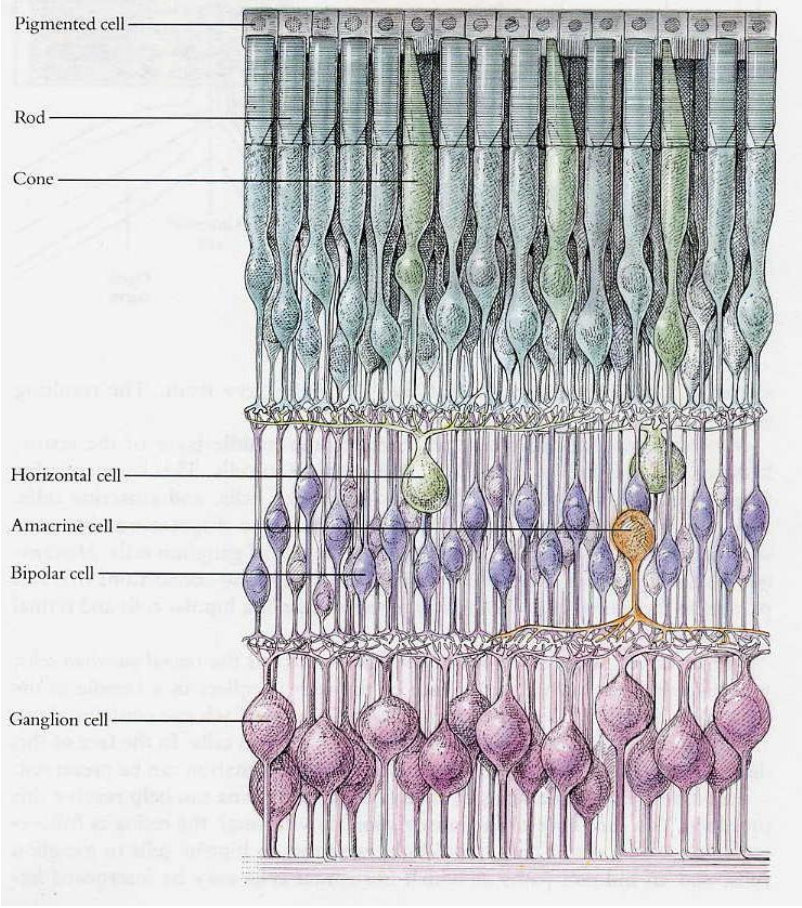

Figure 4 from Hubel, "Eye, Brain, and Vision." 1995.

Rods and cones output to the bipolar cells. The bipolar cell's effective responsibility is to transfer the visual information from the rods and cones to the ganglion cells. The ganglion cells, which converts the light information into action potentials, fires spikes and outputs to the lateral geniculate nucleus (LGN), which acts as a relay station for the information inputs [11]. Since the LGN receives more than just visual information, but also inputs from the cerebral cortex, and the brainstem, LGN may filter visual information before passing it on to primary visual cortex. In particular, both the left and right LGN receives visual input from both eyes. This allows the LGN to send the image of the contra-lateral visual field (opposite side of the visual world) from both eyes to the primary visual cortex on its side.

2.2. Receptive Fields

Before going further into how visual information is processed in visual cortex, we will consider the basic design of the neuronal receptive fields that supply information to visual cortex. The receptive fields of retinal ganglion cells and LGN neurons share the same basic design. This design is that of the center-surround structured receptive field [14]. This structure is of two basic varieties: on-center off-surround, and off-center on-surround (Figure 5).

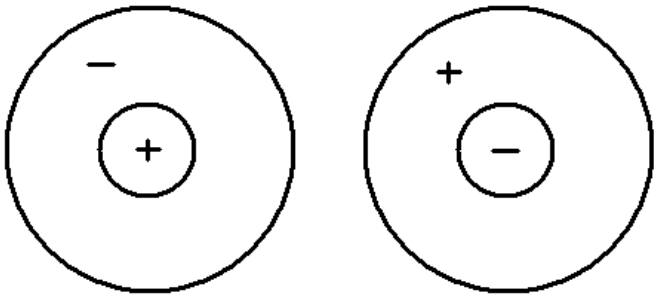

Figure 5 Left: on-center off-surround receptive field

Right: off-center on-surround receptive field

When an on-center segment is illuminated it makes the neuron fire more, when an off-surround segment is illuminated it makes the neuron fire less [11]. Likewise, when the illumination of an on-center segment is extinguished the neuron fires less. When the illumination of and off-surround segment is extinguished the neuron fires more. The opposite scenario applies with off-center on-surround retinal or LGN receptive fields.

The center-surround organization of many retinal and LGN receptive fields has been thought to be combined to create the various types of receptive field organizations found in V1 cortex. Consider that if such center-surround receptive fields arranged along a straight line through the visual field their outputs could be combined to create an orientation selective V1 receptive field [11]. If such a cell is organized to be sensitive with a 90 degrees straight line in sight, then when the 90 degrees straight line is within the center of the receptive field, the cell would fire its output very frequently, as in an excitatory action. However if the straight line is perceived at where the surrounding of the receptive field is, then the cell would inhibit its firing of signal, as in an inhibitory action. The off-center on-surround acts similarly as the example, just in an opposite way. This is one theory of the orientation selectivity of V1 simple cells (Figure 6).

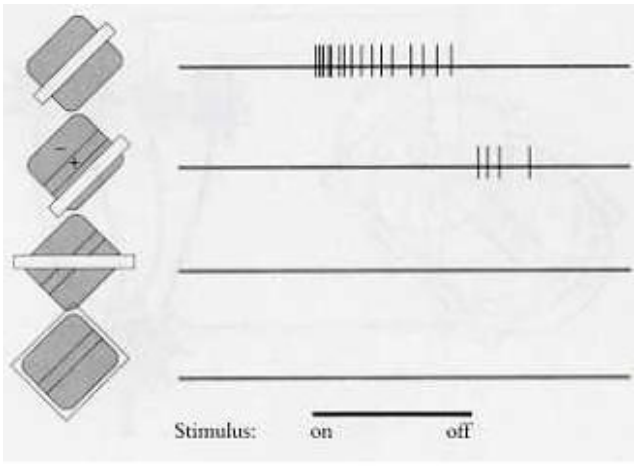

Figure 6 Orientation specificity of V1 simple cell receptive field, white bar is the stimuli. When the white bar is at different orientation in the receptive field, the cell reacts differently. Figure from Hubel, 1995.

2.3. Primary Visual Cortex (V1)

The primary visual cortex, anatomically known as the striate cortex due to white matter stripe through layer IV, is also labeled as V1 to refer to its functional role as first visual processing stage after the LGN. V1 is part of the occipital lobe occupying the posterior tip of the brain. A diverse assortment of neurons in V1 are designated simple cells (for having separate excitatory and inhibitory subfields), complex cells (for their inseparable subfields), and hypercomplex (for end-stop inhibition to long bar stimuli) [11]. All of these cells are higher up in their processing of visual information than retinal and LGN center-surround cells. The receptive fields of V1 simple, complex, and hypercomplex have been thought to be composed of a hierarchical sequence of combined center-surround cell effects

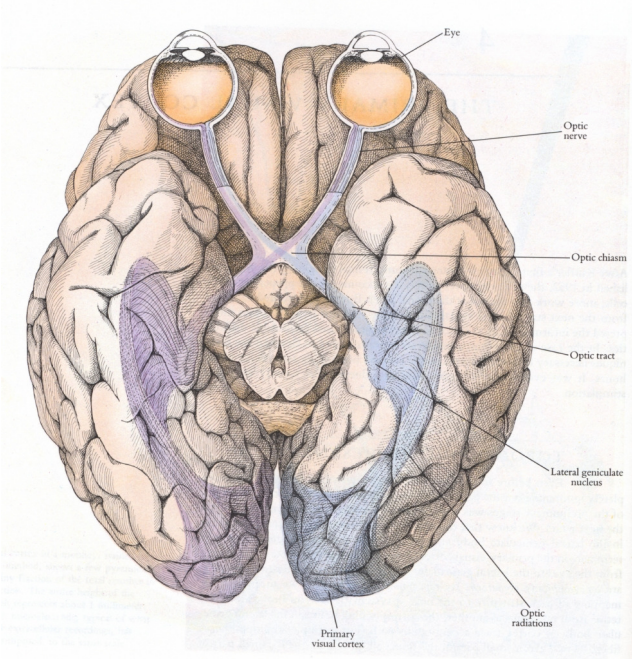

Figure 7 LGN projection to V1, from Hubel, "Eye, Brain, and Vision." 1995.

Figure 7 presents a diagram of the inferior view of the human brain, looking from straight below the brain up into the brain. V1 is at the bottom in this drawing, where it is labeled as primary visual cortex. Each half of the brain, a hemisphere, contains half of V1. V1 is the first major processing stage for the analysis of visual information. In addition to the diverse receptive field properties of V1 cortex, these neurons are also responsive to color and movements in the visual field, as well as some pattern. However, for the detailed and precise processing of the visual input, V1 splits its output information into two somewhat distinctive visual processing pathways: the "What" pathway of Ventral Stream, and the "Where" pathway of Dorsal Stream.

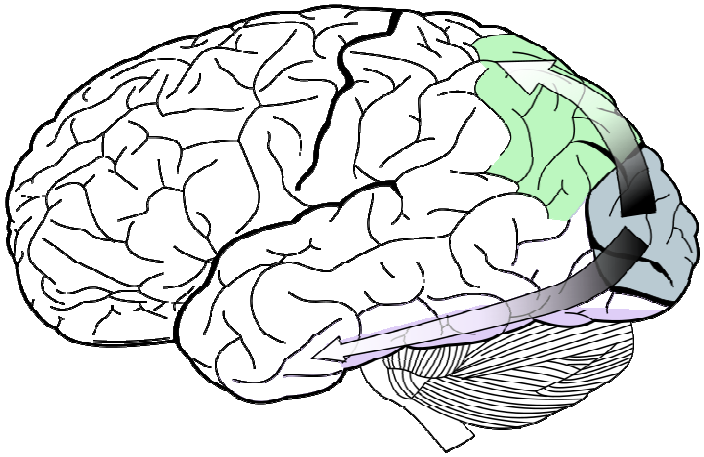

Figure 8 **Blue: Primary Visual Cortex (V1)**

Purple: Ventral steam

Green: Dorsal steam

figure from Wikipedia.com, "Dorsal Stream"

2.4. Ventral and Dorsal Stream ("what" and "where" pathway)

As the primary visual cortex, V1, receives the spikes of action potential firing from the LGN, the information processing starts to split into two parallel processing stream: the ventral stream and the dorsal stream (Figure 8). The ventral stream processes the objects seen in the scene and detects what they are, whereas the dorsal stream processes object locations and motion as well as the full-field motion that results from the observer's self-motion (optic flow) [11].

The path of information flow in the ventral stream takes place in the sequence of areas from V1, to V2, to V4, and then to IT. The path of information flow in the dorsal stream takes place in the sequence of areas from V1, to V2, to MT, and then to MST. Both streams share the substantial contributions to processing in area V1 with divergence of processing within V2 which

is responsible for some color and directional selectivity [11]. V4 is not part of the dorsal stream because V4's major functionality is in processing color. Color information is more important when recognizing objects but much less important when determining the movement or the speed of something that is in motion. In fact, all we need is the light intensity (black/white) to determine objects' motions and self-motion, therefore it makes a lot of sense for dorsal stream, which detects motion, to go past the V4 processing of color, while the ventral stream gets the color information to further determine all the objects from the visual scene (Figure 9).

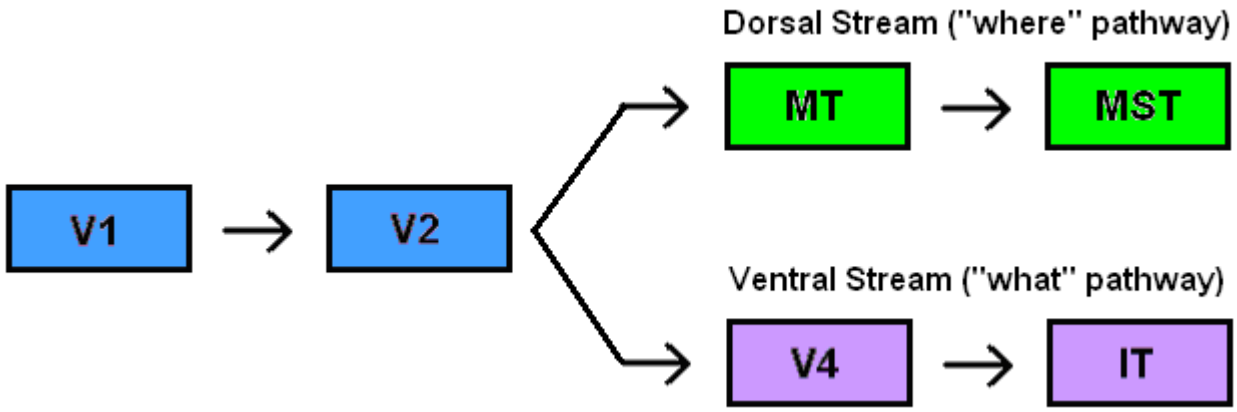

Figure 9, the dorsal and ventral stream.

2.5. Ventral Stream (the "What" pathway)

The ventral stream, which is indicated as the purple blocks along the bottom in figure 9, represents temporal lobe processing of visual data from V1 in parallel with dorsal stream area shown as green blocks. The ventral stream is mostly responsible for object and pattern recognition and identification; therefore it importantly accesses and contributes to long term memory. The major processing station that the ventral stream takes its path consists of V1, V2,

V4, and IT (Figure 10).

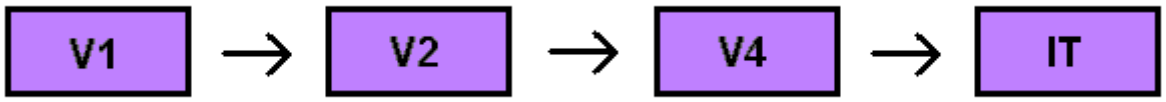

Figure 10, the information flow through dorsal stream extrastriate visual cortical areas.

V1 is, as described earlier, sensitive to color and directional selective stimulus. V2 and V4 share very similar functionalities in terms of color detection and complex cell directional selectivity as V1 [11]. However, as the processing level goes higher and deeper from V1 to V4 then to IT (inferior temporal area), some research indicates that the attentional modulation of neuronal response sensitivities become stronger at the higher stages, although there remains a great deal of disagreement on this point. V4 primarily processes color and shape information, therefore IT has very complex receptive fields due to the large amount of processed information and visual area from the processing of V1 through V4.

Common biologically inspired object detection algorithms that mimic how ventral steam processes shape and color information utilize Gabor filters [20]. Gabor filters with different angles of orientation are able to smooth the image, and filter for a specific orientation by convolution with shaped filter at various angles. For example, applying a Gabor filter that is at 90 degrees (vertical) to an image would output an image with its vertical edges identified.

Figure 11, Gabor Filter 90° (left) convolved with a grey scale image (middle). Result (right) shows the vertical (90°) edges displaying higher intensity (darker areas) than non-vertical parts of the image (lighter areas).

This type of Gabor filter smoothing is very useful for object recognition algorithms that are biologically inspired. By setting up and getting the responses of multiple Gabor filters with different orientation at different locations of an input image, we are able to segment for specific shape of objects from the responses generated [20]. We can also obtain the original color values of the segmented area from the Gabor filters, which help represent the object segmented with more information, therefore completing the ventral-stream inspired object detection algorithm.

2.6. Dorsal Steam (the "Where" pathway)

The dorsal stream, which is indicated as the green blocks along the top in figure 8 represents V1 occipital lobe projections toward the parietal lobe of the brain. The dorsal stream process visual motion data from V1 in parallel with the ventral stream's processing object features. The dorsal stream is mostly responsible for spatial understanding, which recognizes where the objects are and what motion they are in, as well as self motion awareness.

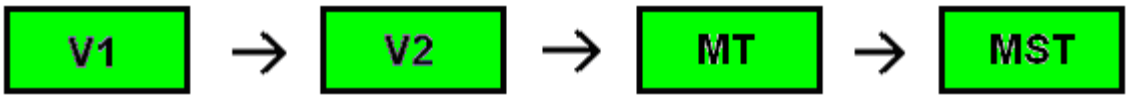

Figure 12, the information flow through dorsal stream extrastriate visual cortical areas.

From V2, the ventral stream continues into V4 for more color processing as stated from the earlier section. The dorsal stream, however, continues into MT (Medial Temporal area) after the basic edge and color processing done from V1 and V2. MT area is responsible for recognizing where objects are located in the scene. As the objects move or as we move, MT keeps us updated with respect to where objects are, therefore enabling us to detect motion over time. Motion detection in general does not require color information about the object, this may be related to the fact that a person isn't able to detect the color and shape details about a car passing by very quickly, but is able to sense that some object was moving though their visual field. MST (Medial Superior Temporal area), being another processing stage after MT, specifically detects the visual motion patterns that result from observer self-motion [4]. These patterns of visual motion from self-motion are referred to as optic flow, which is represented in cortical area MST, which also does not require color information.

Dorsal stream's motion detection processing in MT can be simulated with Gaussian derivative models developed by Dr. Richard Young [22]. A 3-dimentional Gaussian derivative model that is convoluted with an input video is able to detect moving objects with time as its 3rd axis. By generating the GD model with different orientation, it is able to respond to different orientations of motion.

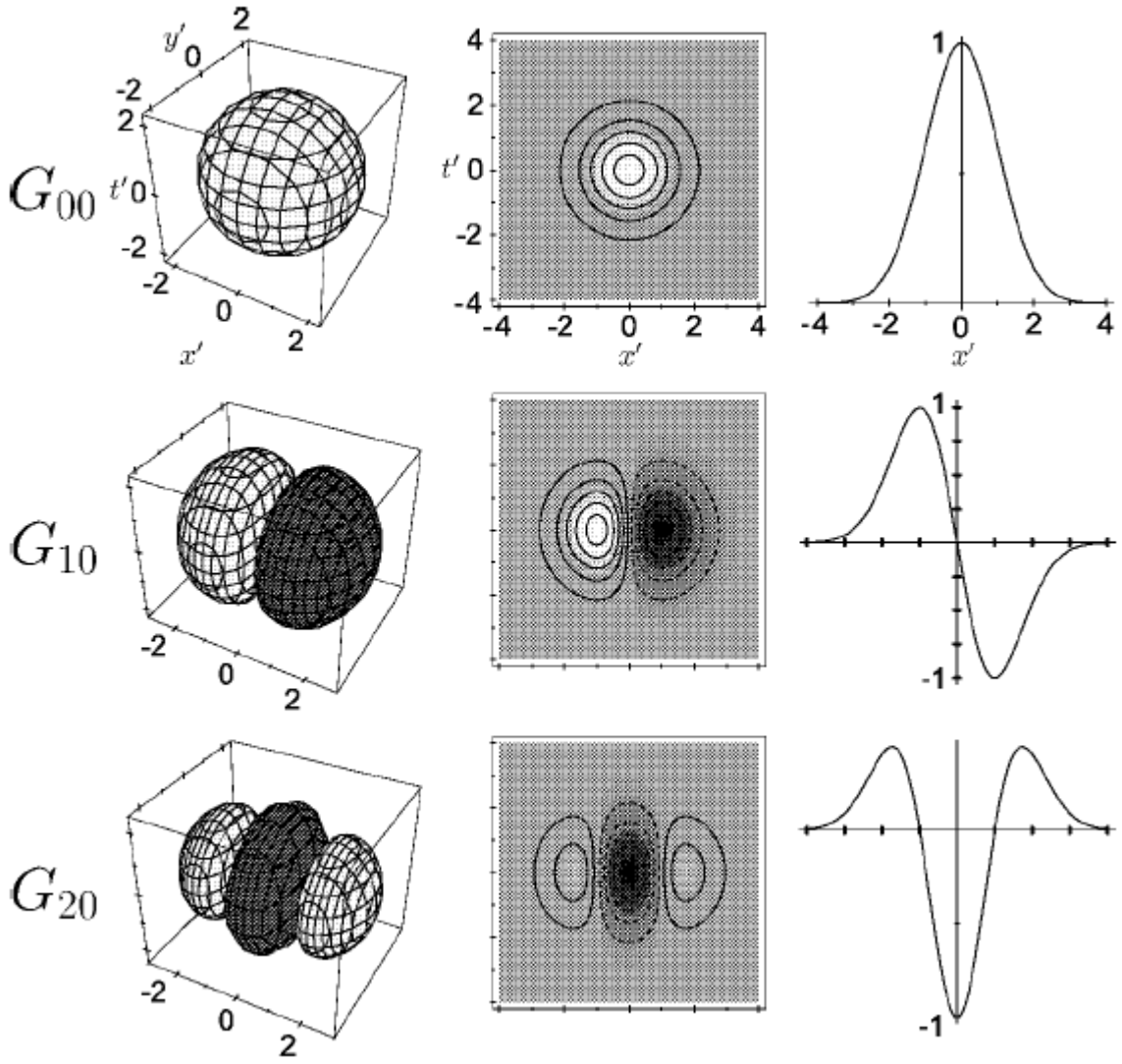

Figure 13, 3-Dimentional Gaussian Derivative Models. G00 as Gaussian function, G10 being the first derivative of Gaussian, G20 being the 2nd derivative. Figure from Young, 2001.

As the GD model is rotated with respect to Y axis, convolved with each time frame of the GD model with every frame from the video of interest sequentially, if any object or edge is moving in similar direction as the rotated GD's orientation, the GD model will respond with higher intensity output from the convolution operation, therefore detecting motion in the video.

2.7. MST and Optic Flow

MST is the next stage of dorsal stream processing after MT. MST is responsible for self-motion detection from optic flow and the neural representation of that visual motion information. Due to being aware of self-motion, a person is able to estimate his heading direction and avoid obstacles even during relatively fast motion through the environment.

Optic flow is the visual input that MST utilizes to process and determine heading direction during self-motion (Figure 14). Optic flow is the radial pattern of visual motion that is created by a person's self-motion. It contains a focus of expansion from which all movement appears to emanate. The focus of expansion (FOE), the singularity where the optic flow cues flow out from, indicates the person's heading direction under most circumstances [15]. By processing optic flow, we are able to navigate around in an environment very efficiently without the need of knowing the details of our surrounding objects, except knowing their location and their relative motion. Optic flow is commonly simulated as being black and white, and these stimuli appear to activate MST neurons effectively, suggesting that the processing of color information is independent at this stage, as is consistent with the dual pathways model described above [4]. MST's representation of visual motion information is so useful that the airplane pilots land the planes with optic flow assisted screen to guide the landing more accurately with ease by headed into the focus of expansion.

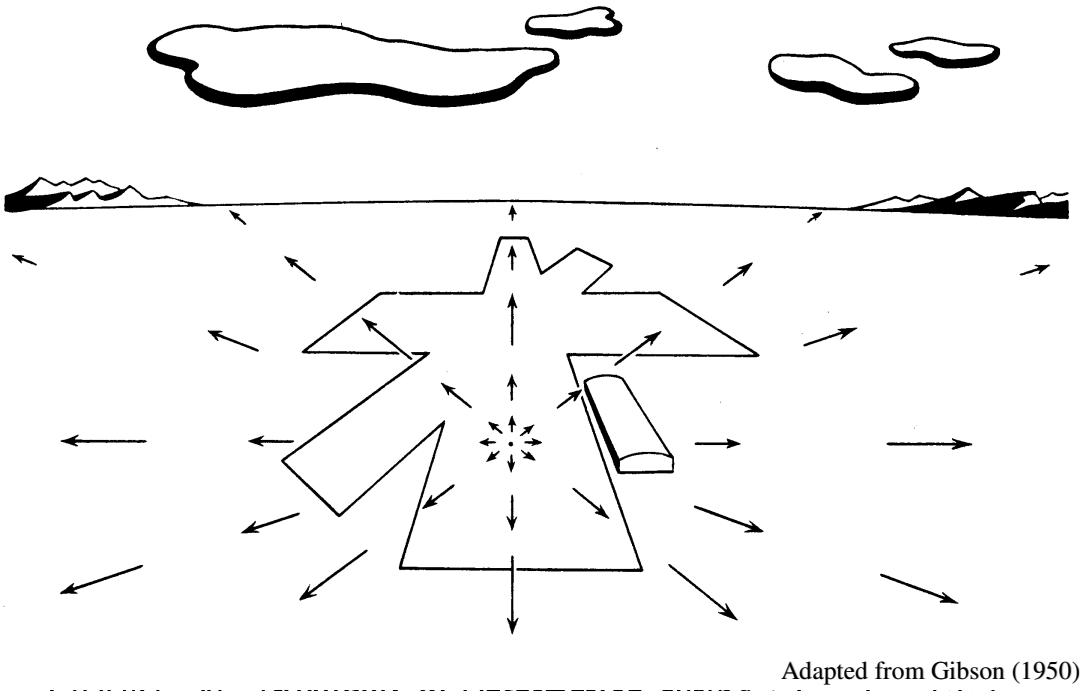

Figure 14, optic flow of a pilot landing its plane.

MST neurons mainly process optic flow representation of our visual input. It is also the next processing level after MT, therefore it is not surprising that its neurons appear to have very complex receptive fields due to its high level of visual motion processing. MST neurons' receptive fields are conventionally known as solid state much like other motion sensitive neurons – the responses of firing rate can be summed up from local motions responses, and it does not alter its tuning of flow selectivity. However, our data reveals interesting findings in which our MST neurons shift its flow selectivity with different optic flow stimuli, sometimes even reversed from its local-motion selectivity. This effect will be discussed and displayed in more details in Methods and Result section.

3. Data

3.1. Neurophysiological Stimuli

The neurophysiological data used in this thesis were collected at University of Rochester Medical Center, Cognitive Neuroscience Laboratory by Drs. Charles Duffy and David Logan with subsequent data management overseen by Dr. William Page. In brief, the responses of single neurons were recorded from the dorsal segment of the medial superior temporal area (MSTd) in the cerebral hemispheres of adult Rhesus monkeys. Surgical preparation began with sedation followed by venous catheterization, endotracheal intubation, and general anesthesia using inhaled isoflurane. Scleral search coils were implanted around the limbus in both eyes [13] to monitor eye position using the magnetic search coil technique [16]. A head holder and bilateral recording cylinders were placed over 2 cm trephine holes centered above area MSTd. Postoperative analgesia with banamine was administered in consultation with the veterinary staff. All protocols were approved by the University of Rochester Committee on Animal Research and complied with Public Health Service and Society for Neuroscience policy on laboratory animals.

The monkeys were trained to sit in a primate chair and perform a visual fixation task. All stimulus presentation trials began with the illumination of a stationary, red fixation point centered on the tangent screen (Figure14). If the monkey maintained fixation (+/-3^{o}) throughout the 5-second trial, an auditory tone was sounded and liquid reward was dispensed. Recording sessions were begun after the animal consistently completed trials with an accuracy of >90%. The stimuli were generated by a personal computer driving a television projector (Electrohome

ECP4100) at 60 Hz to cover the central visual field (90° x 90°) unless otherwise specified.

The monkey maintained visual fixation on a tangent screen during the presentation of all visual stimuli. The display screen is a 90° x 90° rear-projection screen that is 48 cm in front of the monkey. In experiments in which local motion stimuli were presented, the projection was sub-divided into a three by three array (Figure 14). Dividing the viewing area into these nine segments helps localize difference in response when local motion occurs at different places in the visual field. This also allows the possibility of multiple segments combination testing. The nine segments are labeled for implementation usage as follows:

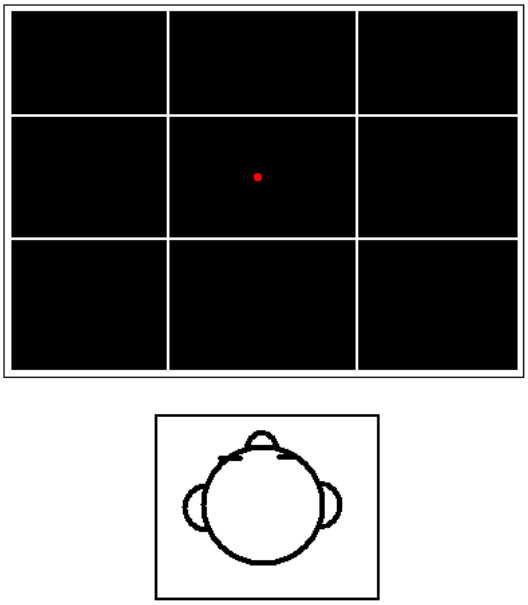

Figure 15, a stationed monkey fixated at the center of the screen as indicated by the red dot. The screen is divided into 3x3 sections as the white division lines indicates (there is no real division line in the recording).

After the monkey fixating at the center of the screen for 500 ms, a 2 second block of motion stimuli was presented. Each block contains 4 different motion stimuli, with each motion stimuli being displayed for 500 ms. The baseline firing rate of a neuron is recorded during the 500 ms fixation interval for each block, and the neuron's firing rate from each stimuli block is averaged over 6 trials of presentation.

Visual motion stimuli are made up of 500 white dots moving toward 1 of the 4 cardinal planar direction on the black background for singles and doubles experiments, while the motion stimuli for optic flow experiment contains a set of 16 global flow motions. Each dot encloses 0.19° at 2.61 cd/m² against a 0.18 cd/m² background. Each dots' initial position is randomly generated in the first frame with random life of 1 – 60 frames in each stimulus. Dots accelerate as a sine x cosine function of their distance from the FOE, maintaining an average speed of 40°/s.

According to different experiments, the display screen may have one or more segments of the 3 by 3 square showing dots moving to one of the eight directions: 0 degrees, 45 degrees, 90 degrees, 135 degrees, 180 degrees, 225 degrees, 270 degrees, and 315 degrees (Figure 15). In the data sheet, they are labeled as integers 1 to 8 as to indicate motion 0° to 315°.

Figure 16, the eight different directions of motion that white dots may be displaying on segments of the screen. From left to right: 0°, 45°, 90°, 135°, 180°, 225°, 270°, and 315°.

There may be only a single patch of the three by three square showing motion with dots

("singles" experiment), there may be a combination of 2 patches showing the same or different motions of dots ("doubles" experiment), and all 9 segments may also be fully displaying the moving dots ("optic flow" experiment). The specifics depend on which experiment is being run at the moment. During each 2 sec motion stimuli presentation block, the singles and doubles stimuli were randomly interleaved in either the "X" or "O" pattern (Figure 16). The sequence of testing is repeated until all stimuli were tested. The optic flow motion stimuli was tested on its own without interleaving any other type of stimuli, and the optic flow motion stimuli contains 16 different full screen motion consists of white dots moving on the black background (Figure 21).

3.2. Neuron Recording

Microelectrode penetrations were made using epoxy-coated tungsten microelectrodes (Microprobe) that were passed into cortex through a transdural guide tube positioned within the recording cylinder [3]. Neural activity was monitored to locate the depth of physiological landmarks, and experiments were initiated whenever neuronal discharges were clearly isolated. Single neuron discharges were isolated using a dual window discriminator and stored with the stimulus and behavioral event markers using the REX experimental control system [10]. Neuron firing data were averaged across the 500 ms period of six to eight stimulus presentations to characterize responses to each stimulus. When a neuron was isolated, we used a hand-held projector to define its approximate receptive field boundaries. We used physiological criteria for identifying MST neurons including their having large receptive fields (>20x20°), which contain the fixation point, with direction-selective responses, preferring large moving patterns rather than moving bars or spots [4]. Location in area MST was confirmed with deeper extension of

penetration across the superior temporal sulcus (STS) to identify the responses of MT neurons. MT was identified as having much smaller receptive fields that are proportionate to the eccentricity of the receptive field center and show greater responsiveness to bar or spot movement than is seen in MST.

The stereotaxic positioning of the recording chambers and the depths of microelectrode penetrations direct neuron recordings into cortical area MST. During the course of these experiments, microelectrode positioning in MST was confirmed by magnetic resonance imaging of the brain with microelectrodes in place. Images were obtained in the sagittal plane on a 1.5 Tesla magnet (General Electric) with fast spoiled gradient echo technique (TR = 23.5, TE = 10.3, 30° flip angle). The MR scans confirmed the location of the electrode tips in the anterior bank of the STS. At the end of experiments on a monkey, electrolytic marks (25 μA x 25 s) were made along the penetration tracks in three guide tubes in each hemisphere. After perfusing the animal and fixing the tissue, posterior cortical blocks were cut in 50-mm thick sections. Every fourth and fifth section was stained by the Nissl and Luxol Fast blue methods, respectively. The electrolytic lesions were identified relative to anatomic landmarks to extrapolate the position of the recording sites.

3.3. Singles Data

The singles data were collected by displaying motion in one of the nine patches at a time for 500 ms. Each testing neuron receives two possible sets of input combinations: X or O type of segment combinations (Figure 16). If a neuron is being tested for an X combination, the neuron will be tested at five segments one at a time: segment 1, 3, 5, 7, and 9 (Figure 17). The O

experiment displays motion at four segments one at a time: segment 2, 4, 6, and 8 (Figure 19).

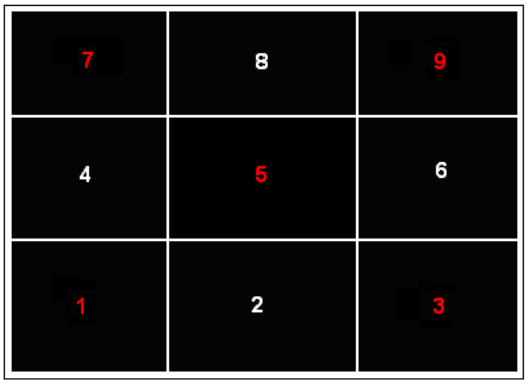

Figure 17, the integer label for each segment of the screen. The X pattern of testing will test only segment 1, 3, 5, 7, which looks like the character X (red labels), while the O pattern of testing will test only segment 2, 4, 6, 8, which looks like the character O (white labels).

Each segment of testing includes four planar directions of motion: 0 degrees, 90 degrees, 180 degrees, and 270 degrees. Therefore, the X testing pattern would result in 20 entries of results.

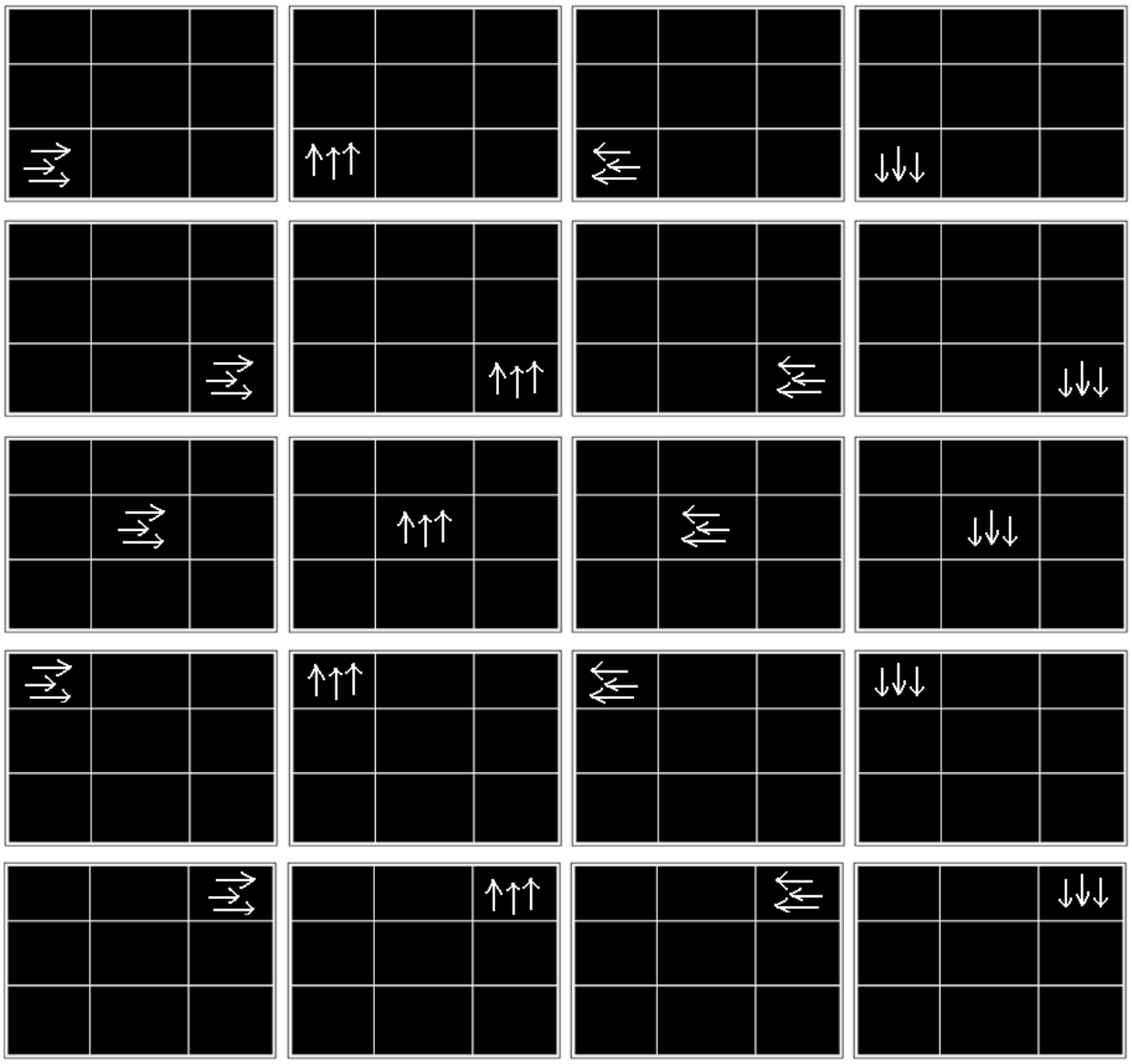

Figure 18, the X pattern of Singles experiment. From left top to right bottom: Segment 1 displays the 4 planar motion (0°, 90°, 180°, 270°) for 4 separate recordings, then recording repeats for segment 3, 5, 7, then 9. The segments arranged like the X character.

0.333333	1	0	0	0	0	0	0	0	0	0.333333	0.952	0.285
0	0	0	1	0	0	0	0	0	0	0		
0.4	0	0	0	0	1	0	0	0	0	0.4		
2	0	0	0	0	0	0	1	0	0	1.154701		
0	0	0	0	0	0	0	0	0	1	0		
0.333333	3	0	0	0	0	0	0	0	0	0.333333		
0	0	0	3	0	0	0	0	0	0	0		
0	0	0	0	0	3	0	0	0	0	0		
49.25	0	0	0	0	0	0	3	0	0	4.888336		
0	0	0	0	0	0	0	0	0	3	0		
0	5	0	0	0	0	0	0	0	0	0		
0	0	0	5	0	0	0	0	0	0	0		
0.5	0	0	0	0	5	0	0	0	0	0.5		
0.5	0	0	0	0	0	0	5	0	0	0.5		
0.4	0	0	0	0	0	0	0	0	5	0.4		
0	7	0	0	0	0	0	0	0	0	0		
0	0	0	7	0	0	0	0	0	0	0		
0.4	0	0	0	0	7	0	0	0	0	0.4		
1.5	0	0	0	0	0	0	7	0	0	1.5		
0	0	0	0	0	0	0	0	0	7	0		

Figure 19, an X pattern recorded neuron (819R02) comma separated data. Each row is a recording of a stimulus. For the first row: first column is the firing rate in spikes per second, column 2 through 10 indicates segment 1 through 9 on the screen. Among the segments, integer 0 represents no motion for that segment of the screen, 1 means there is motion of white dots heading at 0°, 2 means 45°, …, 8 means white dots moving towards 315°. 11th column indicates the standard error of this segment's specific direction firing rate recording in spikes per second, column 12 is the baseline firing rate in spikes per second for this neuron (blank screen), and column 13 is the standard error of this neuron's baseline firing rate in spikes per second. There are a total of 20 entries from an X pattern recorded neuron as this one, due to 5 segments involved in recording 4 planar motions each.

The O testing pattern follows the same procedure as the X pattern, but differs in the segments tested. The O pattern tests segment 2, 4, 6, and 8, with each segment testing four planar direction of motions: 0 degrees, 90 degrees, 180 degrees, and 270 degrees. The result is 16 entries of recording from a single trial.

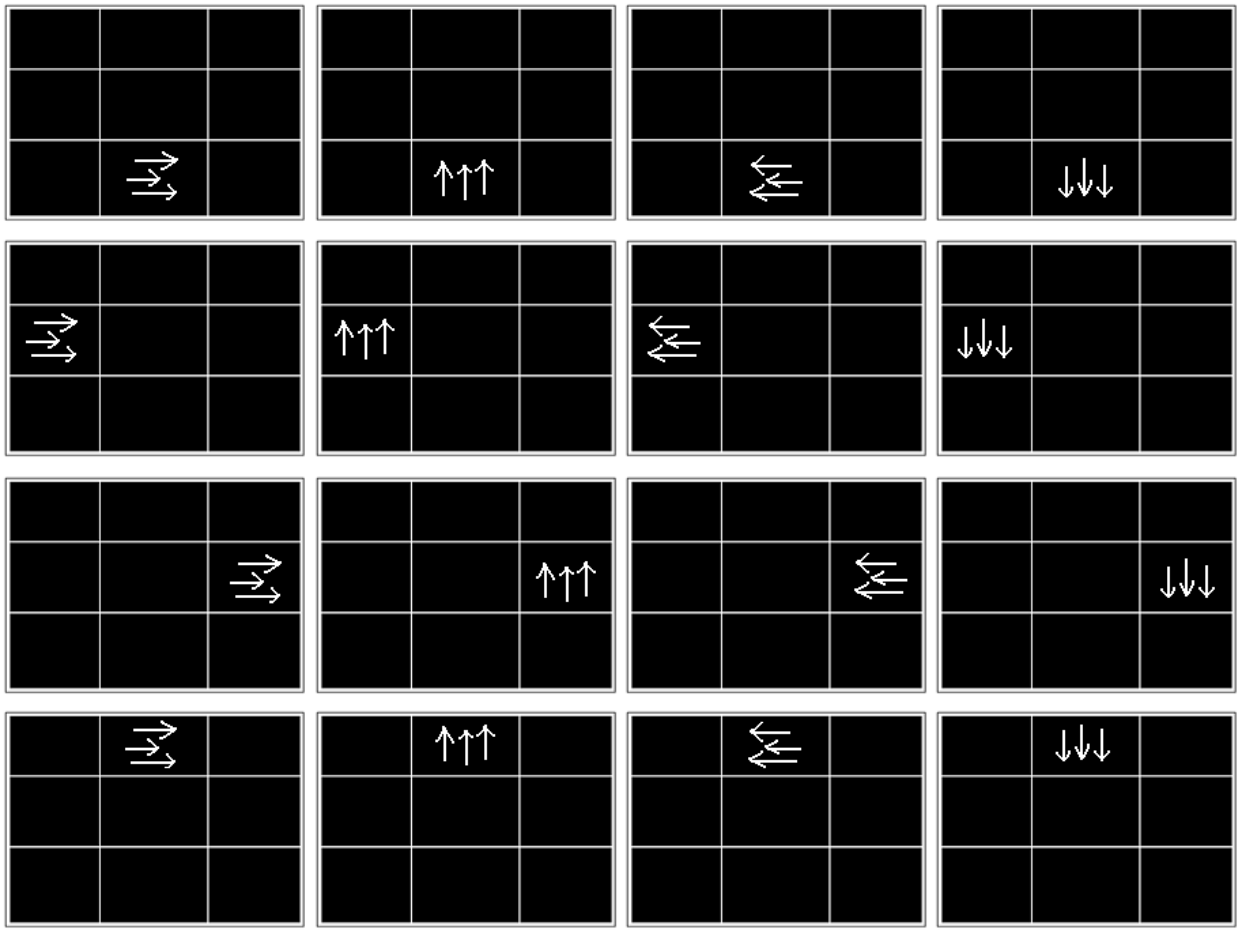

Figure 20, the O pattern of Singles experiment. From left top to right bottom: Segment 2 displays the 4 planar motion (0°, 90°, 180°, 270°) for 4 separate recordings, then recording repeats for segment 4, 6, then 8. The segments arranged like the O character.

6.25	0	1	0	0	0	0	0	0	0	2.25	5.4792	0.6875
4	0	0	0	1	0	0	0	0	0	2		
11.5	0	0	0	0	0	1	0	0	0	2.179449		
5.25	0	0	0	0	0	0	0	1	0	1.973787		
4.6	0	3	0	0	0	0	0	0	0	1.886796		
6	0	0	0	3	0	0	0	0	0	0		
2.8	0	0	0	0	0	3	0	0	0	0.489898		
5.5	0	0	0	0	0	0	0	3	0	0.5		
3.333333	0	5	0	0	0	0	0	0	0	0.666667		
3.2	0	0	0	5	0	0	0	0	0	1.2		
3.5	0	0	0	0	0	5	0	0	0	0.5		
2.8	0	0	0	0	0	0	0	5	0	1.2		
11.33333	0	7	0	0	0	0	0	0	0	3.666667		
10	0	0	0	7	0	0	0	0	0	2.345208		
7.5	0	0	0	0	0	7	0	0	0	2.661453		
2.8	0	0	0	0	0	0	0	7	0	0.8		

Figure 21, an O pattern recorded neuron (819R04) data. The data follows the same format as the X pattern. Only that since in an O pattern recording, 4 segments are involved and each segment is recorded with 4 planar motion, therefore O pattern recorded neuron contains 16 entries.

Some neurons are only tested as an X neuron (only apply X testing pattern and record the firing rate), while some neurons may be tested only on an O pattern. Some neurons are tested with both X and O pattern and result in a total of 36 entries of recording results. Therefore, each neuron's singles data is labeled as X, O, or XO to better identify which testing pattern the neuron were recorded with.

3.4. Optic Flow Data

The optic flow stimuli simulated the self-movement scene for 16 different heading directions (Figure 21). The 16 directions were presented in a pseudo-random sequence until each had been presented during 6-8 successful fixation trials. Each optic flow stimulus consisted of 500 white dots (0.19^o at 2.61 cd/m^2) on a black background (.18 cd/m^2) stimulating the central 90^o X 90^o of the visual field. All dots were replaced by lifetime expiration (33 to 1000 ms) or by a smoothing algorithm that maintained a uniform and consistent dot density across the stimulus in all frames. Dots for these radial patterns accelerated as a sine X cosine function of their distance from the focus-of-expansion maintaining an average speed of 40^o/s.

Optic flow data was collected similarly to the singles data. The main difference is that each flow stimuli displays motion from all nine segments of viewing area, emulating the sensation of a specific self-motion. There are a total of 16 flow stimuli recording for each neuron. The 16 different motion combinations from the entire viewing field are illustrated below:

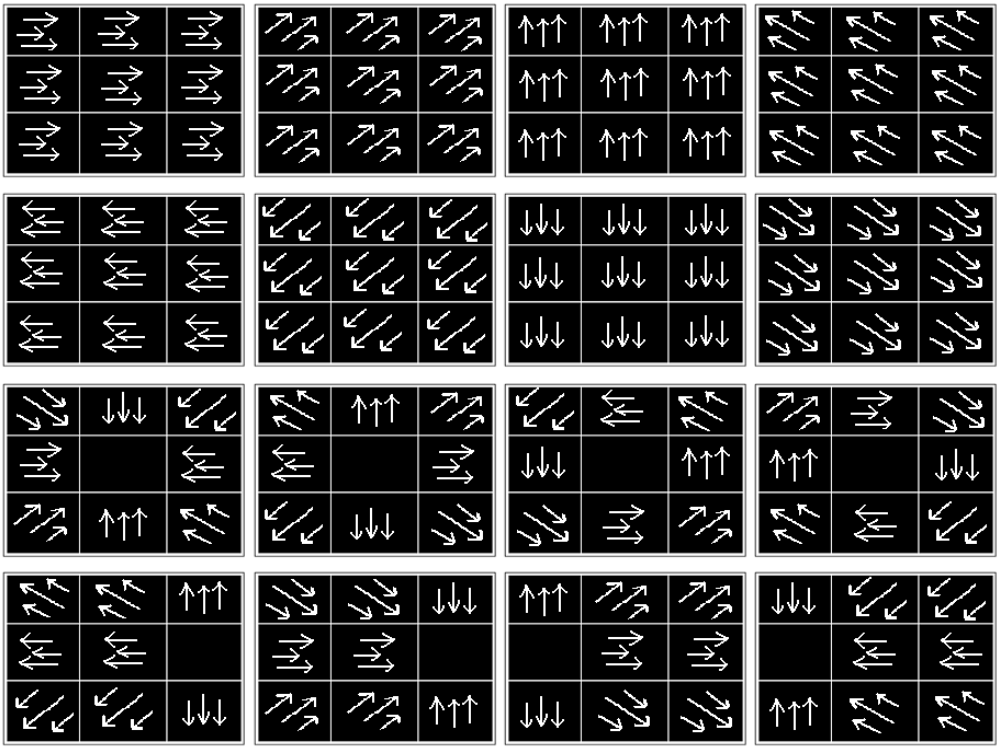

Figure 22, flow stimuli, total 16 of them. Stimulus 1 through 16 is ordered from top left to top right, then end as the lower right corner as the 16th stimulus. Each of those 16 flow stimulus has most of the segments displaying motion. White arrows indicate the white dot's motion direction within that segment, where all 9 segments combined simulates self-motion of the opposite direction from the dot's motion. i.e. flow stimulus 9 has dots moving inward, which simulates an backward self-motion to the viewing subject; flow stimulus 16 displays dots moving inward-left, which simulates backward-right self-motion to the subject.

15	1	1	1	1	1	1	1	1	1	1.154701	9.75	1.75
23	2	2	2	2	2	2	2	2	2	1		
21.66667	3	3	3	3	3	3	3	3	3	3.282953		
8	4	4	4	4	4	4	4	4	4	0		
6	5	5	5	5	5	5	5	5	5	1.414214		
22.5	6	6	6	6	6	6	6	6	6	1.5		
27.75	7	7	7	7	7	7	7	7	7	3.326034		
30.33333	8	8	8	8	8	8	8	8	8	2.333333		
14.25	2	3	4	1	0	5	8	7	6	1.973787		
14.75	6	7	8	5	0	1	4	3	2	1.931105		
6	8	1	2	7	0	3	6	5	4	0.816497		
17.33333	4	5	6	3	0	7	2	1	8	1.452966		
4.5	6	6	7	5	5	0	4	4	3	0.5		
20.75	2	2	3	1	1	0	8	8	7	1.887459		
11.5	7	8	8	0	1	1	3	2	2	2.661453		
10.6	3	4	4	0	5	5	7	6	6	1.122497		

Figure 23, sample flow data from neuron 819R04. The flow data sheet follows the format from the singles data, the apparent difference comes to almost fully-filled stimulus numbers from column 2 through 10, which represents motion being displayed from segment 1 to 9 on screen.

3.5. Doubles Data

The key of this thesis work is the collection and the analysis of the doubles data. The doubles data are collected similarly as the singles data, except that during each testing, two segments display motion simultaneously instead of just one. Since there are two segments showing motion at the same time instead of one, we call it “doubles” data. To better organize the testing of doubles testing pattern, a “hot spot” is selected from one of the nine segments. The hot spot is a segment from one of the segments tested from a neuron's singles trial. Therefore, an X neuron's hot spot could be segment 1, 3, 5, 7, or 9 (Figure 23); an O neuron's hot spot could be segment 2, 4, 6, or 8; an XO neuron would have 2 hot spots: one from the X pattern and another one from the O pattern segments. The hotspots are selected as the most excitatory spot from the single’s recordings. The hot spots are also a reference spot, in which each hot spot is paired with a “test spot” to form the doubles experiment. The test spot also must be one of the segments tested from the neuron's singles run. Therefore, an X neuron's doubles experiment contains a total of 64 entries of recording; an O neuron's doubles experiment contains a total of 52 entries of recording; an XO neuron's doubles experiment may contain 116 entries since it contains a hot spot from the X pattern and a second hot spot from the O pattern.

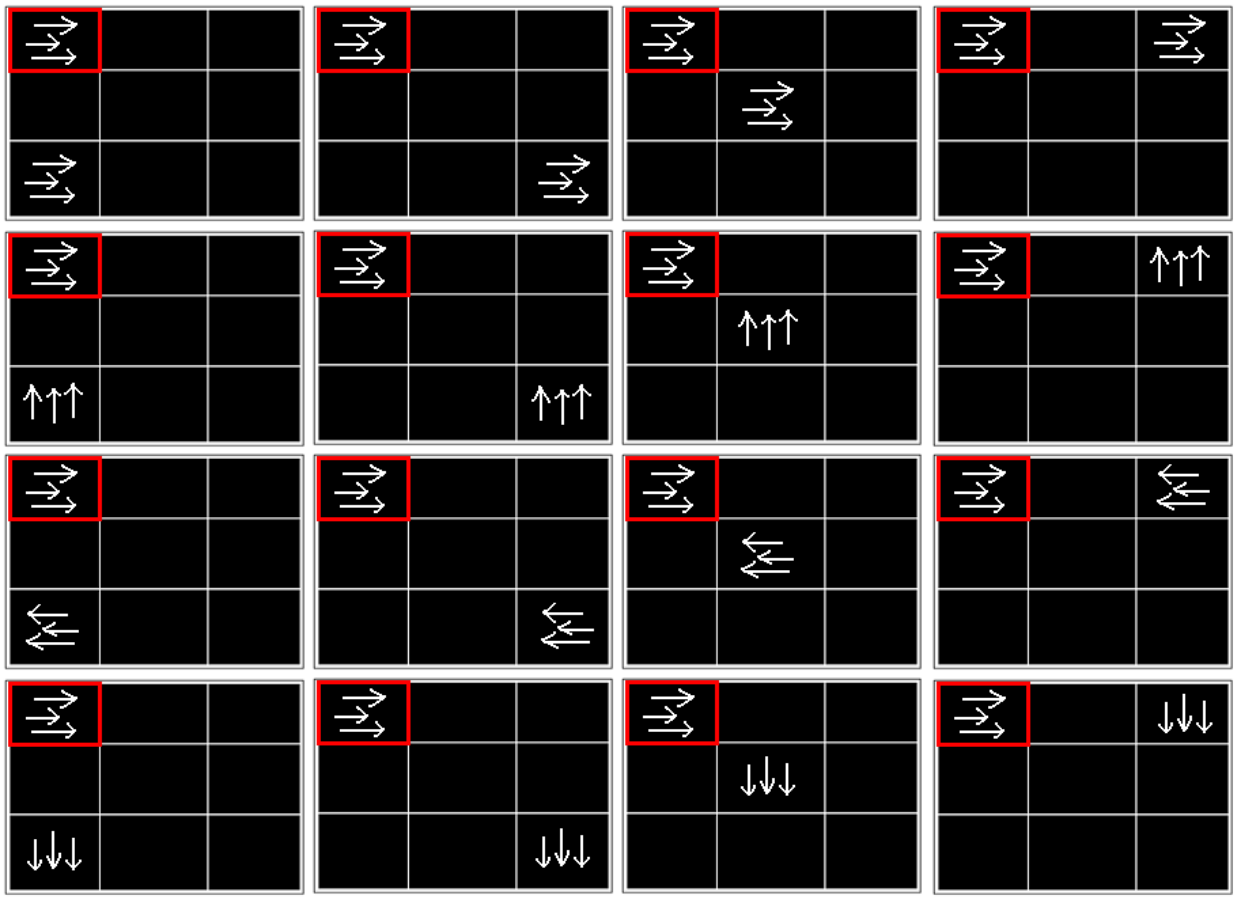

Figure 24, doubles stimulus hot spot #1 first 16 stimulus. As the figure shows, each "doubles" stimulus displays 2 segments of motion for recording. There is a "hotspot" segment in which is always present, pairing with another spot we call it "test spot". In this case, the hotspot is the 7th segment, and since the 7th segment is a part of the X pattern, the test spots are the 4 other segments that are part of the X pattern recording. This figure is the first 16 double stimuli for an X neuron, where the hotspot is heading 0°. The next 16 stimuli would have the hotspot moving at 90° pairing with the test spots; then 180°, and ends with 270°, completing the 4 planar motion that are displayed for recording.

63.333	1	0	0	0	0	0	1	0	0	14.24	24.767	7.6
68	0	0	1	0	0	0	1	0	0	0		
8.5	0	0	0	0	1	0	1	0	0	6.1305		
99	0	0	0	0	0	0	1	0	1	8.7369		
2.5	3	0	0	0	0	0	1	0	0	1.893		
30.667	0	0	3	0	0	0	1	0	0	14.678		
30.8	0	0	0	0	3	0	1	0	0	18.803		
47	0	0	0	0	0	0	1	0	3	41		
4.2	5	0	0	0	0	0	1	0	0	2.2891		
1	0	0	5	0	0	0	1	0	0	0.57735		
12.25	0	0	0	0	5	0	1	0	0	7.7715		
1.5	0	0	0	0	0	0	1	0	5	1.5		
22.333	7	0	0	0	0	0	1	0	0	7.4461		
9	0	0	7	0	0	0	1	0	0	4.1473		
164	0	0	0	0	7	0	1	0	0	5.5678		
86.333	0	0	0	0	0	0	1	0	7	17.13		

Figure 25, doubles sample data from neuron 819R10. Again, the data sheet follows the same format as the singles and flow data sheet. This data is the recording of when hotspot is moving towards 0°, as the 8th column (7th segment on screen) is showing the integer 1 through out the whole experiment, while pairing up with other X pattern segments moving toward a planar direction. There are 4 test spots and 1 hotspot in a X neuron, and we test 4 planar motions per segment, therefore there are 16 entries for 1 planar motion of the hotspot, making the total experiment having 64 entries from all 4 planar motion recordings of the hotspot.

3.6. Interaction Effects in Doubles Recordings

It is commonly accepted in the field of neuroscience that local motion responses can be "add up" to form the total flow response of a neuron, and that a neuron's flow selectivity is mostly consistent with its local motion selectivity summed up, which would suggest that the separately collected singles data recordings would be fairly consistent with the neuron's flow recordings if we puzzle together the appropriate combinations of the singles responses. However, from the doubles hot spots recordings, we have noticed that at certain situations when a combination of two segments are on, the resulting neuron firing rate can be as different as opposite of the neuron's singles data firing rate in the same segments. In one of the more clear cases, neuron 819R10 seems to be displaying a reversal of selectivity effect triggered by the 7th segment: 819R10's singles has its X segments responsive when the motion on the screen is moving to the left in general (Figure 25), however in the doubles recording, when the 7th segment being the hotspot is showing rightward motion on screen, the neuron's selectivity of other x segments becomes reversed of its singles selectivity, they all becomes rightward excitatory (Figure 26).

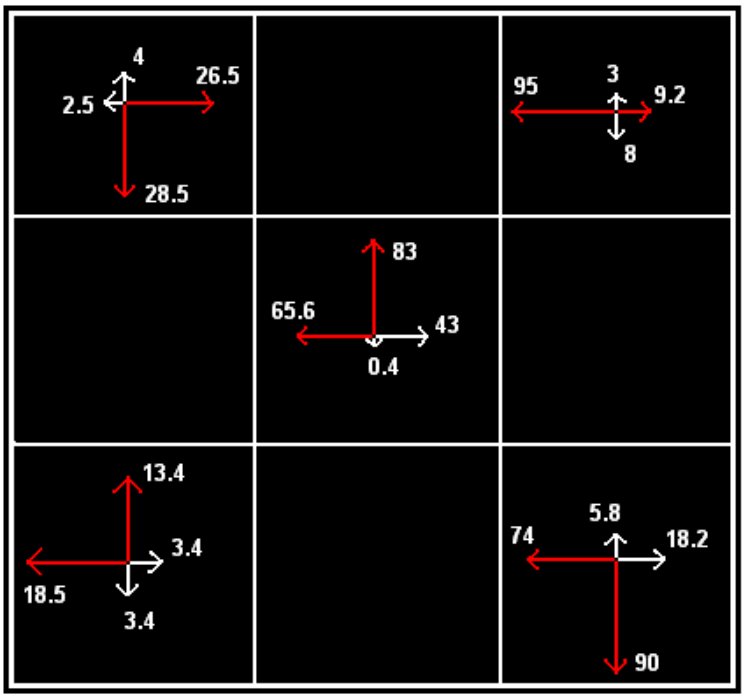

Figure 26, neuron 819R10 Single's recording in terms of arrows. Each segment's firing rate responses from each planar motion is plotted; the length of each arrow indicates the strength of the neuron's response when that motion is displayed within that segment. The strongest two responses are colored as red for easier viewing, which indicates mostly a leftward selectivity from this singles recording of neuron 819R10.

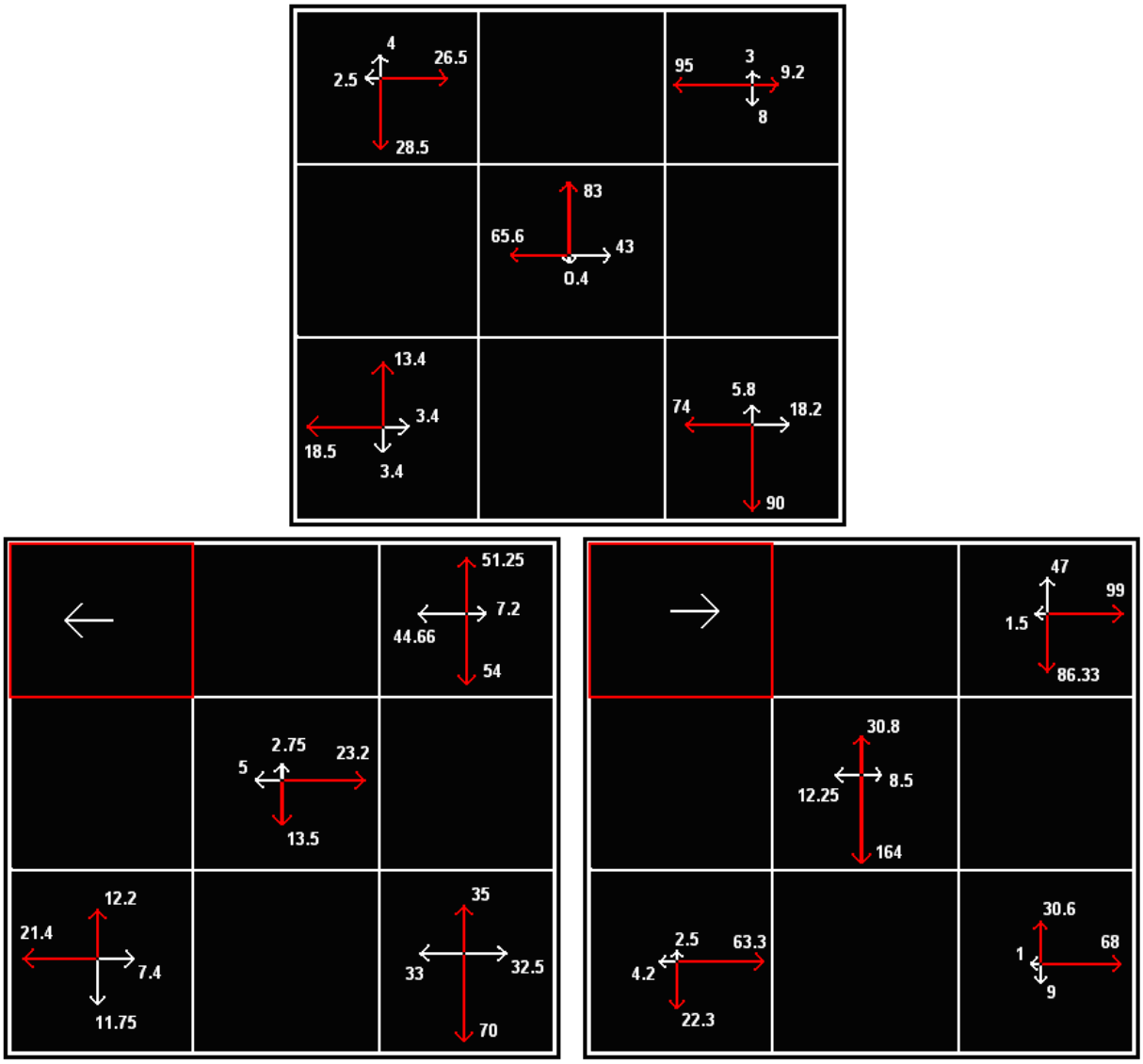

Figure 27, comparison of 819R10's Singles X pattern arrow plot, 819R10's Doubles X pattern hotspot 180° plot, and 819R10's Doubles X pattern hotspot 0° plot. The bottom 2 plots are the double's plots when the hotspot (7th segment, having a red square) is showing 180° movement and its corresponding X patterned test spots, and when the hotspot is showing 0° movement with its X patterned test spots. It is apparent that when the hotspot is showing 180° movement, the test spot's selectivity is more similar to that of its single's recording compared to when the hotspot is showing 0° movement: a clearly reversed selectivity from its singles recordings.

From the above firing rate illustrations, it is apparent that when specific combinations of two segments are showing motion, the 2 segments interact and produces a drastically different response comparing to just one of the 2 segments are being tested. The shift or the reversal of the responses may also be a type of state-switching, where it is triggered by the hotspot's motion stimulus, in which it looks more like a template matching having the hotspot's motion as its reference. This finding explains why when puzzling together singles segmental responses to predict flow responses is a flawed approach, since interaction requires more than one segment that is displaying motion. The resulting responses from the doubles interaction also indicates that a neuron's flow selectivity is much more complex than simply adding up local motion selectivity, that it requires interaction effects to capture a better global selectivity of flow stimuli, resulting in a much more efficient neuronal receptive field.

4. Methods

4.1. Training of the Dual Gaussian Model

The aim for the models is to see if singles and doubles model can predict their neuron's flow responses. We designed dual-Gaussian models of each MST neuron's responses to the singles and doubles local motion responses. Each neuron's dual-Gaussian model is first trained by fitting its singles data and then, in a separate step, trained by using its double data. Both models are derived using the GA. All trainings are done in 3 separate trials of the GA, to provide an index of the reliability of the model, particularly with respect to the avoidance of local minima may obscure the actual global minimal error model.

4.1.1. Dual Gaussian Singles Models

The function of choice to model the MST neuron's singles data firing rates is the Normal Distribution function; also called the Gaussian function. It was chosen as a reasonable and widely employed approximation to single neuron response directionality functions (Figure 27). Dual models were used to accommodate the common impression that local motion mechanisms include independent excitatory and inhibitory, or less often two excitatory or two inhibitory mechanisms. The Gaussian function takes the following form:

$$G(\mu,\sigma) = e^{\frac{-\mu^2}{2\sigma^2}}$$

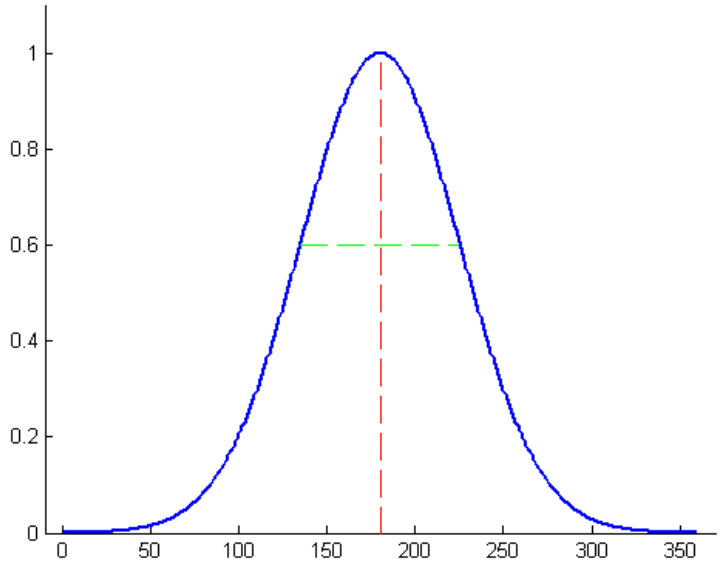

Figure 28, Gaussian curve, μ = 180, σ = 45. As employed in this modeling effort, the ordinate represents normalized neuronal firing rate and the abscissa represents local motion stimulus direction.

Since the data is pre-organized into nine different segments, we would need at least nine Gaussian functions for each segment's firing rate data. The Gaussian function represents the preferred direction of motion for each segment. To visualize this, the x-axis of the Gaussian curve represents the angle (direction) of the segment's stimulus motion, with a range of 0 to 359 degrees and plotted to label the segment's preferred direction as 180^{o} from figure 27; the y-axis represents the neuron's firing rate when that stimulus direction is presented (Figure 27). Therefore a Gaussian curve's μ value represents the preferred direction for a specific segment's data, while σ value represents the selectivity of that segment's firing rate responses. To take into account potential excitatory and inhibitory responses in each response segment of a neuron's receptive field, we added a polarity indicator (P) for the Gaussian, which can be either +1 or -1 for excitatory or inhibitory representations, respectively. To match the intensity of the firing rate

for each segment i, a gain constant (C) is applied to the Gaussian curve as well. The complete function is therefore:

$$response_i = C_i * G(\mu_i, \sigma_i) * P_i$$

We specified two Gaussians per segment to accommodate both excitatory and inhibitory responses in a segment of the receptive field. In addition, the dual Gaussian models can fit the bipolar (bi-directional) response functions observed in some segments. Finally, summing the responses from all nine of dual Gaussian functions with the neuron's singles baseline (B) creates a full accounting of the firing rate data in response to a local motion stimulus. These baseline values were recorded during recording periods in which no motion stimulus is presented on the screen, and is taken to be a good indicator of a neuron's firing rate threshold between its excitatory state and inhibitory state. Therefore, to obtain a response of a 9-segment singles dual Gaussian receptive field models from any flow stimulus requires the following function:

$$response_{\text{total}} = B + \sum_{i=1}^{9} C_{1i} * G_1(\mu_i, \sigma_i) * P_{1i} + C_{2i} * G_2(\mu_i, \sigma_i) * P_{2i}$$

4.1.2. Clamping

There is also a need to clamp any negative total response from the dual Gaussian model to 0 instead of using the negative value. The reason is that neurons with strong inhibitory

responses are limited to firing at zero spikes per second, and there are no negative firing rates in extracellular single neuron recordings. Therefore clamping negative total response to zero for training the model captures this aspect of the recorded data. Our experience is that this clamping yields better models.

4.2. Genetic Algorithm – Singles Model Training

After setting up the dual Gaussian functions for all 9 segments of the receptive field (total of 18 Gaussians), each Gaussian's parameters were tuned by the GA (genetic algorithm) to produce the final summed response that match the singles or doubles data for that segment. To obtain the proper values for each of the variables of the dual Gaussian functions for each segment, the GA optimizes all of these variables.

4.2.1. Initialization

To initialize the modeling of each neuron, 2550 individual candidate dual Gaussian models are randomly generated, with each individual Gaussian having the following variables to be optimized: **C**, **μ**, **σ,** and **P.** Each candidate model also known as an *individual* of that generation in the GA, is the 9-segment model that contains a dual Gaussian for each segment. Therefore an individual contains 18 Gaussian functions with the above variables that will be optimized throughout the GA process, and a fitness score indicating how well this individual is preferred. **C** is initialized randomly to be between 0 and 200, μ is initialized randomly to be between 0 to 359, σ is initialized randomly to be between 0 to 90, and **P** is initialized randomly

between 0 to 15, with integer larger than 7 representing positive polarity, and negative otherwise.

4.2.2. Selection

For each neuron, each individual model's fitness score is calculated, then the top 25 individuals are selected for the next phase. The fitness score function combines two different aspects of each model's fit to the neurophysiological data. The first fitness function calculates the absolute error of an individual model's firing rate responses to the neurophysiological responses. The absolute error fitness function takes absolute value of the difference between the model's response and its corresponding single's stimulus recorded response, then the difference is divided by the standard error of this stimulus' singles recording. This way, larger and smaller standard error becomes meaningful in the training of the model.

$$Fitness_{absE} = \sum_{i=1}^{20,16,36} \frac{\left| response_{model_i} - response_{data_i} \right|}{standardError_i}$$

The second fitness function calculates the grouping error according to k-means clustering algorithm. We apply a k-means clustering algorithm to the neurophysiological data assuming three response clusters for each neuron that corresponds to classifying all responses as low, medium, or high firing rates. In many cases, this clustering recognizes excitatory responses, baseline firing responses, and inhibitory responses. Therefore, by having k-means clustering to find 3 clusters through out a neuron's singles recording, each recorded stimulus response can be

classified as group 1 (inhibitory group), 2 (baseline/no response group), and 3 (excitatory group).

$$Fitness_{groupE} = \sum \left| kMeans(response_{model}, 3) - kMeans(response_{data}, 3) \right|$$

The fitness score for each model therefore includes calculated for both absolute error and group error fitness scores. All of the individual models within the initial population are assessed the same way to select 25 elite individual models from both fitness functions to make a total of 50 (overlapping models are allowed) selected elite individuals to go into the next phase of GA.

2	54	25	41	5	52	132	39	1
2	166	123	7	13	17	2	21	3
2	117	232	11	10	172	295	43	7
2	40	262	27	1	93	118	31	1
2	35	52	20	10	20	145	79	10
2	165	217	8	4	163	21	83	7
2	195	291	50	7	55	46	46	3
2	70	93	42	6	135	243	4	13
2	93	211	32	1	64	108	5	3
257.67	29	0	0	0	0	0	0	0

Figure 29, a randomly generated initial singles dual-Gaussian model (individual) by the GA of neuron 712R02. Row 1 through 9 represents receptive field model's 1st to 9th segment selectivity dual Gaussians, 10th row represents the 2 fitness scores: absolute error is 257.67, and group error is 29. Receptive field models all follow the same format as this example comma separated data file. For row 1 to 9, the first column represents how many Gaussians are in effect for that segment of the receptive field model; column 2 to 5 are the values for the first Gaussian: column 2 is the Gain-Constant; column 3 is μ, means the tuning direction preference; column 4 is σ, indicates how selective this Gaussian is; column 5 is the polarity of this Gaussian – 8 or larger being positive and other wise negative polarity. Columns 6 through 9 are the 2nd Gaussian's parameters which all follows the same format as column 2 to 5.

4.2.3. Crossover

Each individual model is consisted of genes, which are represented as binary bits. An individual model's genes are its variables that need to be optimized by the GA: **C**, **μ**, **σ,** and P. The genes of an individual are crossed over with another individual (Figure 29), and the individuals are provided from the Selection process. The 25 lowest absolute error individuals are crossed over with the 25 lowest k-means grouping error individuals in the hope that their crossed-over offspring will have both characteristics: better point to point matching and lower variance. Each of the 25 lowest total error individuals are crossed over with each of the 25 lowest grouping error individuals, and each parent produces four offspring. When crossing over from the 2 parents, we are crossing over the parameters that correspond to each other: gain constant to gain constant, μ to μ, σ to σ, and polarity to polarity from the 2 parents.

The four offspring from each parents are generated by randomly cutting from an index point for each of the variables bit strings, split the variable bit string into two pieces from the index point selected, then combine left piece from parent 1 first to right piece from parent 2 after, right piece from parent 2 first to left piece from parent 1 after, left piece from parent 2 first to right piece from parent 1 after, and right piece from parent 1 first to left piece of parent 2 after. If any of the resulting crossed-over variables contains an invalid number that is larger than the pre-set limit, such as 500 for μ, the value is then set back to the maximum number that value is allowed, which is 359 in this case. After all 4 parameters of a Gaussian from each parents are crossed over successfully, the 4 resulting parameters together represent the newly generated offspring from the parents. The total offspring is 2500, adding the 50 elite parent individuals back to the new population pool would make this new generation of population totaling 2550

individuals.

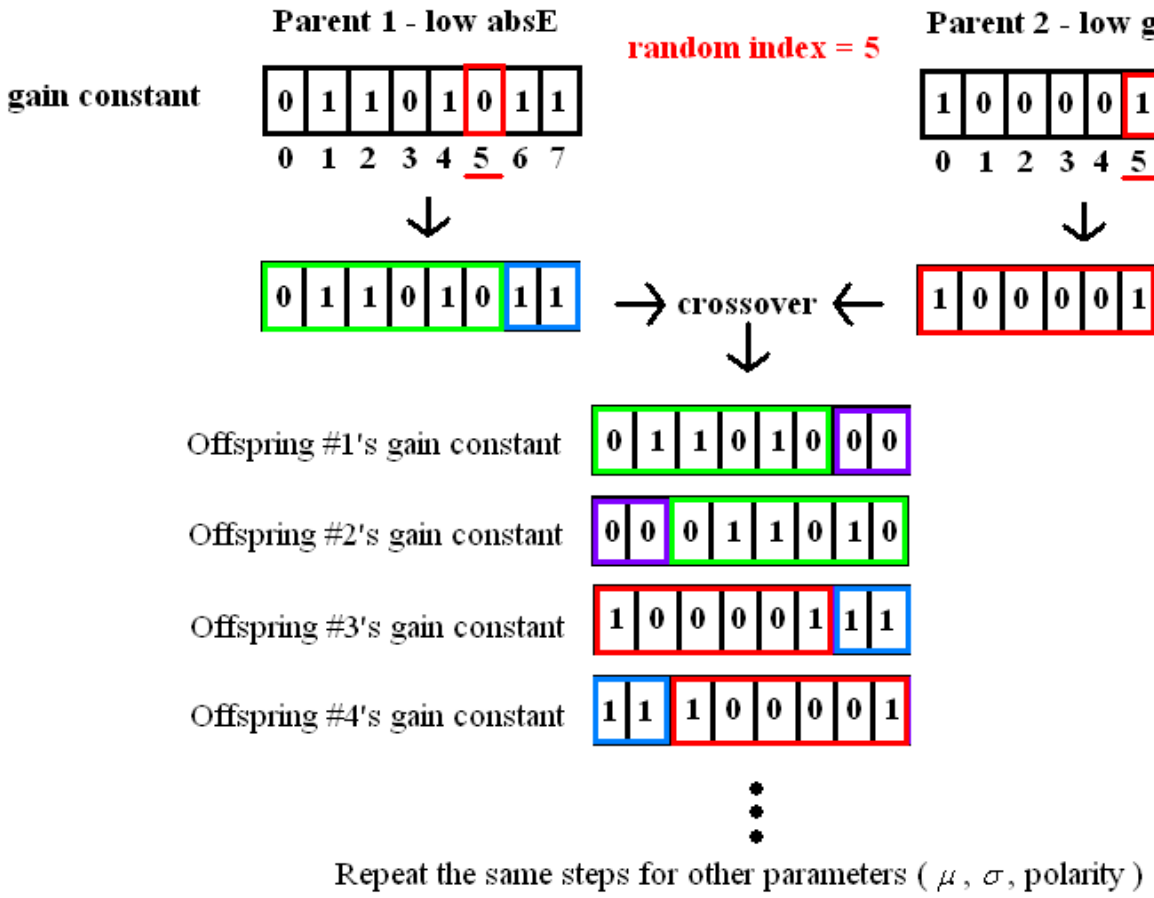

Figure 30, crossover of 2 parent's gain constant.

4.2.4. Mutation

In case of any individuals that are locked in possible local minimum from the vast search space, mutations of the genes are needed. The mutation factor is set as 0.05, and whenever a random constant between 0 and 1 is less than 0.05, the mutation process will take place for any candidate variable from an individual. For the variables that are to be mutated, a random index is selected, and the variable's bit string would then have its bit at that index toggled from 0 to 1 or

from 1 to 0 (Figure 30). Possible mutations are considered for every variable for all individuals.

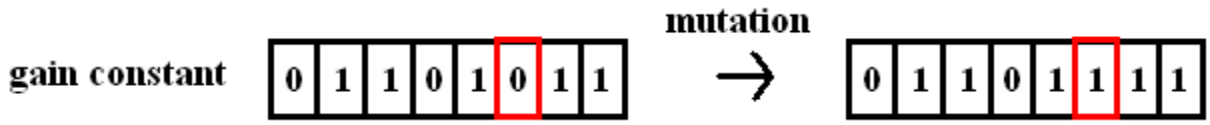

Figure 31, example mutation of a given gain constant bit string. The randomly selected bit is toggled.

The resulting population becomes the new generation, and is sent back into the selection process for the loop. A singles dual Gaussian model is expected to take 75 generations of looping in order to achieve a satisfactory result, whereas for doubles templates X and O would need just 35, due to less data and missing segment firing rates.

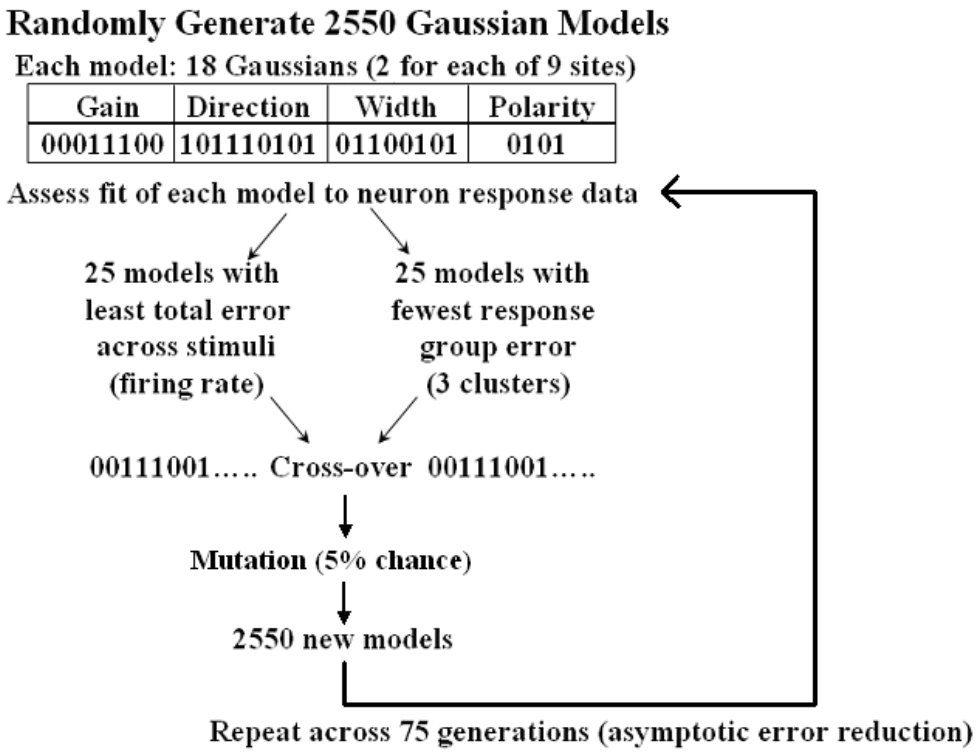

Figure 32, flow of GA for singles dual Gaussian model training.

4.3. Genetic Algorithm - Doubles Model Training

Doubles dataset is different from the singles dataset, in which doubles experiment tests a pair of segment instead of a single segment from the singles experiment. Therefore, this difference requires some small modification of the GA training method, as well as how to utilize the trained models in flow prediction.

4.3.1. Dual Gaussian Doubles Model and Template-Matching

Since the doubles data consists of responses to the selected hotspot paired with a test spot, some adjustments are required for the GA to find a suitable dual Gaussian model. For each doubles data file, the hotspot takes one of four planar directions, which is paired with all four directions of the test spots of either the X or O configuration. In contrast to singles data in which each segment evokes directional firing rates of its own, doubles data contains firing rates for a pair of segments. For the GA to find a dual Gaussian model for the doubles data, we do not assign any Gaussian or firing rate data to the hotspot, we only try to have GA find the appropriate parameters for the test spot's dual Gaussian, while using the paired firing rate as the response to the test spot that the GA tries to fit.

The doubles data is fed into the GA to search for the optimized dual Gaussian curve for each of the test spot's segments. Note that for the hotspot, however, does not contain any Gaussian functions, hotspot will only has identifiers indicating which direction it was tested. The way we think how doubles data work is what we called as "template-matching": each hotspot

direction serves as a template, that when we use the doubles model to predict flow responses, we use the doubles template in which the hotspot's direction matches the flow stimulus's direction at hotspot's segment (Figure 32).

There is a small difference between how doubles data is trained by the GA and that of the singles: the singles models were trained by the GA optimizing all 9 segments' dual Gaussian together, while the doubles models were trained by the GA optimizing just a pair of hotspot and test spot data at a time, then put back together into a full segments model. Besides the training efficiency, there is technically no real difference between the two approaches of training as long as the GA converges to a solution model over the generations. However, the doubles GA training experienced difficulty in finding a good solution for some neurons, and by dividing the training set into smaller data sets solved this problem. Therefore, the divide and conquer efficiency was needed for the doubles GA training sessions.

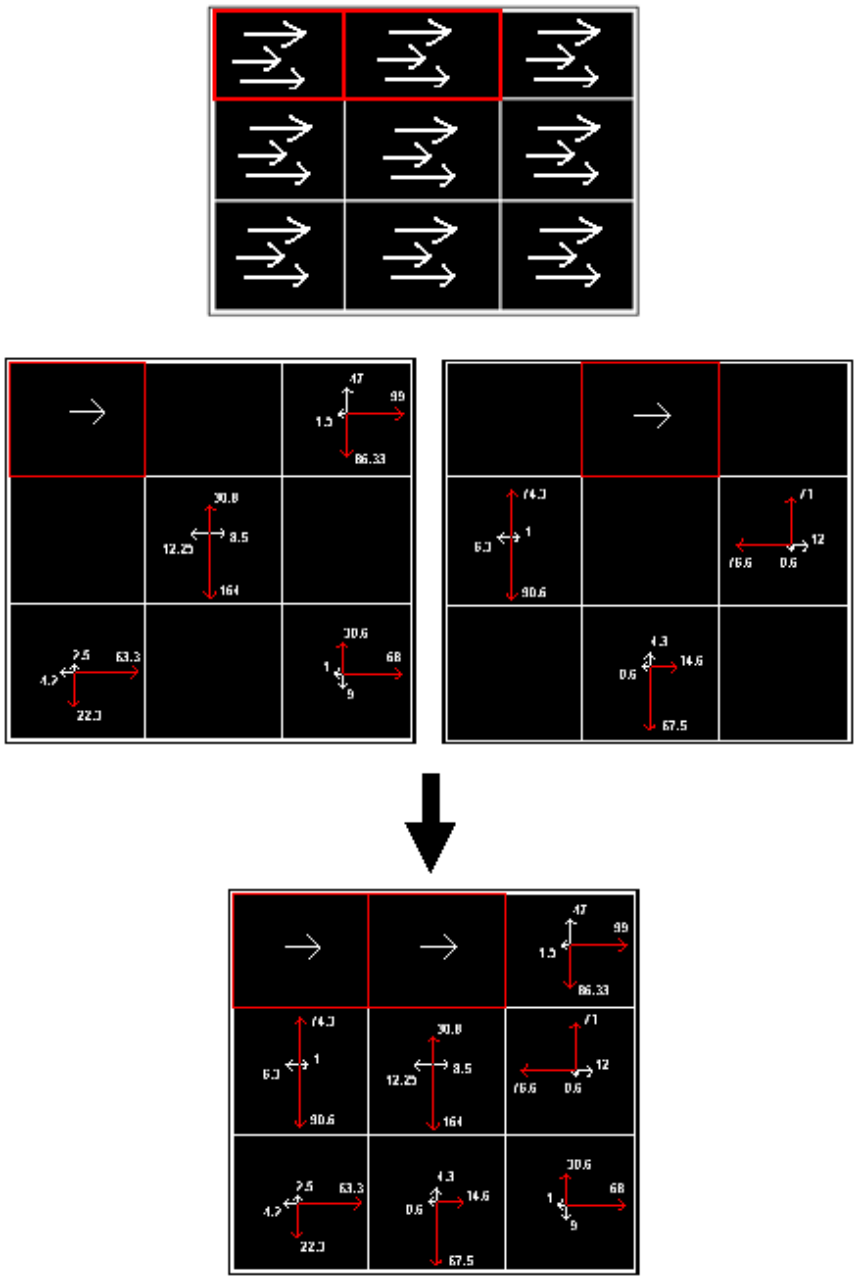

Figure 33, neuron 819R10's doubles template for flow stimulus 1. This template is constructed by finding the recording which has its hotspot direction matching the flow stimulus that we are trying to predict, and for neuron 819R10, it has its X hotspot at the 7th segment, and O hotspot at the 8th segment, therefore combining the X and O hotspot that are pointing at 0° gives us the template that will be used for flow stimulus 1's prediction.

4.3.2. Doubles Diagonal Hotspot Data Interpolation

The singles data contains four planar direction's firing rate responses for X, O, or both patterns together. The doubles data was recorded the same way as singles. However, for singles-to-flow prediction we just feed the singles model through the flow's entire 16 stimuli. For the doubles-to-flow prediction, we create templates for matching the segmental directions in each of the optic flow stimuli. The problem with this is that flow was recorded with diagonal motions, whereas neither singles nor doubles were recorded with any diagonal motion, singles and doubles were only recorded with the 4 planar motions. Therefore, in order to construct diagonal hotspot motion templates, we interpolate for the double's diagonal hotspot motion's test spot firing rates from the data we have.

The doubles data was recorded by presenting just one of the four planar direction motion stimuli for a hotspot segment paired with a test spot segment. To interpolate for a neuron's doubles data X pattern hotspot 45° and X test spot firing rates, simply take the average of hotspot 0° firing rates and 90° firing rates for every tested segment. Repeat the same steps through all of the other diagonal motion of the hotspot for doubles until all of the diagonal hotspot and test spot firing rates are generated.

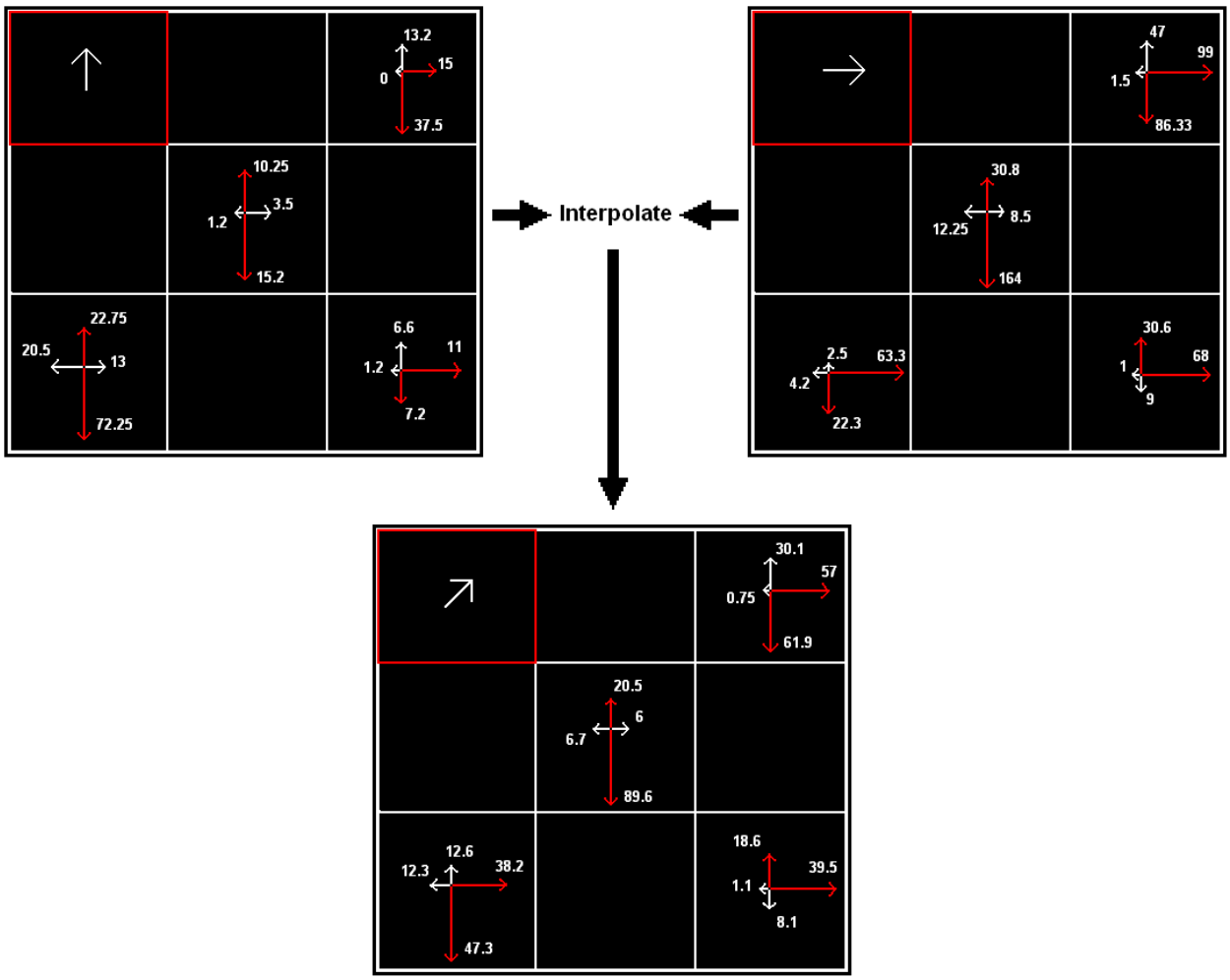

Figure 34, interpolated data of neuron 819R10 X pattern hotspot at 45°. To interpolate for this neuron's X pattern hotspot at 45°, firing rates from each recorded segment's motion are averaged.

4.4. Gain Modulation

While we observed the reversal effect of local motion interaction from the doubles data, it is also possible that by turning up/down the relative gain of a sub-region region's strength of influence on the overall firing rate, we may find better flow predictions from the singles recordings. Therefore, we are also going to explore this gain modulation effect by turning up or down the gain constant of each Gaussian from each segment. To find the optimized gain factors, a neuron's singles dual Gaussian model is put into the GA, and the GA would then try to search for *one* set of gain modulation variables that would influence the singles dual Gaussian model in ways such that it best fits all 16 of the flow responses. To implement this gain modulation mechanism, it is important to remember that the dual Gaussian model contains two Gaussian functions per segment, therefore there are two ways of implementing gain modulation.

4.4.1. Nine Gain Factors

In this approach to gain modulation, we specify one volume variable for each of the nine segments of singles data to add up to a total of nine gain factors (1 for each segment). This approach assumes that each receptive field segment's two Gaussian function's gain constants are influenced by the same segmental gain factor, a gain factor for that spatial segment of the receptive field. The gain factor is initialized randomly in the GA with the range of 0 to 10, a gain factor that is higher than 1 represents an increase in volume by 10 times the gain factor; less than 1 mean a decrease in volume by the 10^{th} of the gain factor, and 1 represents no change.

4.4.2. Eighteen Gain Factors

In this approach to gain modulation, we specify two separate gain factors for each of the nine segments, meaning each of the two Gaussian functions of each segment is influenced by a different gain factor. Therefore, two gain factors per segment for all nine segments of singles data create a total of eighteen gain factors to be optimized by the GA. In some ways, the 18 gain factor approach may be especially interesting since to change the gains of both Gaussians per segment may represent similar meaning as directional shift. The 9 gain factors experiment strictly turns both Gaussians up or down in strength, which is purely segmental dominance as comparing to the 18 gain factor which may display directional shift in addition to segmental dominance.

4.5. Optic Flow Prediction

When developing a computational model, the model needs to be able to mimic the effect of what it was modeled upon. In this work, our models of the MST neurons will also have to be able to perceive optic flow stimulus. Therefore, after the models are optimized by the GA, they need to demonstrate their ability in predicting optic flow stimulus, while reflect the data they modeled from. Another aspect of this research is to demonstrate that doubles dual Gaussian models are able to predict the optic flow responses as well as the singles dual Gaussian models, with some doing significantly better due to the discovery of receptive field interactions from the doubles data.

4.5.1. Singles to Flow Prediction

For a GA optimized singles dual Gaussian model to predict its flow responses, we test each singles model segment's dual Gaussian function to the corresponding flow segment's motion stimuli. This step is repeated for all nine singles segments, then the results are summed across the nine segments of that neuron. Notice that any negative response is clamped the same way as the models were trained by the GA. It is also important to know that flow recordings and singles recordings from the same neuron usually has a fluctuation in baseline, sometimes the difference is very large. During the GA training of the singles models, singles baseline value was added to the segmental summed response; therefore, for the prediction of flow by the singles model, the singles baseline will also be added to the summed segmental response as the final response output.

To measure how good of a prediction a model is to the flow stimuli, we take the absolute difference between the model's response and the recorded flow response. Although flow recordings also had multiple trials therefore yield standard errors per stimulus, we do not take the standard error into account like the training of singles and doubles model since it is predicting a different data set. As for group error, we also take the group error difference in the prediction, and when we measure a goodness of prediction, it will be determined mainly by group error. The reason why we use group error as goodness of prediction is because every neuron fires differently, therefore the range of different neuron's firing rates makes the max firing rate across neuron non-uniform. However when we measure group error, it is always in groups of 3, therefore k-means group error is a good way to measure a prediction's goodness, and can be compared across neuron.

Over half of the singles recordings were completed for both X and O pattern; however, the remainder of the singles recordings have only X or O pattern. In a case when a neuron only has X pattern recording, the resulting absolute response was multiplied by 9 / 5; in a case when a neuron only has O pattern recordings, the prediction absolute response was multiplied by 9 / 4. As for k-means group error, all of the X patterned singles was tested on flow stimulus 1 through 8, and 13 through 16, and the O patterned singles was tested on flow stimulus 1 through 12, while the singles model that contains both X and O will be tested on all 16 flow stimulus. The X or O patterned singles model was tested only on part of the flow stimulus because their corresponding doubles template has its hotspot at the not-tested flow stimulus' focus of expansion, therefore to make the singles prediction result comparable to its corresponding doubles models, singles needs to skip the flow stimulus where its doubles model does not have an appropriate template for. The k-means group error would also need to be modified for an X or O patterned singles model: the resulting group error was multiplied by 16 / 12. This step is to normalize the output so that the error numbers will be comparable against the singles models that has both X and O pattern combined.

4.5.2. Template Matching Flow Prediction with Doubles Dual Gaussian Models

The interaction effects are hypothesized as hotspot driven; meaning when the hotspot segment receives a stimulus that has a certain direction of motion, the various interactions such as reversal effect is then activated at another segment. Therefore, in order for doubles dual Gaussian model to be able to predict flow responses, the doubles model needs to be separated into 16 different models for each of the 16 flow stimulus, which has the doubles hotspot motion

direction matching the flow's motion stimulus direction at the hotspot's segment.

4.5.3. X and O Doubles Template

Since the doubles data was done the same way as the singles in the setup of X and O segments, they are able to predict flow responses separately as an X doubles template, or as an O doubles template if a neuron does not have both X and O pattern recording present. The process is similar to flow prediction from singles, if there are missing segments from a receptive field model, that segment will output 0 as its segmental response. Because the hotspot is always paired up with a test spot when the experiment was taken in which the hotspot was assigned 0 firing rate during training, therefore when a doubles X model is put together, the summed response will be multiplied by 8 / 4 whereas the O model's segmentally summed response will be multiplied by 8 / 3 (not 9/3 because there is a hotspot that started with 0 firing rate which is not counted.) In the case where the doubles model was trained from both X and O pattern of recording, such model's flow prediction will not need to be multiplied by any factor since it contains full 9 segment dual Gaussians.

The hotspots of a given doubles data set was selected by the top firing singles segment. In some cases when a neuron's doubles' X model hotspot happens to be at a segment that is the focus of expansion for certain flow stimulus, the prediction of such flow stimulus will use the neuron's appropriate O model template to obtain a response, vice versa for the O model hotspot being some flow stimulus' focus of expansion. In the case where a doubles model does not have any corresponding template, such flow stimulus is skipped of prediction.

The goodness of the prediction of any doubles template set is measured the same way as

the singles to flow prediction: group error difference. Absolute error is also derived as a reference value, but the actual ranking in which model is doing better is by comparing the group error difference.

5. Results

5.1. Singles Model

Singles Models were trained very successfully by the GA. The overall error rate dropped precipitously in the first few generations and asymptotically stabilized as subsequent generations progressed toward the final 75th generation. Below I illustrate these effects in neuron 712R02 from the total of 52 neurons. Plots from all of the neurons are included in the Appendix.

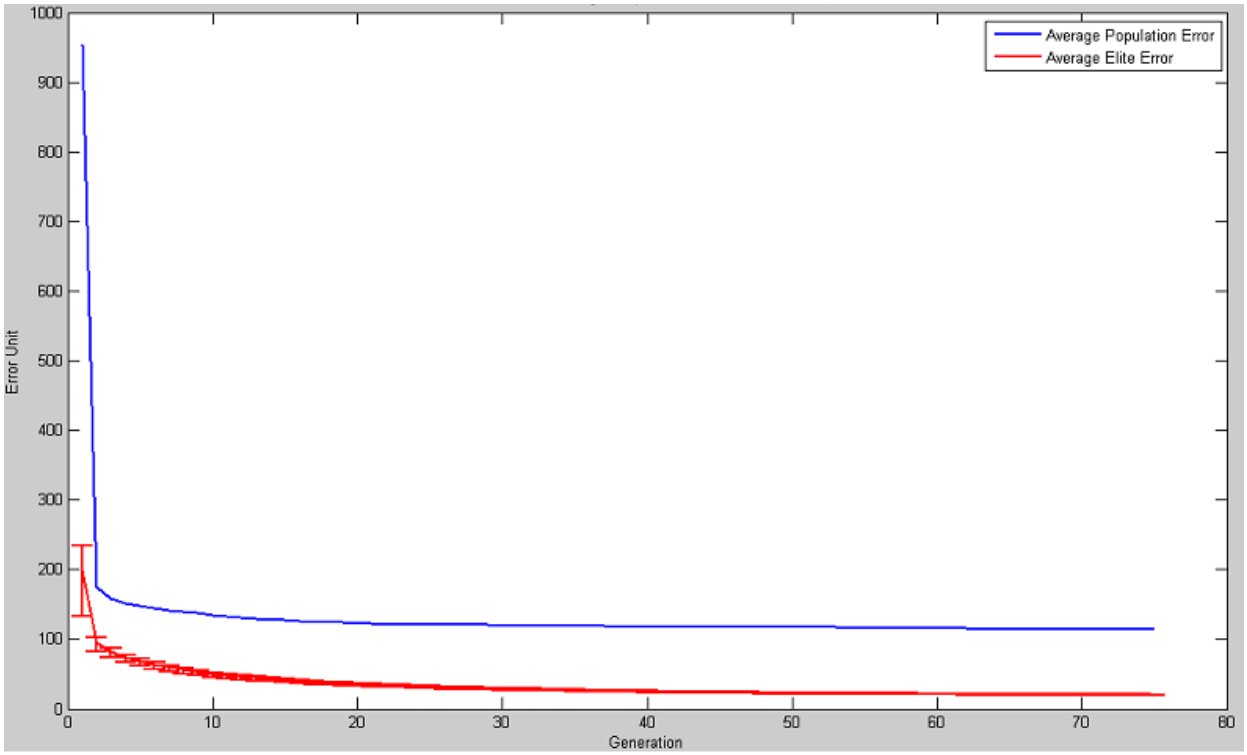

Figure 35, convergence plot of all 52 neurons, repeated across 3 GA trials, showing average total error across GA generations. This plot shows that as the genetic algorithm runs from generation 1 through 75, the total error reduces quickly and asymptotically stabilizes to the individual models converged at the end of the fitting procedure. The red line, is the average Elite (best 25 models) among the population in absolute error, has an error bar representing the range of the elite's error, which has also converged to be very small across successive generations.

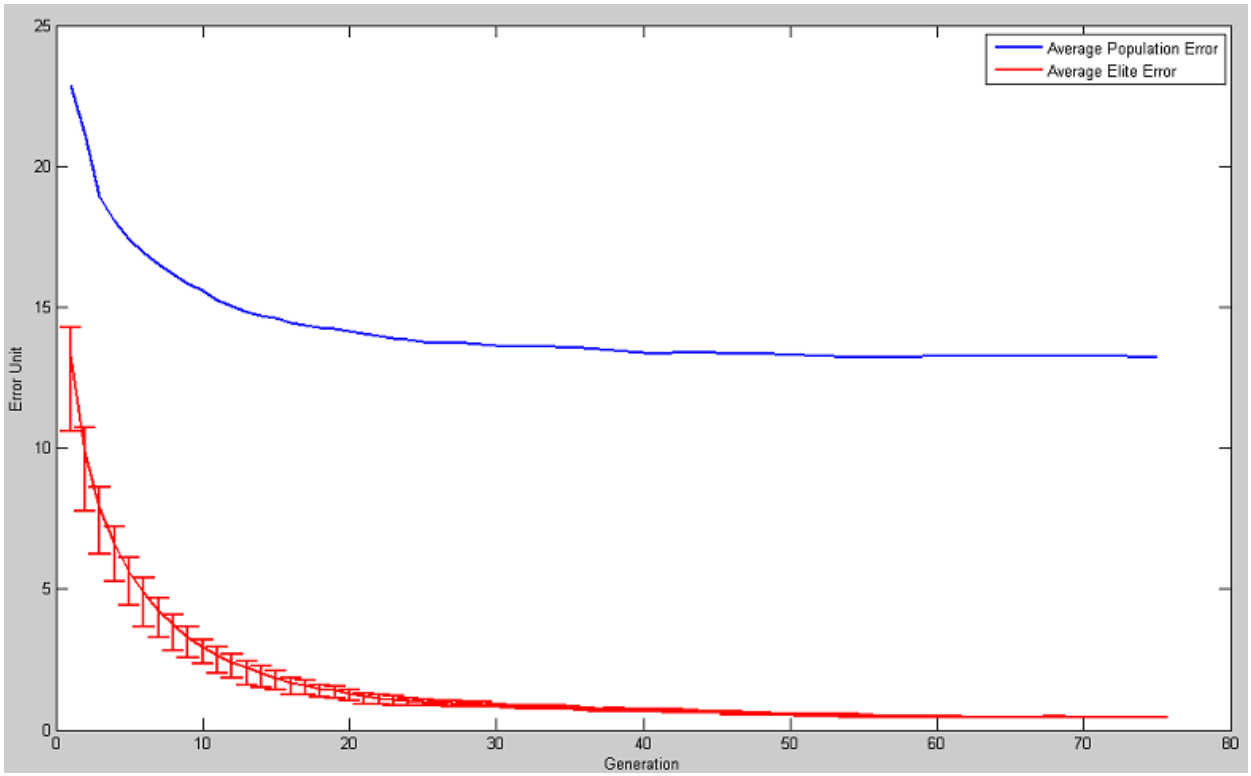

Figure 36, convergence plot of all 52 neurons for all 3 trials for each neuron showing sample averaged k-means group error. This plot shows that as genetic algorithm runs from generation 1 through 75, the group error reduces and asymptotes as each individual model converges to a stable solution in the end. The red line is the average Elite (best 25) models among the population as measured by group error. The error bar shows the range of the elite's error, which has also converged to be very small across successive generations.

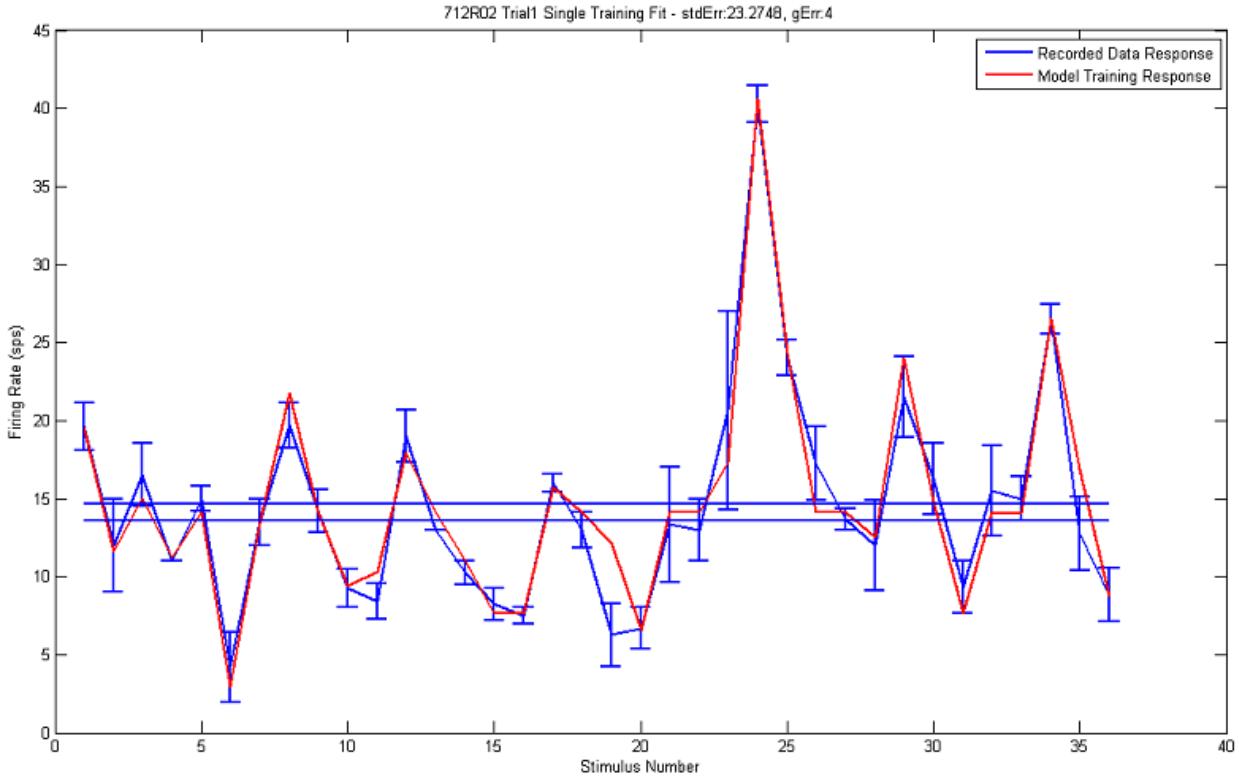

Figure 37, neuron 712R02's singles training trial 1 training response profile plot. As the plot shows, the model (red line) was trained successfully to fit its responses to each of the singles stimulus recorded responses (blue line).

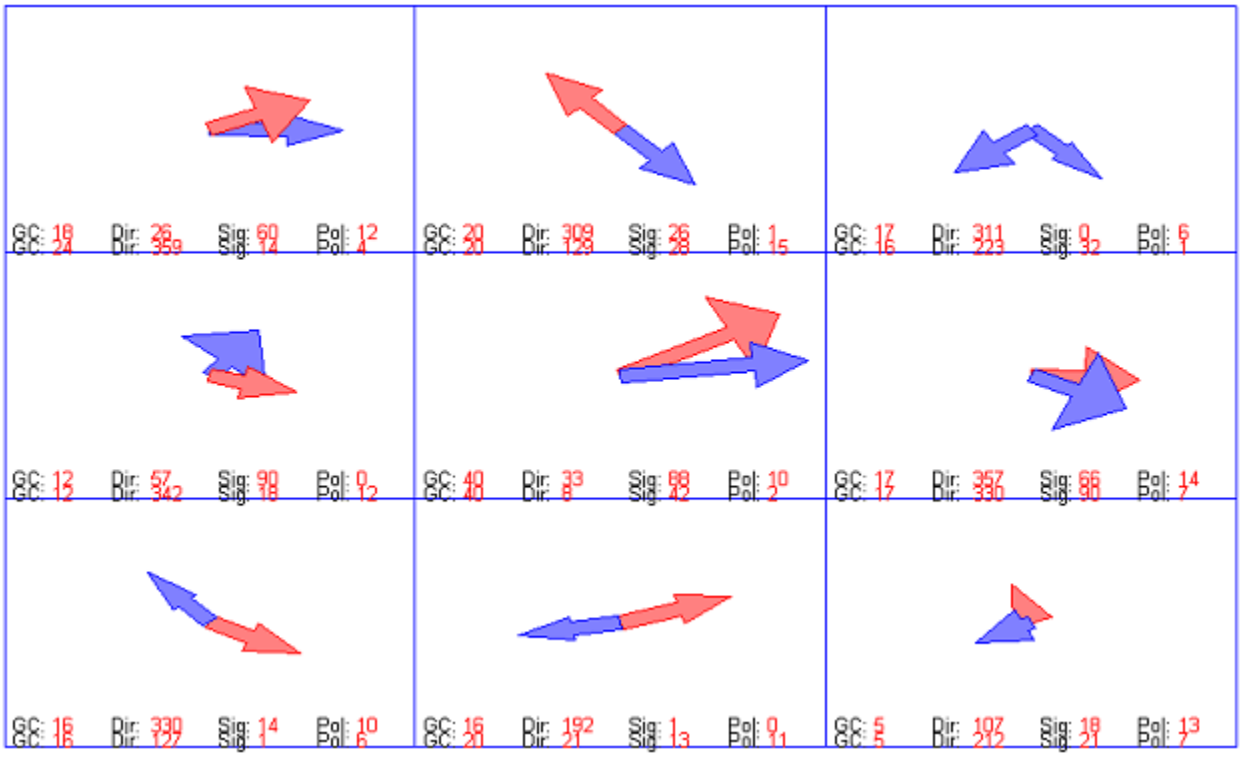

Figure 38, neuron 712R02 singles resulting model, trial 1. This is a graphical display of the model that was generated by the genetic algorithm from 712R02's singles responses. Each arrow represents a Gaussian, therefore each segment contains 2 arrows representing our dual-Gaussian model. The red arrow indicates excitatory responses, whereas the blue arrow indicates inhibitory responses. The length of the arrow indicates the overall strength (gain factor) of that segment, and the width of the arrow head indicates how selective that Gaussian is. The actual numbers that specify each arrow's information are the text below the arrows within each segment.

5.2. Doubles Model

Doubles Models were also trained very successfully by the genetic algorithm. The overall error rate drops and asymptotes successively across generations during progress toward the final, 75th generation. Since we have a total of 52 neurons, we have selected neuron 712R02 to show the individual performance and model plots. All of the plots are included in the Appendix.

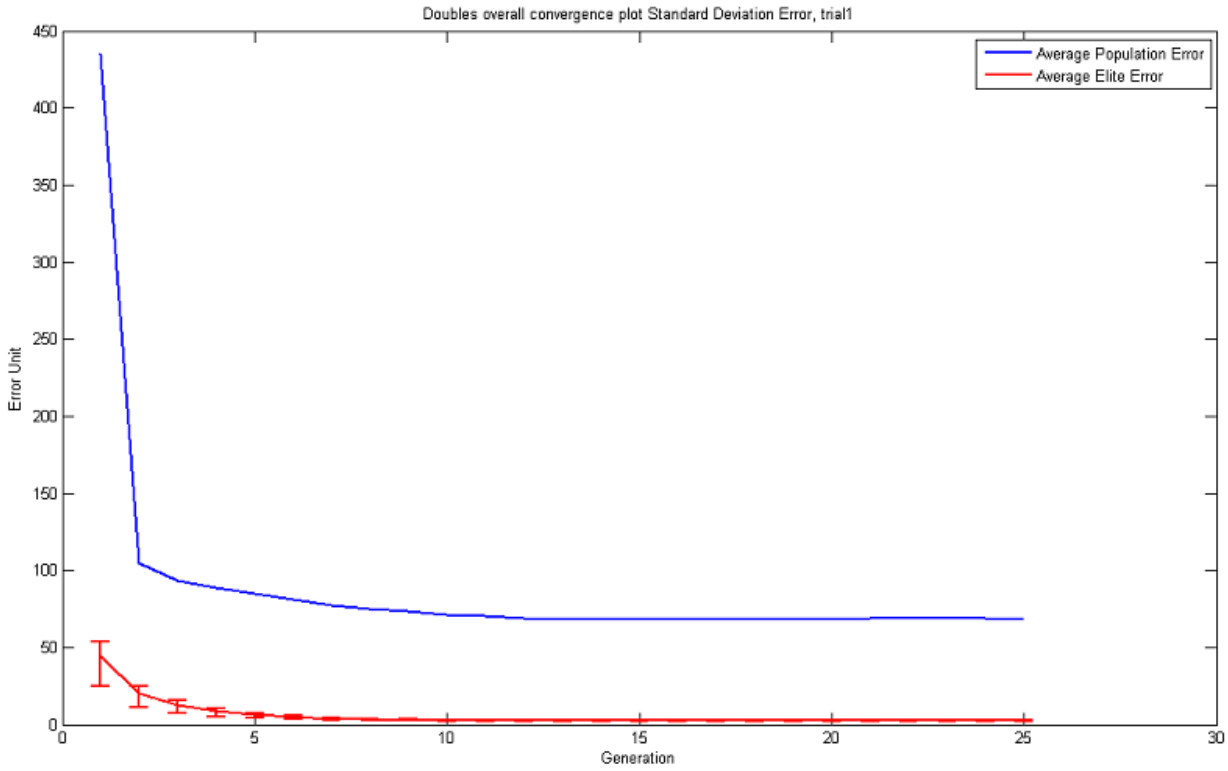

Figure 39, Doubles model convergence plot for all 3 GA trials of all neurons averaged in absolute error. The Doubles experiment was run with 25 generations per hotspot directional template in contrast to the Singles' 75 generations because Doubles are trained with hotspot directional templates which result in fewer entries for the Gaussian to fit comparing to Singles. The plot shows a nicely converged doubles training session, with the variance also converging very quickly.

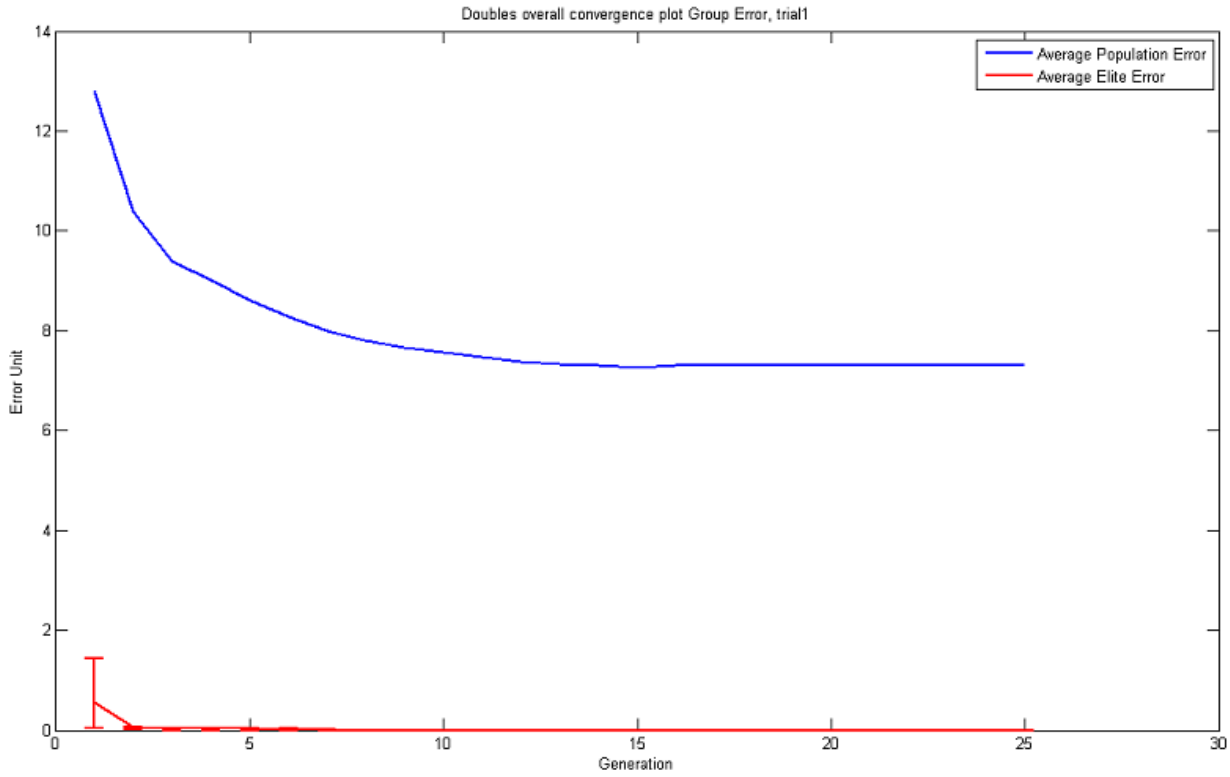

Figure 40, Doubles convergence plot for across all 3 trials and all neurons in k-means group error. Due to fewer data entries that need to be fitted, 25 generations suffices for the training of Doubles templates. The group error training of the genetic algorithm went especially well, the elites mostly have average group error lower than 1. That is largely due to fewer entries to fit against. However the steadily flattened convergence line shows very successful training of the doubles template models with dual-Gaussian design.

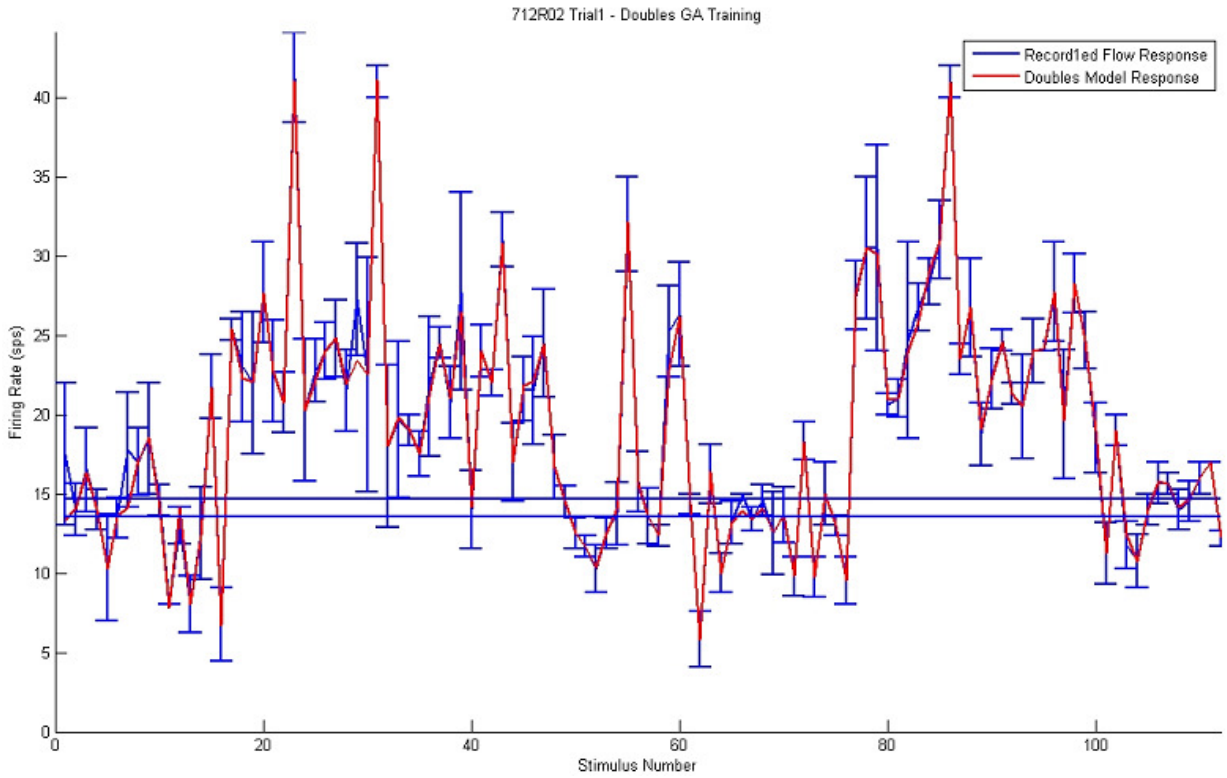

Figure 41, neuron 712R02 doubles' trial 1 with both X and O hotspot entries combined GA training response profile. This plot shows neuron 712R02's doubles' model training result. As the model's response (red line) matches the neuronal responses in the Doubles experiment (blue line) almost perfectly, indicating a very successful training session of the doubles' dual-Gaussian models.

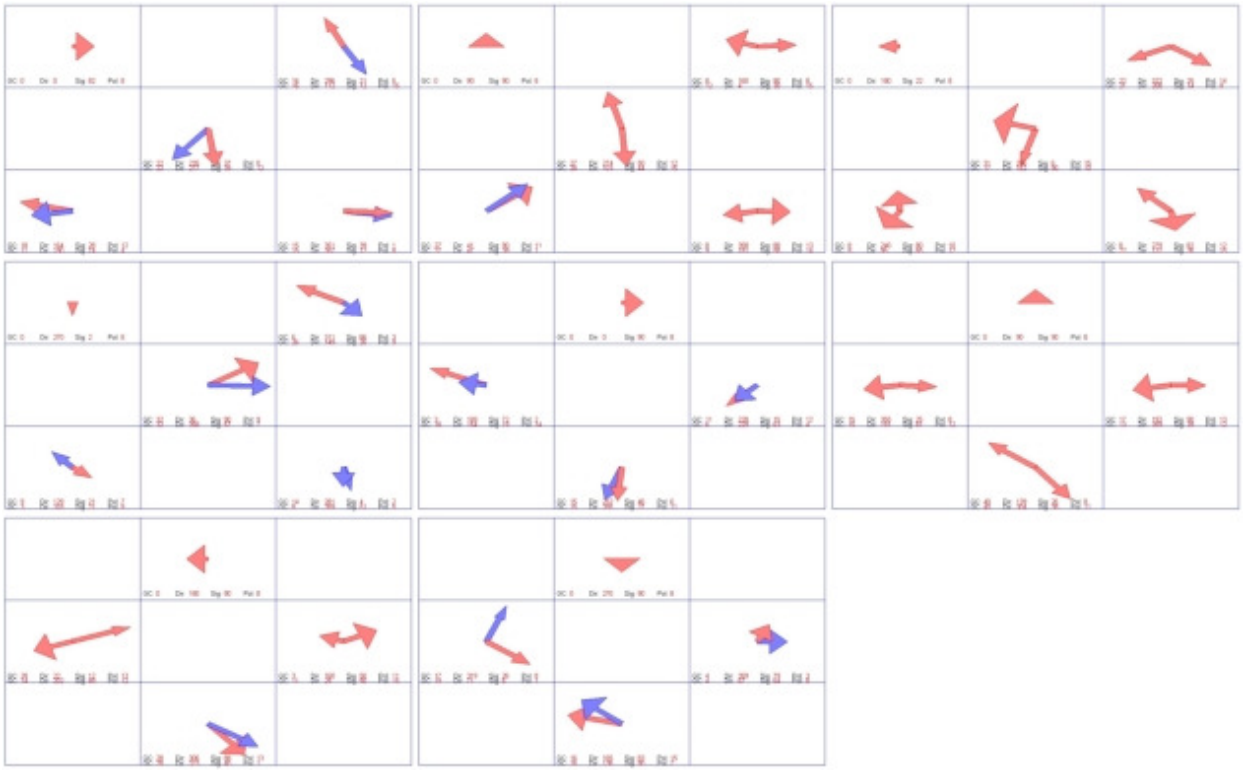

Figure 42, neuron 712R02's doubles' X and O hotspot models from trial 1. The first 4 models are the X patterned doubles' model from 712R02's trial 1 training. As the X pattern's hotspot is located at the 7th segment, the X doubles model has its 7th segment displaying the hotspot's direction. The next 4 models are the O patterned doubles' models, where the hotspot is the 8th segment.

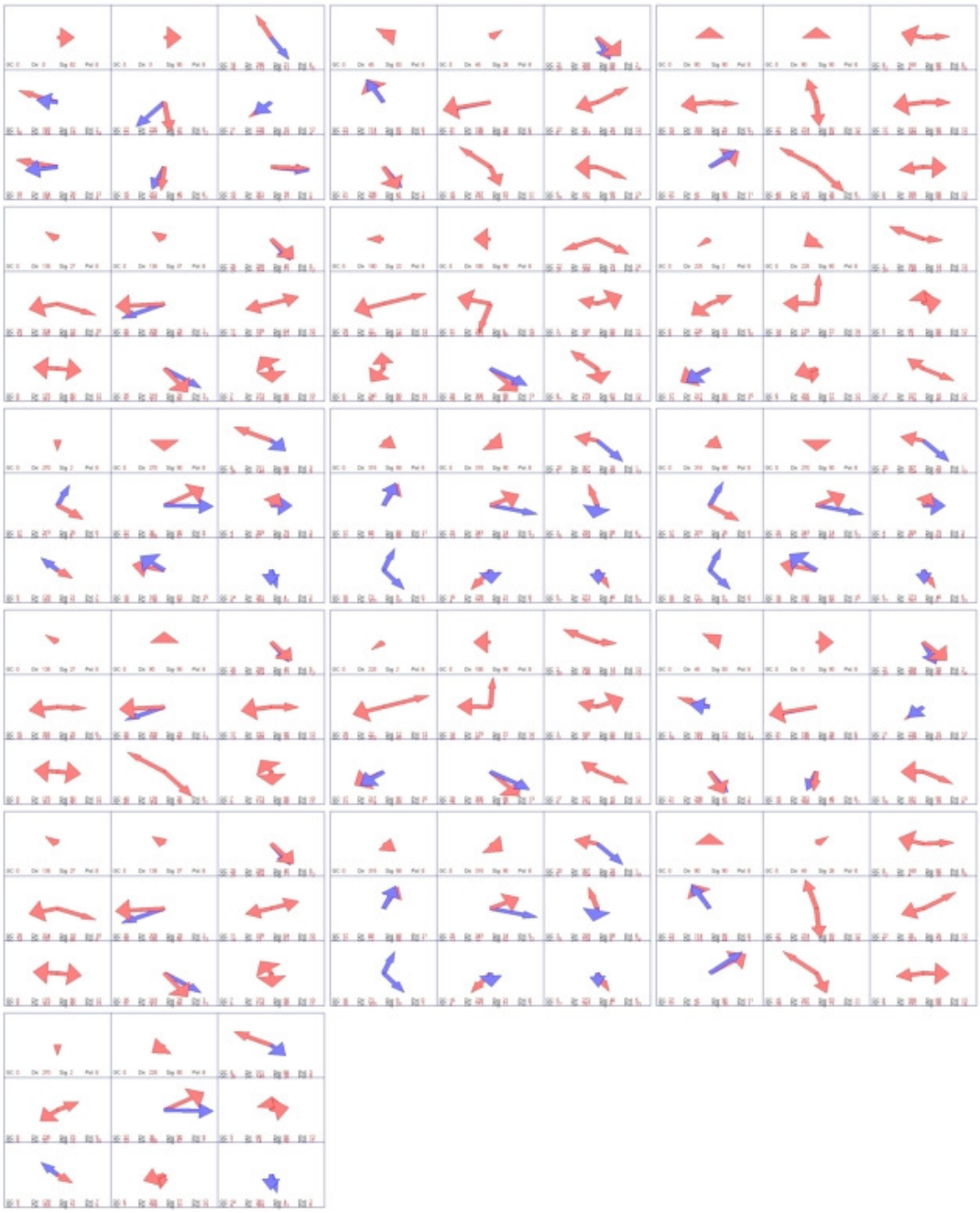

Figure 43, neuron 712R02 doubles template models for flow prediction. As in the models display, the X hotspot (7th segment) and O hotspot (8th segment) are combined to form various templates that predict responses to each of the flow stimuli. The templates are formed by matching the doubles' hotspot direction with the same flow's segmental direction per stimulus.

5.3. Flow Prediction

The GA has successfully trained the dual Gaussian models to fit singles and doubles data separately, resulting in 2 sets of models for each of the 52 neurons (a singles set and a doubles template set). The GA then fits sets of gain factors to transform the singles model to better fit its flow responses further. To test their flow prediction performances, we test each of the singles and doubles template models with the 16 flow stimuli and check the neuron model's responses against the neuron's recorded flow responses. Gain modulations of nine and eighteen gain factor models are also evaluated to determine how much the gain modulated singles models have improved after the transformations.

5.3.1. Singles to Flow Prediction

Each singles model predicts 12 or 16 flow responses depending on if it is an X or O singles model, or both X and O. Each neuron's singles model predicts flow with 2 different goodness-of-prediction measures: absolute error difference and k-means group error difference. However, since each neuron's firing rate and baseline varies, we cannot compare each neuron's prediction fitness by absolute error. We therefore use k-means group error as the goodness of prediction measurement that we can compare across neurons.

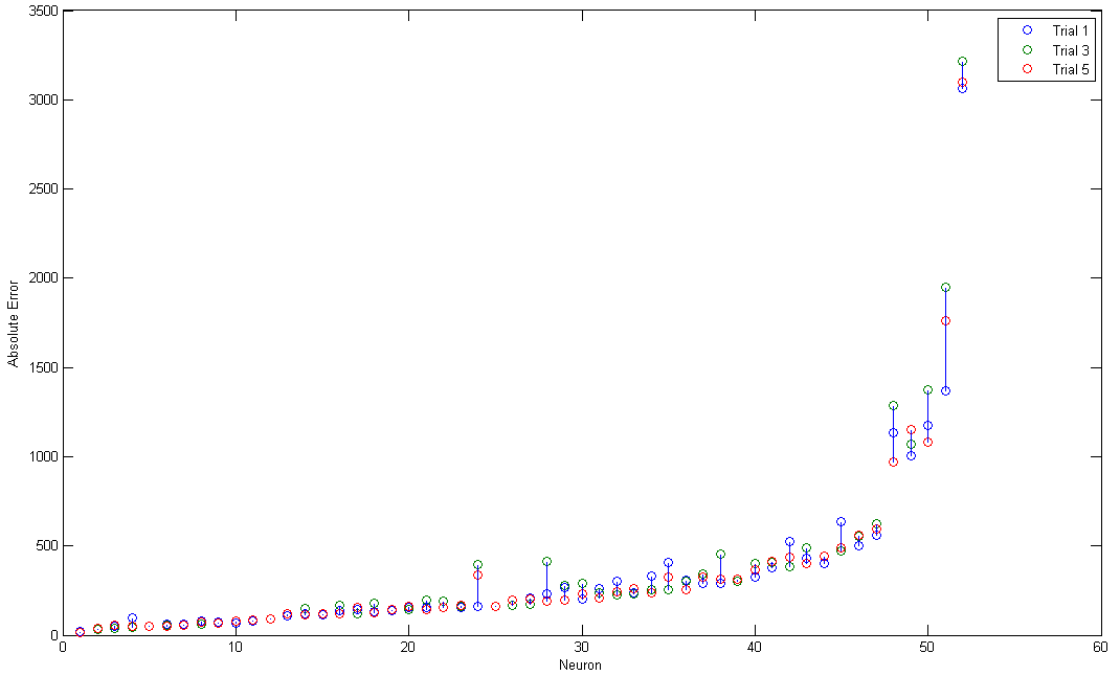

Figure 44, singles predicting flow overall performance from neuron 1 through 52 in absolute error. Note that this plot's x axis is sorted from the lowest error neuron flow prediction to the highest. Each neuron's prediction error is shown for the 3 separate GA trials (3 circles in each column). Since the different trials represent possibly better local minimal of model error, we pick the lowest flow prediction trial as the neuron's flow prediction.

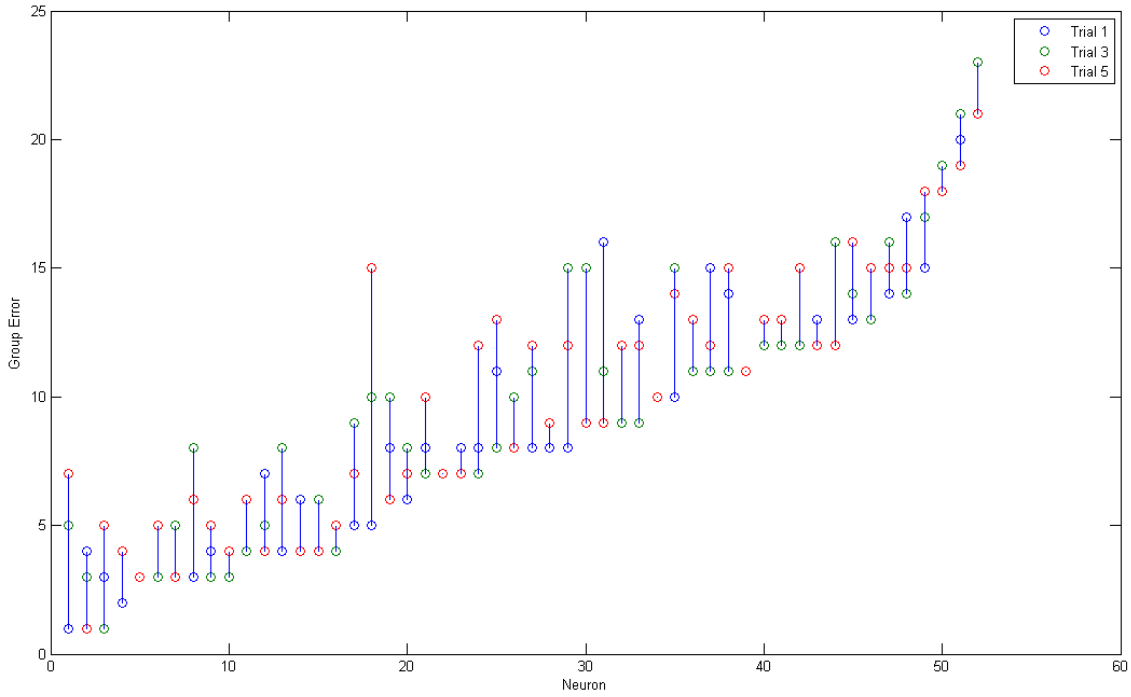

Figure 45, overall performance of singles model predicting optic flow responses from neuron 1 through 52 as measured by average in group error. Similar to figure 43, this plot is sorted by the lowest group error per each neuron across 52 neuron's singles flow prediction. The mean of the group error throughout 52 neurons is 8.1 with a standard deviation of 4.7. The three circles in each column represent the group error for each of the three trials of the represented neuron.

Neuron	Lowest Er	Lowest Gr		Trial 1 Er	Trial 1 Gr		Trial 2 Er	Trial 2 Gr		Trial 3 Er	Trial 3 Gr
712R02	499	13		499	13		552	14		558	16
712R05	304	7		316	8		304	7		316	10
712R06	293	3		293	3		456	3		315	3
712R07	37	3		49	5		37	3		53	5
819R01	163	7		163	7		398	7		339	7
819R02	154	3		156	3		188	5		154	3
819R03	234	11		237	11		234	11		260	13
819R04	121	8		142	11		121	8		158	13
819R07	114	4		121	4		149	4		114	6
819R09	172	7		209	8		172	7		204	7
819R10	1368	14		1368	14		1952	16		1763	15
819R11	56	8		63	10		56	10		57	8
819R12	472	1		639	1		472	5		488	7
819R14	65	12		71	12		65	12		70	13
819R16	61	9		78	15		61	15		73	9
819R17	561	8		561	8		627	11		595	12
819R18	44	7		97	8		44	7		52	12
819R19	400	1		430	4		491	3		400	1
819R20	210	8		260	8		235	9		210	9
819R21	116	12		116	12		119	12		121	13
819R22	52	19		60	20		53	21		52	19
819R24	82	12		82	12		84	12		85	15
819R25	89	21		93	21		92	23		89	21
819R26	143	12		156	13		143	12		160	12
819R27	139	11		139	15		144	11		144	12
819R28	31	12		33	12		31	16		36	12
819R31	288	3		288	3		343	8		326	6
819R32	163	10		163	10		163	10		163	10
819R33	377	15		377	15		409	17		411	18
819R34	969	9		1137	16		1287	11		969	9
819R35	127	5		132	5		181	9		127	7
819R37	201	4		201	7		288	5		234	4
819R39	237	11		331	14		253	11		237	15
819R41	194	6		267	8		279	10		194	6
819R42	326	9		326	12		401	9		366	12
819R44	254	4		408	4		254	8		326	6
819R45	188	8		231	8		412	15		188	12
819R47	16	4		18	6		16	4		16	4
819R48	382	10		526	10		382	15		439	14
819R51	254	4		309	6		302	6		254	4
819R52	51	11		52	11		52	11		51	11
819R53	120	14		136	17		169	14		120	15
819R54	1082	18		1177	19		1375	19		1082	18
819R56	1005	13		1005	15		1072	13		1152	15
819R57	157	4		157	5		159	4		166	5

819R58	401	1		401	3		440	1		440	5
819R59	3065	5		3065	5		3216	10		3096	15
819R60	165	2		165	2		167	4		194	4
819R61	145	6		156	6		198	8		145	7
819R62	226	9		303	13		226	9		243	12
819R63	111	3		111	4		120	3		121	5
819R64	70	3		70	4		81	3		82	4
Mean:	318.3462	8.153846									
STDEV:	478.3616	4.741906									

Figure 46, singles predicting flow overall performance data. This data sheet shows the absolute error and the group error prediction results from each of the 3 trials, and the lowest of the 3 trials. Since singles have different firing rates and baselines per neuron, the mean and standard deviation of absolute error is less meaningful than group error's mean and standard deviation, which is comparable across all neurons.

5.3.2. Doubles to Flow Prediction

The doubles models predict responses to optic flow for 12 or 16 optic flow stimulus templates, depending on whether the doubles were recorded in the X, O or XO patterns. Doubles template models also predict flow stimulus by absolute error difference and k-means group error difference as with the Singles models. The difference between the Singles and Doubles predictions is that the Doubles can be limited to a subset of optic flow stimuli that have templates that can be encompassed by the pattern of segments recorded in the configuration of double stimuli used in that neuron.

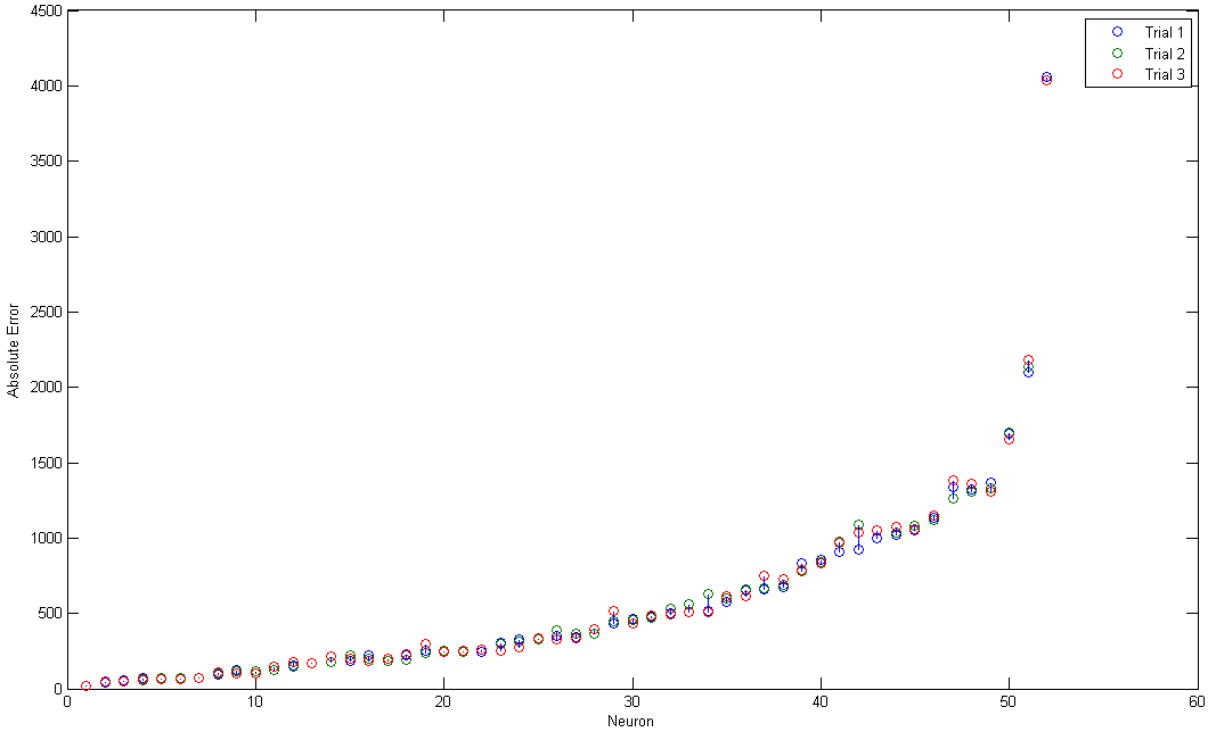

Figure 47, doubles predicting flow overall performance from neuron 1 through 52 in absolute error. This plot's x axis is sorted from the neuron with the lowest error flow prediction to the highest. The three circles for each column represent the prediction result from the 3 separate trials of each neuron's doubles model. Since the different trial represents possible better local minimal of model error, we pick the lowest flow prediction trial as the neuron's flow prediction.

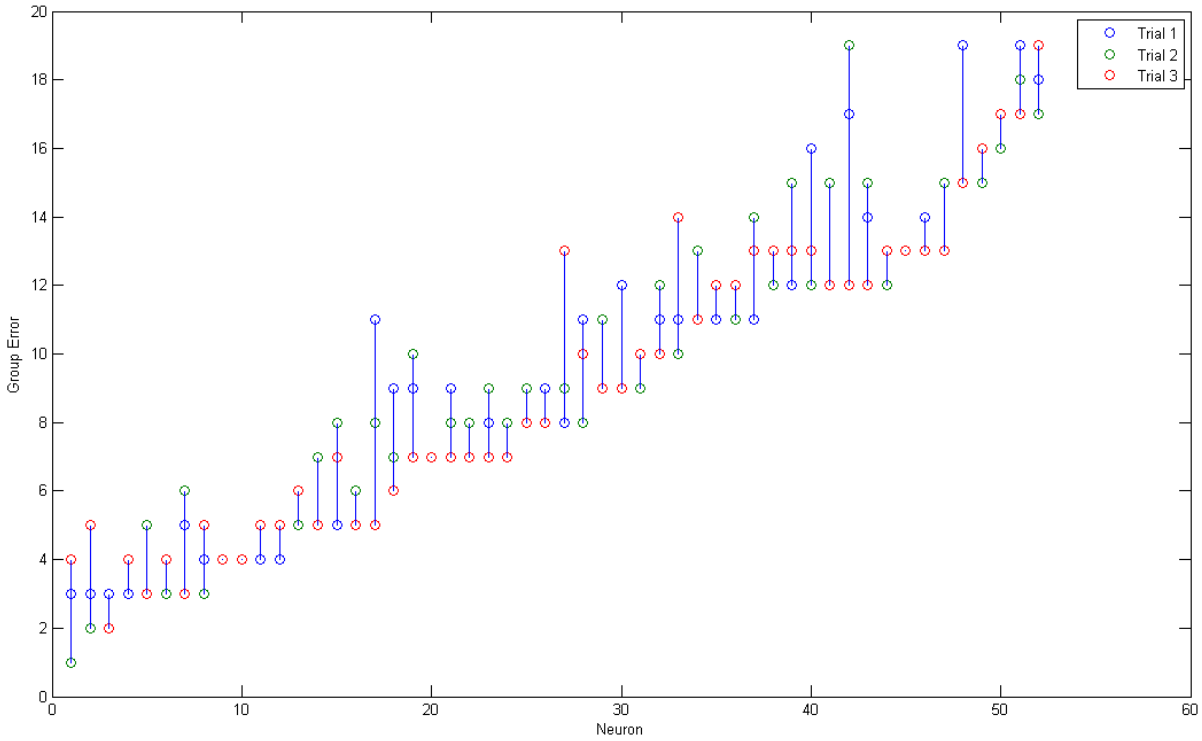

Figure 48, doubles predicting flow overall performance from neuron 1 through 52 in group error. Format as in Figure 43, this plot is also sorted by the lowest group error per each neuron across 52 neuron's doubles flow prediction. The mean of the group error across the 52 neurons is 8.3 with a standard deviation of 4.2.

Neuron	Lowest Er	Lowest Gr		Trial 1 Er	Trial 1 Gr		Trial 2 Er	Trial 2 Gr		Trial 3 Er	Trial 3 Gr
712R02	510	10		511	11		564	12		510	10
712R05	276	6		326	9		316	7		276	6
712R06	1122	3		1132	3		1122	4		1149	4
712R07	248	5		248	5		261	5		263	6
819R01	325	7		331	9		325	10		338	7
819R02	662	7		662	7		666	7		752	7
819R03	247	13		256	13		247	13		252	13
819R04	188	12		188	13		188	12		197	13
819R07	330	8		349	8		388	9		330	8
819R09	181	3		181	3		223	5		202	3
819R10	1266	11		1338	13		1266	13		1386	11
819R11	241	10		252	11		241	10		297	14
819R12	677	5		677	5		686	7		728	5
819R14	65	12		69	12		69	15		65	13
819R16	61	12		65	16		75	12		61	13
819R17	435	12		435	12		446	15		519	12
819R18	194	3		224	3		194	3		230	4
819R19	1309	9		1325	11		1309	11		1359	9
819R20	1655	5		1690	5		1701	8		1655	7
819R21	56	11		69	11		56	12		62	12
819R22	46	15		56	19		46	15		51	15
819R24	97	13		97	14		100	13		106	13
819R25	38	13		38	13		52	15		49	13
819R26	180	7		213	9		180	8		217	7
819R27	169	16		169	16		169	16		169	17
819R28	121	12		124	17		121	19		146	12
819R31	436	2		467	3		454	2		436	5
819R32	101	3		101	5		120	6		103	3
819R33	337	12		346	14		366	15		337	12
819R34	1310	5		1371	5		1328	6		1310	5
819R35	363	8		397	9		363	8		397	8
819R37	577	8		577	8		598	9		616	13
819R39	1000	8		1000	11		1051	8		1054	10
819R41	2103	7		2103	8		2137	8		2179	7
819R42	780	9		830	12		780	9		791	9
819R44	910	4		910	4		977	4		969	4
819R45	99	5		122	11		115	8		99	5
819R47	16	4		16	4		16	4		16	4
819R48	611	7		650	8		663	9		611	7

819R51	254	4		302	4		298	5		254	5
819R52	68	11		69	11		69	11		68	12
819R53	184	17		224	19		197	18		184	17
819R54	1023	17		1023	18		1033	17		1077	19
819R56	493	15		503	16		534	15		493	16
819R57	243	9		243	9		251	9		247	10
819R58	926	3		926	4		1090	3		1036	5
819R59	4033	11		4056	11		4033	14		4037	13
819R60	830	4		853	4		837	5		830	5
819R61	1053	7		1053	7		1084	8		1058	7
819R62	512	12		517	13		631	12		512	13
819R63	144	1		152	3		144	1		180	4
819R64	470	2		480	3		470	2		484	2
Mean:	568.75	8.365385									
STDEV:	673.4282	4.23815									

Figure 49, doubles predicting optic flow responses. This data sheet shows the absolute error and the group error prediction results from each of the 3 trials, and the lowest of the 3 trials. Since doubles have different firing rates and baselines per neuron, the mean and standard deviation of absolute error is less meaningful than group error's mean and standard deviation, which is comparable across all neurons.

5.3.3. Singles Gain Modulation – 9 Gain Factors

After singles models were trained from the GA, we apply the Gain Modulation transformation over the resulting singles model from each neuron. This is to try to simulate segmental dominance strictly in terms of the magnitude of each segment's strength. This experiment is to try to see if segmental dominance can explain the interaction effect. The 9 gain factor experiment is to apply 1 multiplicand to each segment's two Gaussians together, and see how the affected model from this transformation can better fit the flow responses. We think that 9 gain factor illustrates turning up and down the magnitude of each segment's strength, without changing any directional preference.

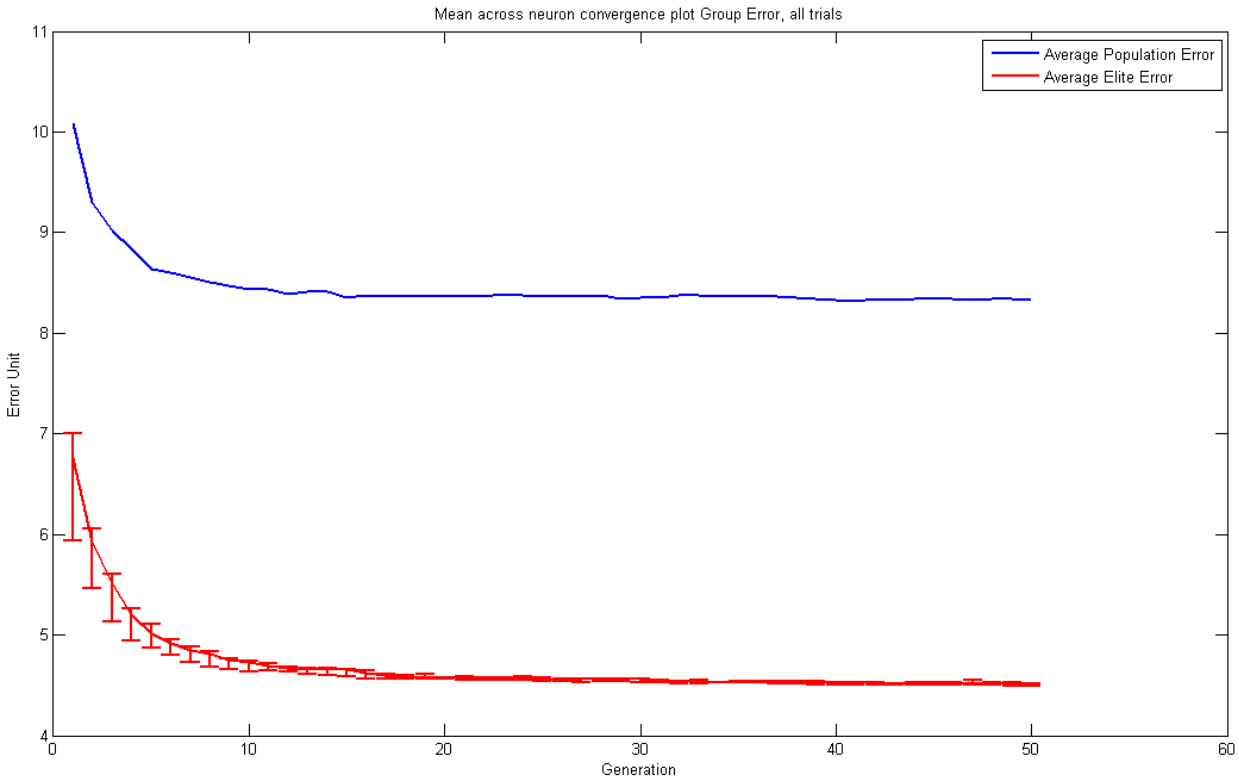

Figure 50, singles GM09 gain factor training convergence plot for across all 3 trials and all neurons in k-means group error. The plot shows that the GA has converged very well to find a set of 9 gain factors that can transform a given singles model to respond similarly as its flow responses, with the average resulting group error being around 4.5 across elites from all 3 trials. This is very significant because this means segmental dominance can potentially be the answer to the interaction that is happening to the singles models.

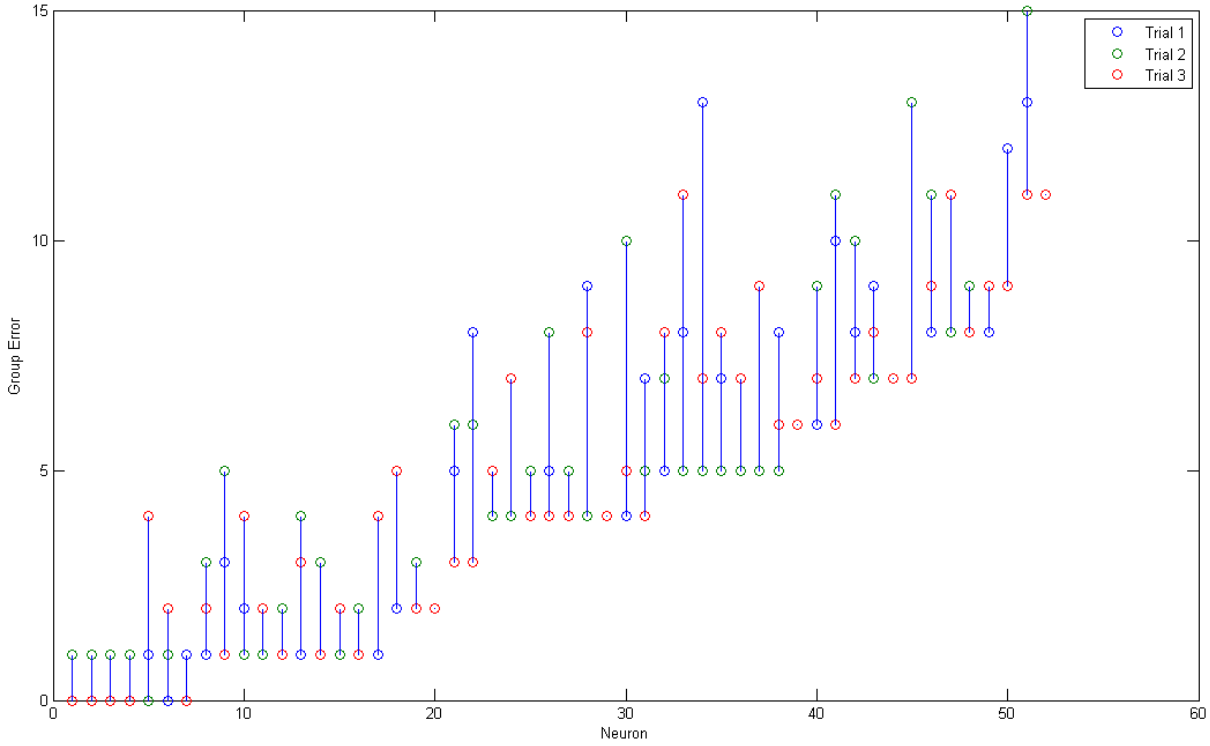

Figure 51, singles GM09 transformed models flow fitting performance plot. This plot is showing that across all 52 neurons, the GM09 transformed singles models can fit their flow responses very well, with 7 of the neurons fitting their flow responses perfectly in terms of the 3 groupings. This plot is sorted by lowest group error neuron.

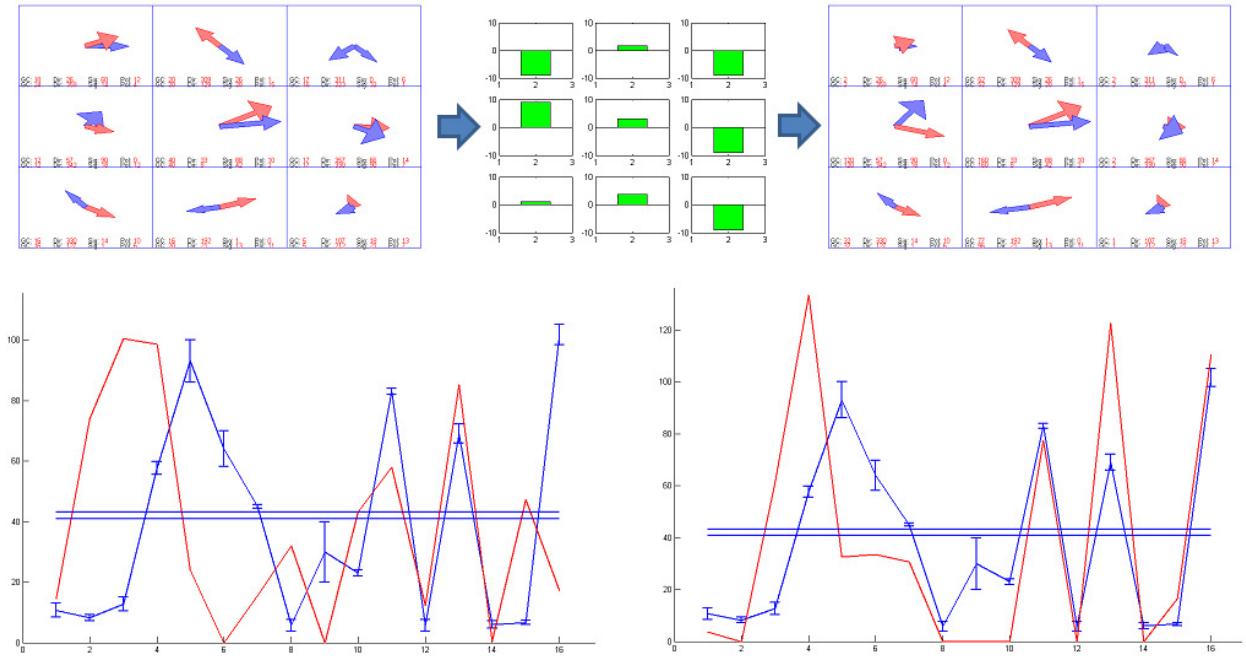

Figure 52, neuron 712R02 singles GM09 transformation plot from trial 1. The top portion of this graph shows the singles model from 712R02 trial 1 at the left, then the bar graph shows each segment's change in magnitude (change in gain factor), which then becomes the model at the right, the GM09 transformed singles model of neuron 712R02. The bottom portion shows the original 712R02 singles model's flow prediction result, and the right portion shows the GM09 transformed 712R02's fit to flow response, notice that by turning some segment's gain value up or down, the newly transformed model can fit the flow better, making the group error go from 13 to 5. We can sort of see a pattern for this neuron as well: the GA found the set of gain factors that turns the "volume" of the right side of this neuron way down, and by turning up segment 4 significantly seems to do the trick of fitting the flow better.

Neuron	Singles Lowest Group Error	GM09 Lowest Group Error
712R02	13	5
712R05	7	3
712R06	3	0
712R07	3	0
819R01	7	1
819R02	3	1
819R03	11	4
819R04	8	4
819R07	4	1
819R09	7	1
819R10	14	7
819R11	8	1
819R12	1	0
819R14	12	7
819R16	9	5
819R17	8	8
819R18	7	4
819R19	1	1
819R20	8	7
819R21	12	8
819R22	19	11
819R24	12	6
819R25	21	7
819R26	12	11
819R27	11	5
819R28	12	8
819R31	3	0
819R32	10	2
819R33	15	9
819R34	9	3
819R35	5	5
819R37	4	4
819R39	11	5
819R41	6	4
819R42	9	6
819R44	4	1
819R45	8	4
819R47	4	4
819R48	10	4
819R51	4	2

819R52	11	8
819R53	14	5
819R54	18	6
819R56	13	5
819R57	4	2
819R58	1	0
819R59	5	1
819R60	2	0
819R61	6	1
819R62	9	4
819R63	3	1
819R64	3	0
Mean:	8.153846	3.884615
STDEV:	4.741906	2.994464

Figure 53, singles comparing to singles GM09 transformed flow fit table. As the table shows, almost all neuron's group error drops tremendously after the GM09 transformation. It is important to know that since the 9 gain factors are initially chosen from random by the GA, as the generation goes the GA refines the gain factors to transform each singles model to best fit their flow responses. Due to local minimum issues, it is possible for the transformation to produce higher group error rate than the original model, although very rare.

5.3.4. Singles Gain Modulation – 18 Gain Factors

After applying 1 gain factor to each segment, we also tried to apply 2 separate gain factors to the two Gaussians from each segment, totaling 18 gain factors. This approach is more complicated since the result represents not just segmental dominance, but by tweaking every single Gaussian of all segments, it may represent directional shift as well. Therefore this approach may illustrate similar mechanism as the doubles interaction effect, or the mechanism may just be something entirely different. Nevertheless, this approach is worth a try and we have very good results from GM18.

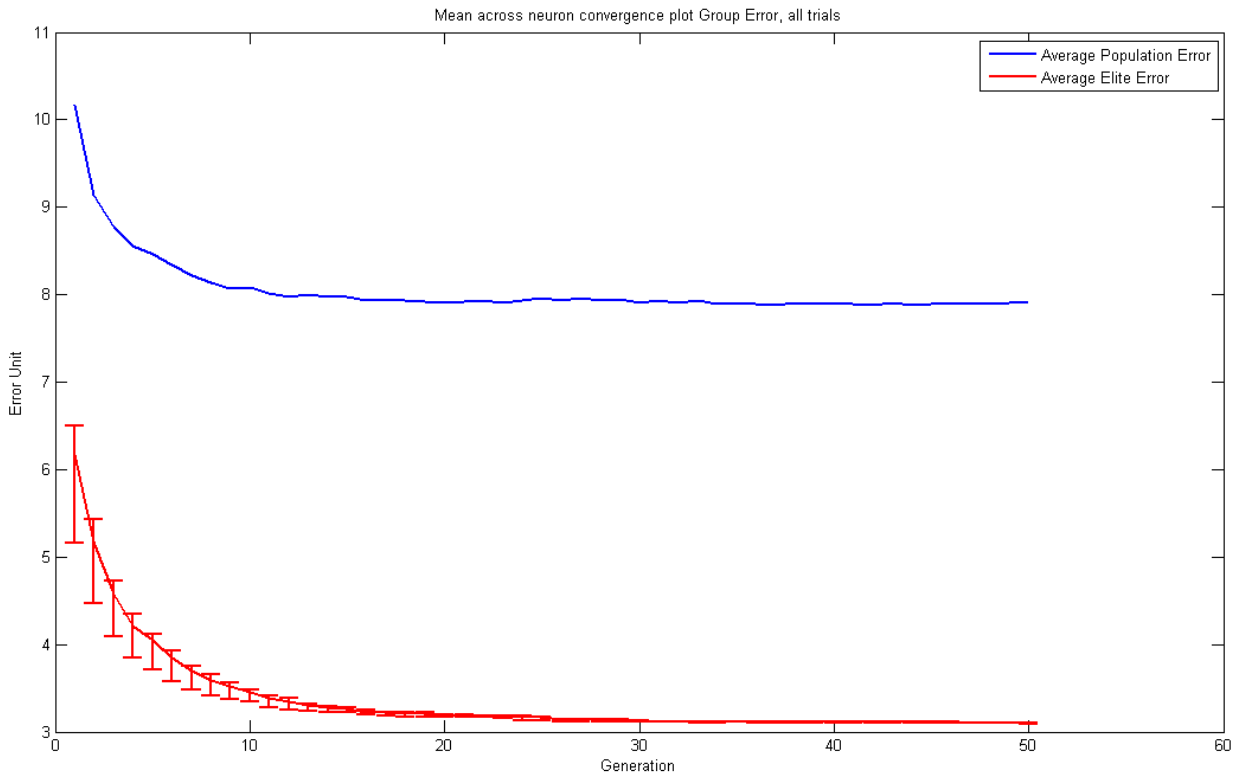

Figure 54, singles GM18 gain factor training convergence plot for across all 3 trials and all neurons in k-means group error. The plot shows that the GA has converged very well to find a set of 18 gain factors that can transform a given singles model to respond similarly as its flow responses, with the average resulting group error being around 3.2 across elites from all 3 trials. It is not surprising that GM18 does even better than GM09, since we are now doubling the degrees of freedom of this GM transformation.

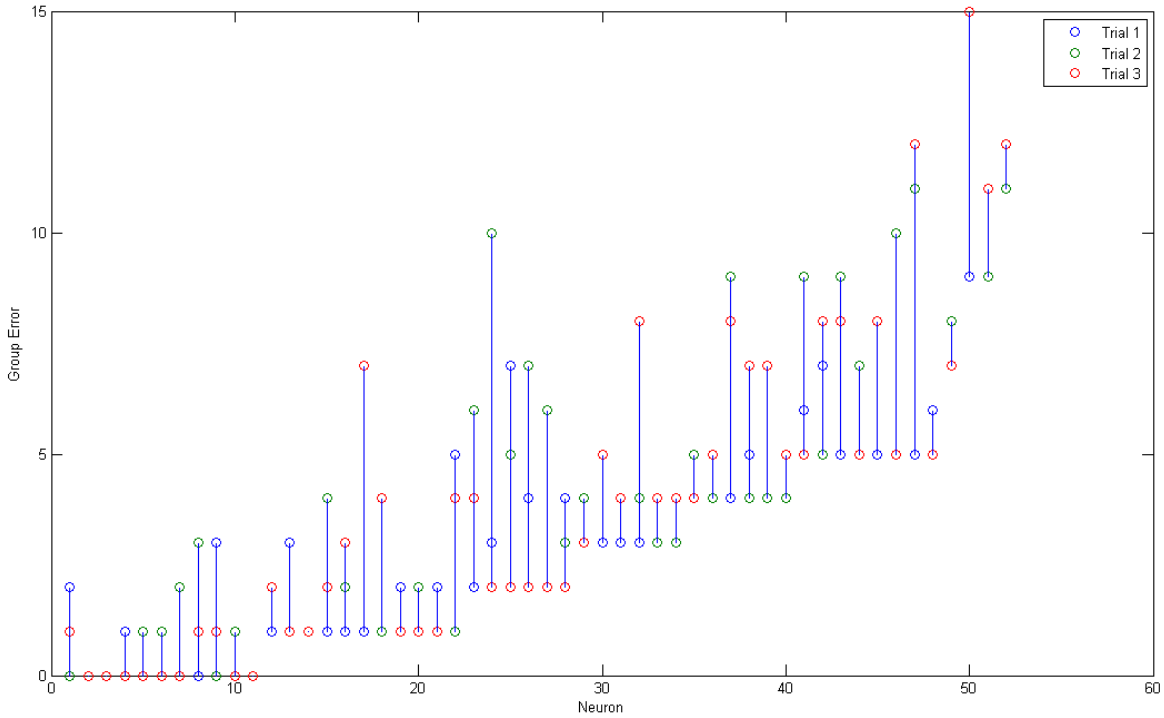

Figure 55, singles GM18 transformed models flow fitting performance plot. This plot is showing that across all 52 neurons, the GM18 transformed singles models can fit their flow responses very well, with 11 of the neurons fitting their flow responses perfectly in terms of the 3 groupings, which is even higher than GM09's 7 neurons that fitted its flow responses perfectly. This plot is sorted by lowest group error neuron.

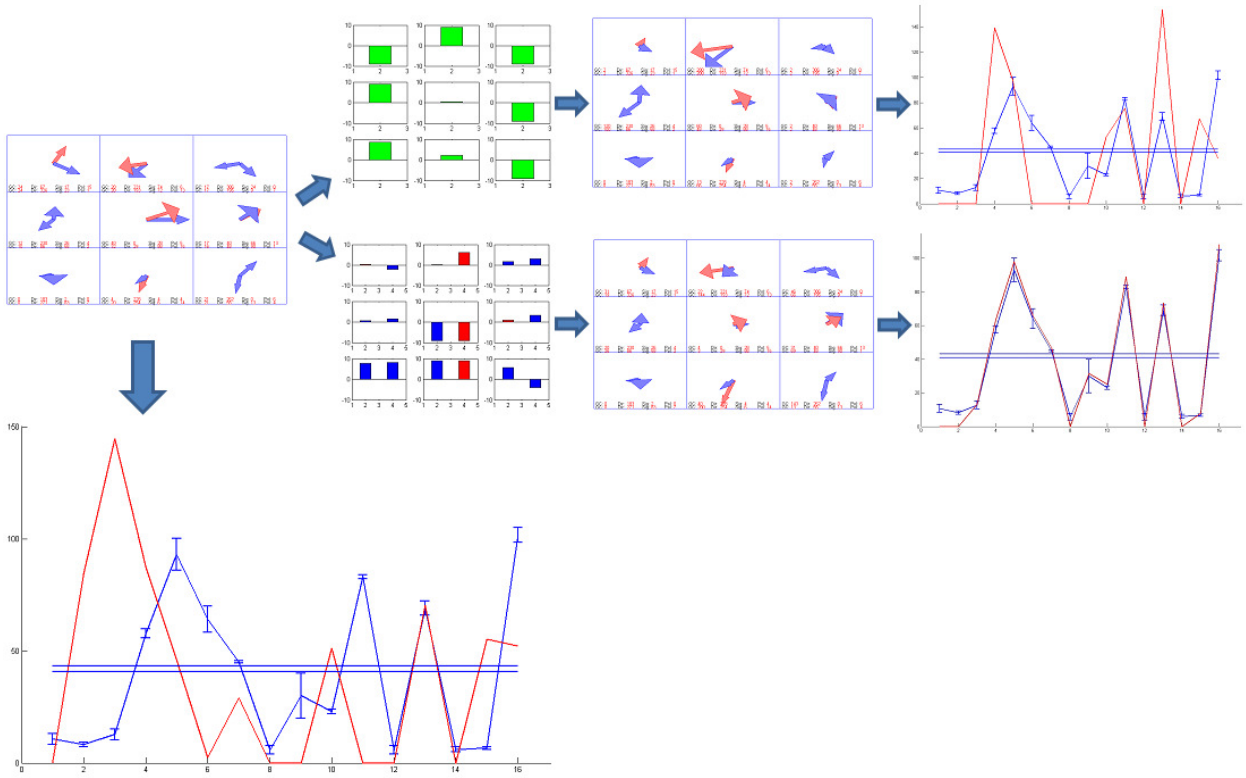

Figure 56, neuron 712R02 singles original vs GM09 transformation vs GM18 transformation trial 2 graph. The top left model is the original singles model from trial 2, which predicts its flow responses with group error of 14 shown bottom; the singles model gets transformed by GM09 at the top, and fits of its flow improved to group error of 7; singles model gets transformed by GM18, the changes are represented in the bar graph with blue bar indicating the change for the inhibitory Gaussian and red bar as the change for the segment's excitatory Gaussian, further improves the flow fit to a perfect group error of 0. It is very amazing how 1 set of 18 gain factors can transform this singles model to fit its flow response perfectly! Although it works very well, it is a potential concern that 18 gain factors are giving the model too many degrees of freedoms that just let any model be able to fit any flow, however not all neuron can produces a perfect fit like this with GM18, therefore such concern of too many degrees of freedom requires further investigation.

Neuron	Singles Lowest Group Error	GM09 Lowest Group Error	GM18 Lowest Group Error
712R02	13	5	0
712R05	7	3	4
712R06	3	0	0
712R07	3	0	0
819R01	7	1	1
819R02	3	1	3
819R03	11	4	1
819R04	8	4	4
819R07	4	1	1
819R09	7	1	1
819R10	14	7	5
819R11	8	1	1
819R12	1	0	0
819R14	12	7	4
819R16	9	5	5
819R17	8	8	5
819R18	7	4	3
819R19	1	1	0
819R20	8	7	5
819R21	12	8	5
819R22	19	11	9
819R24	12	6	5
819R25	21	7	11
819R26	12	11	9
819R27	11	5	4
819R28	12	8	5
819R31	3	0	0
819R32	10	2	2
819R33	15	9	2
819R34	9	3	2
819R35	5	5	1
819R37	4	4	3
819R39	11	5	3
819R41	6	4	2
819R42	9	6	3
819R44	4	1	0
819R45	8	4	4
819R47	4	4	1
819R48	10	4	3
819R51	4	2	0

819R52	11	8	7
819R53	14	5	5
819R54	18	6	2
819R56	13	5	2
819R57	4	2	1
819R58	1	0	0
819R59	5	1	1
819R60	2	0	1
819R61	6	1	0
819R62	9	4	1
819R63	3	1	4
819R64	3	0	0
Mean:	8.153846	3.884615	2.711538
STDEV:	4.741906	2.994464	2.561682

Figure 57, the complete table for singles vs GM09 vs GM18's flow fit. This table shows that GM18 further improves the average flow fit group error as well as the standard deviation of the average flow fit group error from GM09. Again although very rare, due to the random initial gain factors and local minimum problem, as GA runs and tries to find the best sets of gain factors, it is possible for GM18's resulting flow fit error to be higher than GM09 or even the original singles' flow prediction.

5.4. Performance Comparisons

We now compare the singles, doubles, and gain modulated singles models to each other as a way to analyze their recorded data. The singles models are models that consists of summed local motion selectivity, which retains its state throughout the flow prediction; the doubles models are different templates that are triggered by the matching hotspot direction to the flow stimulus; the GM (gain modulated) singles models were designed to demonstrate how segmental dominance may improve a neuron's flow perception. By comparing the 3 different types of model performances, the different characteristics of each model type may be better illustrated.

5.4.1. Singles vs Doubles in Flow Prediction

Singles-to-flow prediction has an average k-means group error of 8.15 and standard deviation of 4.74, whereas the Doubles-to-flow prediction has an average k-means group error of 8.36 and standard deviation of 4.24. while these numbers can considered roughly equivalent with respect to the two data set's flow prediction performance, it is important to know that out of the 52 neurons, 29 of which from the doubles data set predicted its flow responses the same or better than its singles counterpart.

Singles Prediction				Doubles Prediction		
Neuron	Lowest Er	Lowest Gr			Lowest Er	Lowest Gr
712R02	499	13			510	10
712R05	304	7			276	6
712R06	293	3			1122	3
712R07	37	3			248	5
819R01	163	7			325	7
819R02	154	3			662	7
819R03	234	11			247	13
819R04	121	8			188	12
819R07	114	4			330	8
819R09	172	7			181	3
819R10	1368	14			1266	11
819R11	56	8			241	10
819R12	472	1			677	5
819R14	65	12			65	12
819R16	61	9			61	12
819R17	561	8			435	12
819R18	44	7			194	3
819R19	400	1			1309	9
819R20	210	8			1655	5
819R21	116	12			56	11
819R22	52	19			46	15
819R24	82	12			97	13
819R25	89	21			38	13
819R26	143	12			180	7
819R27	139	11			169	16
819R28	31	12			121	12
819R31	288	3			436	2
819R32	163	10			101	3
819R33	377	15			337	12
819R34	969	9			1310	5
819R35	127	5			363	8
819R37	201	4			577	8
819R39	237	11			1000	8
819R41	194	6			2103	7
819R42	326	9			780	9
819R44	254	4			910	4
819R45	188	8			99	5
819R47	16	4			16	4
819R48	382	10			611	7
819R51	254	4			254	4
819R52	51	11			68	11
819R53	120	14			184	17
819R54	1082	18			1023	17

819R56	1005	13			493	15
819R57	157	4			243	9
819R58	401	1			926	3
819R59	3065	5			4033	11
819R60	165	2			830	4
819R61	145	6			1053	7
819R62	226	9			512	12
819R63	111	3			144	1
819R64	70	3			470	2
Mean:	318.3462	8.153846		Mean:	568.75	8.365385
STDEV:	478.3616	4.741906		STDEV:	673.4282	4.23815

Figure 58, singles performance vs doubles performance plot. The highlighted neuron numbers are the ones that the doubles template model predicts the same or better than its singles counterpart. There are 29 out of 52 neurons of which that does the same or better with its doubles model than singles models.

To look at the results in more detail, 29 of the 52 neurons do the same or better with doubles models compared to singles models; this represents 56% of all the tested neurons. However since some singles are more planar resolvable than the others (perhaps not all neurons require interaction such that 819R10 has displayed, that local-motion summed model is enough), we can further group the results into 3 groups: all group error range, singles group error of 5 or higher, and singles group error of 10 or higher. By looking at the results from this point of view, we can see if doubles model help more for those singles that are predicting flow worse, meaning that interaction effect may be required for those worse flow predicting singles neurons. As it turns out, when we consider all group error in the 52 neurons: among the 36 neurons with singles group error equal or higher than 5, 22 show doubles doing better than singles; among the 19 neurons with singles group error equal or higher than 10, 14 show doubles doing better than singles.

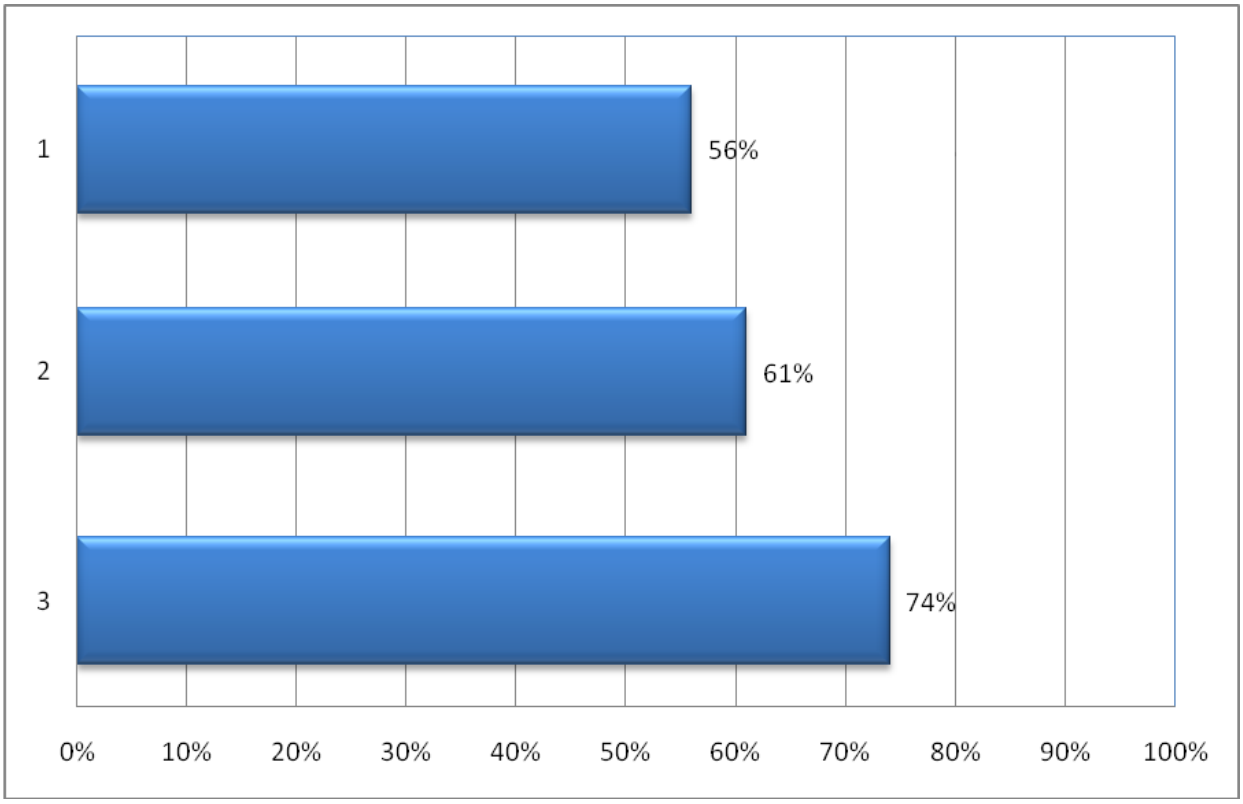

Figure 59, doubles vs singles in 3 classification comparisons. X axis represents the percentage of neurons in which the doubles has lower error than singles, and the Y axis represents the 3 different classifications. Classification 1 are neurons with singles to flow prediction group error of 0 or higher (all neurons); classifcation 2 are neurons with singles to flow prediction group error of 5 or higher; classification 3 are neurons with singles to flow prediction group error of 10 or higher, meaning mostly the ones that singles just do not predict flow very well at all. The plot shows that the neurons that do worse with singles, tend to do better with doubles indicating that those neurons need interaction effects incorporated in the double data to properly predict optic flow responses.

5.4.2. Doubles Model with Interaction Effects

From figure 26, we illustrated the finding of the reversal effect from neuron 819R10's doubles data comparing to its singles data. This is our first example neuron that demonstrates possible segmental interaction effects. The flow prediction numbers show that neuron 819R10's prediction improved from singles model's 14 to doubles template models' 11. While the improvement is clear but not massive, the reversal effect is clearly making the model to predict flow better comparing to singles locally summed model.

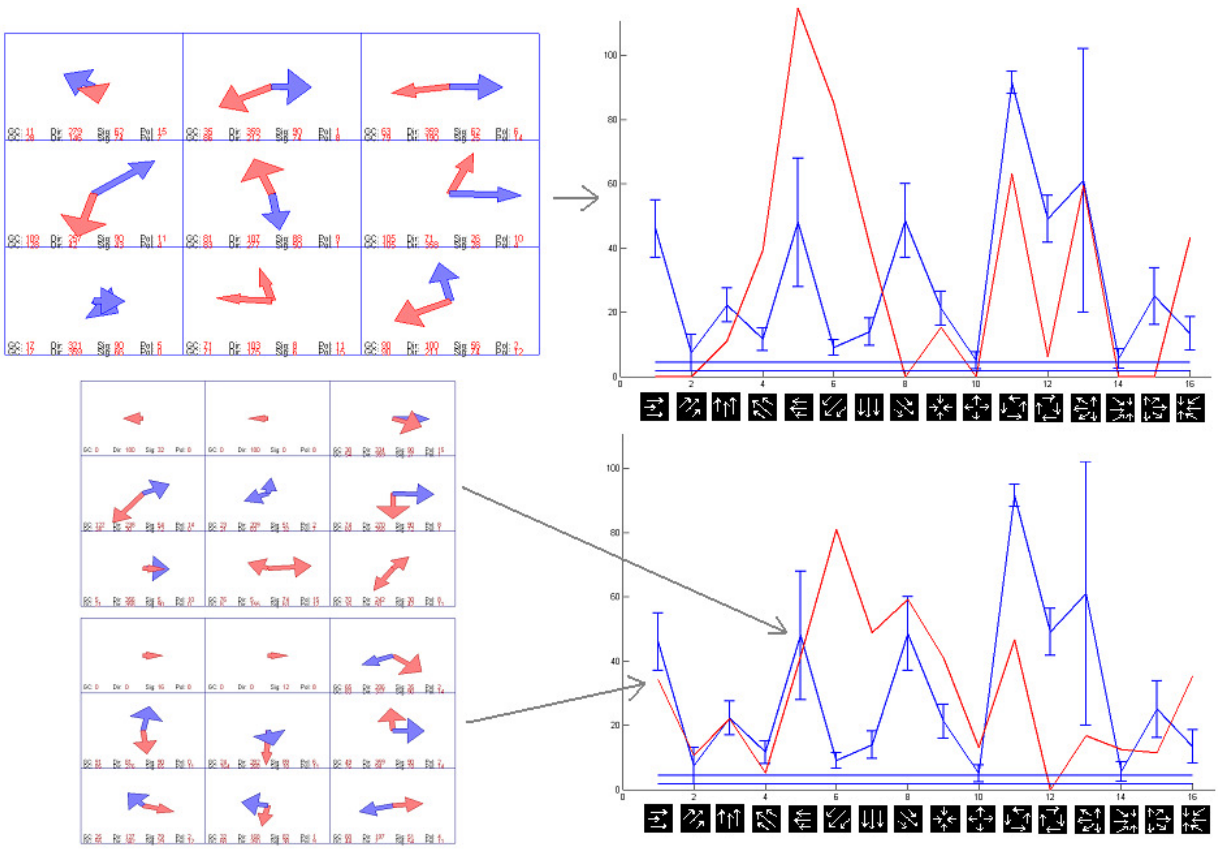

Figure 60, neuron 819R10's singles and doubles to flow prediction comparison (group error of 14 for singles vs group error of 11 for doubles). The top portion is the singles model and singles to flow prediction result from 819R10; the bottom portion is the doubles template #5 and doubles template #1, and the full doubles to flow prediction result from 819R10. For the prediction result, the blue lines are the recorded firing rates in response to the optic flow stimuli (iconically illustrated in black box below the X axis); the red lines are the models' predictions of the responses to the flow stimuli. The predictions are normalized by the mean of data and model responses for better viewing. As the plot shows, the singles model clearly indicates an overall excitatory leftward selectivity with strong rightward inhibition. However from figure 26, we saw that when the doubles hotspot were tested with rightward motion, the neuron seems to become selective to rightward motion, reversed

from its singles leftward selectivity. With the doubles template #1, where the hotspot 7 and 8 are pointing to the right, indicates when the neuron receives rightward motion input at hotspot 7 and 8. The receptive field from template #1 clearly shows that the X segments reversed its selectivity comparing to its singles model, therefore making it fit the flow response much better comparing to the singles model's inhibitory response. The doubles template #5 has its hotspot at segment 7 and 8, are pointing to the left, indicating when the neuron receives leftward motion input at hotspot 7 and 8. From doubles template #5, the model retains its leftward selectivity back with some minor segmental direction change which also made the flow response fits better comparing to its massive leftward selective singles model.

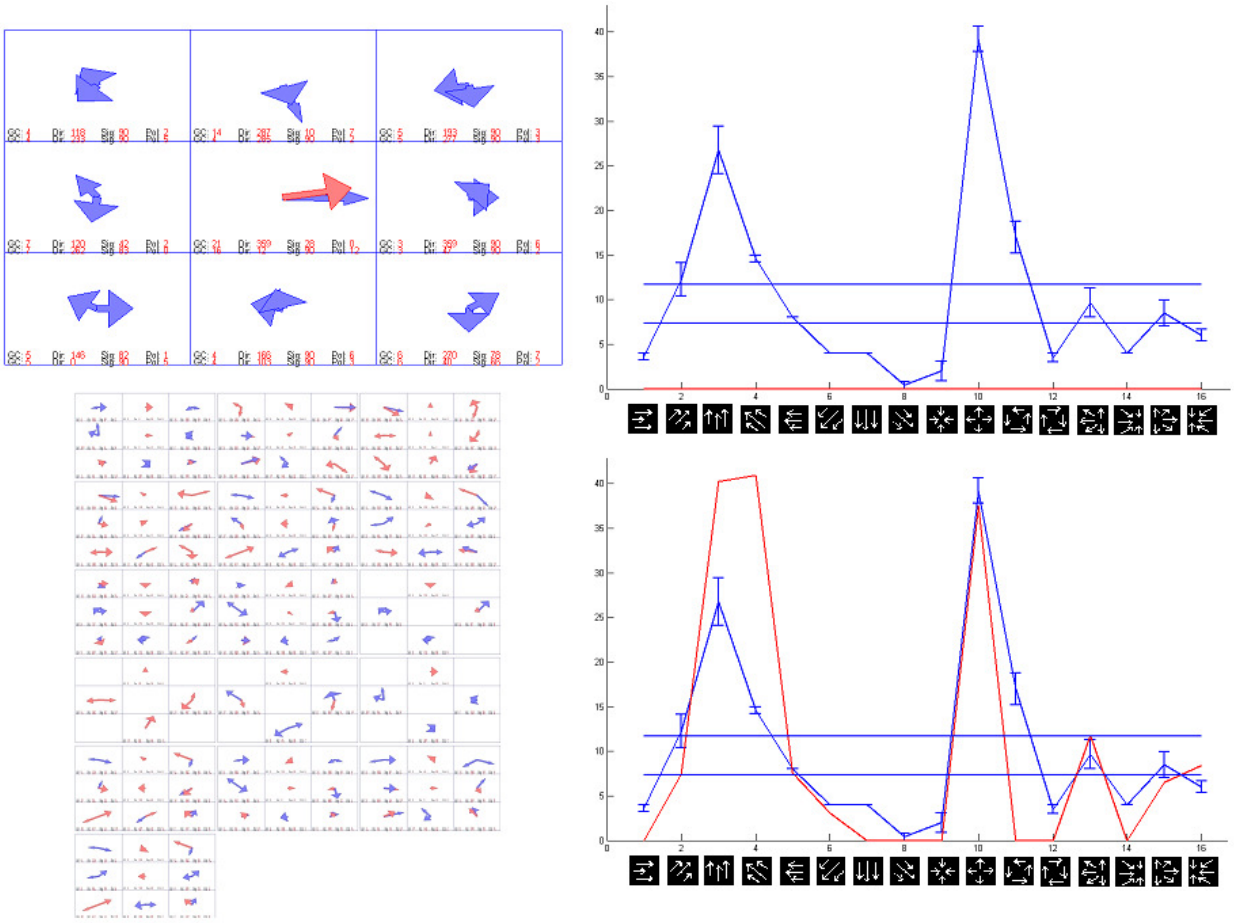

Figure 61, neuron 819R32's singles and doubles to flow prediction comparison (group error of 10 for singles vs group error of 3 for doubles). The top portion is the singles model and singles to flow prediction result from 819R32; the bottom portion is the doubles template #1 to #16, and the full doubles to flow prediction result from 819R32. As the singles model shows, this neuron seems to be an overwhelmingly inhibitory neuron, in which it really does not respond to any of the local motion stimuli except those in segment #5 so that it contains fully inhibitory dual-Gaussians. Thus, it is not surprising that its flow prediction was that all responses are inhibitory, here clamped at 0 firing rates. Although the singles recordings showed widespread inhibition, its flow recordings were showing a good profile of excitatory, baseline, and inhibitory responses. Its doubles templates - each template

driven by the hotspot's matching direction to the stimulus's segmental direction, do predict flow much better for this neuron. In order to match those excitatory responses like the flow recordings, we see the doubles showing some polarity-reversal and directional-shifting effects, with which matched the flow responses almost perfectly in terms of group errors.

It is worth pointing out that although we see some very interesting interaction effects when certain stimuli are presented, doubles do not predict optic flow response that much better than the singles. The main reason may be that the doubles were collected by hotspot and test spot paired recording, and only 4 planar motions were involved, all diagonal motion firing rates were interpolated rather than from actual recordings. This proves to be a major issue since the way we utilize doubles data is to make the doubles model hotspot-triggered templates. If the neurons were indeed hotspot triggered in order for segmental interactions to take place as we hypothesized, the wrong hotspot recording will result in minimal or no segmental interactions. The hotspots were chosen from the most active firing segment, but there is no guarantee that a segment that drives the interaction must be the highest firing segment, it may simply be a segment that fires baseline values and still be the triggering spot, perhaps then we need the correct "key spot" that triggers interaction rather than using the hotspots.

Regarding interpolated diagonal motion firing rates, there may be specific interaction such as directional reversals, which take place at some diagonal motion directions that are included in the optic flow stimuli, but not tested by the doubles and hence could not be captured by the doubles model. Interpolated diagonal direction firing rates is the best we can do but may be inaccurate. Take figure 51 as example, flow stimulus #6 is a fully diagonal motion stimulus with motion going toward bottom left. Neither the singles nor the doubles templates were producing anything inhibitory for that stimulus when the neuron's flow response was very low. We can speculate that perhaps there may be segmental interactions evoked by that stimulus just like stimulus #1's reversal effect, but since we do not have the actual recorded data, the interpolated diagonal firing rates may be off by a large margin due to the missing interaction effect.

Although doubles data were gathered for only a small subset of possible paired stimulus conditions, the data was gathered systematically using the reasonable approach of hotspot and test spot pairs. If indeed the doubles reveal the key-spot driven interaction effects, chances are some of the 52 neurons that we've tested have hotspots that are the actual key spots for segmental interactions, therefore revealing significant interaction effects. Therefore, doubles to singles comparison overall performance was be considered a demonstration of the principle rather than a full comparison of the potential effectiveness of segmental interactions in shaping optic flow responses. More extensive sampling of the doubles stimulus space might yield better optic flow predictions with the less planar resolvable neurons in which segmental interactions might be more prevalent. Now that we know the interactions can occur, and account for clear improvements of optic flow predictions in some neurons, we can design a more thorough data collection doubles data in future studies.

5.4.3. Doubles vs Gain Modulation 9 and 18

After the doubles interaction effect has been demonstrated, doubles needs to be compared to GM09 and GM18 to determine if the effect of doubles interaction and GM's segmental dominance are similar. It is no doubt that GM09 represents pure segmental dominance effect with its single gain factor per segment transformation. However, it is very difficult to say what exactly GM18 illustrates. GM18 includes the segmental dominance effect from GM09 with its gain factors, while adding possible directional shift with its separate gain factor for each Gaussian from each segment. Could GM18 be the mixture of GM09 and doubles, meaning it includes both segmental dominance, and the change in Gaussian's directional preference that

results from segmental interactions? Or perhaps GM18 is just giving each model too many degrees of freedom to operate from, and then inevitably resulting in great fits for most of all neurons? By putting them together into 1 chart may be easier to resolve this issue.

Neuron	Singles Lowest Group Error	GM09 Lowest Group Error	GM18 Lowest Group Error	Doubles Lowest Group Error
712R02	13	5	0	10
712R05	7	3	4	6
712R06	3	0	0	3
712R07	3	0	0	5
819R01	7	1	1	7
819R02	3	1	3	7
819R03	11	4	1	13
819R04	8	4	4	12
819R07	4	1	1	8
819R09	7	1	1	3
819R10	14	7	5	11
819R11	8	1	1	10
819R12	1	0	0	5
819R14	12	7	4	12
819R16	9	5	5	12
819R17	8	8	5	12
819R18	7	4	3	3
819R19	1	1	0	9
819R20	8	7	5	5
819R21	12	8	5	11
819R22	19	11	9	15
819R24	12	6	5	13
819R25	21	7	11	13
819R26	12	11	9	7
819R27	11	5	4	16
819R28	12	8	5	12
819R31	3	0	0	2
819R32	10	2	2	3
819R33	15	9	2	12
819R34	9	3	2	5
819R35	5	5	1	8
819R37	4	4	3	8
819R39	11	5	3	8
819R41	6	4	2	7
819R42	9	6	3	9
819R44	4	1	0	4
819R45	8	4	4	5
819R47	4	4	1	4
819R48	10	4	3	7
819R51	4	2	0	4

819R52	11	8	7	11
819R53	14	5	5	17
819R54	18	6	2	17
819R56	13	5	2	15
819R57	4	2	1	9
819R58	1	0	0	3
819R59	5	1	1	11
819R60	2	0	1	4
819R61	6	1	0	7
819R62	9	4	1	12
819R63	3	1	4	1
819R64	3	0	0	2
Mean:	8.153846	3.884615	2.711538	8.365385
STDEV:	4.741906	2.994464	2.561682	4.23815

Figure 62, singles vs GM09 vs GM18 vs doubles table. As the table shows, doubles and singles are nearly the same, therefore doubles are having a very difficult time doing better than either GM09 or GM18 for any neuron. There are 4 neurons that are highlighted by yellow which doubles is doing the same or better than both GM09 and GM18, but the improvement from those neurons' doubles models is not very significant. One reason is that doubles data were not completely gathered – the hotspot may not be the key spot that actually triggers proper interactions; and missing data points are very likely to be providing more interactions that help the neuron to better predict flow responses.

6. Summary and Conclusion

This thesis reports a four stage project devoted to developing receptive field models of MST neuronal responses to optic flow. The four stages are: model design, model training, model assessment, and model modification. During the early phases of the model design stage, we tried several different methods that included Gaussian derivative models [22], feed-forward neural networks, single Gaussian models, and finally dual-Gaussian models. Gaussian derivative models are specific models for motion detection, which did not fit into the neuronal firing rate model scope of this project. Feed-forward neural networks could be trained from the neurophysiological data, but their black-box operation made it impossible to make sense of the internal structure of the neural network in terms of receptive field properties. Single Gaussian models were the first real step forward, allowing us to train, test, and predict recorded data. However, we recognized the need to accommodate the common occurrence of bi-directionally selective receptive field segments. Adding a second Gaussian per segment allowed us to model the bi-directional selectivity. The design phase went very well, we learned from the draw-backs of each previous designs and dual-Gaussian proved to be a robust model design for this project.

Since this project focused on neuronal firing rate modeling, we tried to maintain a close adherence to biologically inspired implementations. Therefore, we used an evolutionary algorithm – genetic algorithm -- to train and fit the models to the recorded data. We spent a long time finalizing the specifics of the cost function, which defines how the GA measures the goodness of a model. The overall convergence from figure 34, 35, 38 and 39 showed the successful GA training phase and demonstrates that the models were able to converge to a solution and fit the data very well.

Our efforts to predict the optic flow responses of each neuron with the trained models were both interesting and satisfactory. The interaction effect that we observed in the doubles recordings (Figure 26) showed marked improvement at predicting flow better than its singles counterpart (Figure 57). The doubles data of some neurons showed interesting effects such as polarity-reversal with neuron 819R32, that confirms the segmental interaction exists, without which some of the neurons cannot correctly predict the neuron's optic flow responses. These observations raised the question of whether directional shifts and reversal effects may be the product of simple segmental dominance? With such a question in mind, we added a segmental gain-modulation transformation step after the trained singles models. The results of GM-to-flow fit were amazingly good, with some of the neurons almost perfectly matching the flow responses with 18 gain factors. However, it is difficult to compare the underlying principles of GM and doubles templates, since GM is turning all the gain values up or down just once, while the doubles models are multiple hotspot driven templates. Other issues to be considered are that: both GM-9 and GM-18 are giving the models too many degrees of freedom, and that the GM model training uses the fit to the optic flow responses, effectively giving the answer back to the fitting process.

The results of the doubles analysis and GM results indicate that segmental interactions exist, and it is required for some neurons to perceive optic flow correctly. The interaction can be directional reversal effects, polarity reversal, or segmental gain dominance. These effects may occur individually or simultaneously, all of which might help the neurons to more efficiently process optic flow stimuli. This thesis work is only the first attempt to unlock the existence and the complexity of the interaction effect with dual-Gaussian models. Further experimental refinements can be based on the analysis of this work to explore the underlying receptive field

mechanisms of MST neuronal optic flow selectivity.

7. Future Work

There are plenty of steps to continue this work in order to either improve the result from the same recorded data, or utilize the models from this thesis. Those include data interpolation, data collection, validity of gain modulation, and machine vision applications.

Since all the data were recorded with just the mix of 4 planar motions except for the flow stimulus, we may try to interpolate the data for the diagonal motion firing rates for all singles and doubles data sets. By doing so, the training of the models by the GA will become more difficult, since there will be many more responses the model has to match, and the resulting model may be very different from that seen in this work. It will be a concern, however, that the interpolated data are not part of the recorded data, which may possibly distort some of the prediction results.

Data collection will also need to be enhanced to accommodate the key-spot activation hypothesis. More data analysis from the results of this thesis work will need to be done to design a systematic way of extracting possible key-spots from the singles and/or doubles recordings of each neuron. To include both of these considerations, we might propose studies in which the visual stimuli may include diagonal motion for a more complete recording set, as well as fully pair up all key-spot with the rest of the 8 test spots. New type of recordings such as “triples data” recording responses to three simultaneously presented local motion stimuli, but these efforts my be limited by the practical constraints on neurophysiological recording time.

Gain modulation transformation of the singles model provided very valuable results, and raised very interesting questions as well. It is clear that GM09 represents pure segmental dominance effect, while the exact meaning and the validity of GM18 remains unclear. Further investigation of GM18 will need to be compared with a more completely gathered doubles data,

in order to discover the underlying mechanism of GM18's change upon the singles models. By studying how each segment's gain is turned up or down, there may be a pattern of how regions of a receptive fields may affect each other in terms of Gaussian magnitude, and the GM18's change in individual Gaussians that results into possible directional shift may also result in similar effect as doubles' interaction effect from further experiments.

The models resulting from this work can be utilized as part of a machine vision system's self-motion sensor. Several ideas include training a neural network with the 52 neuron singles and/or doubles models as its input, with an output integer indicating the type of self-motion the machine is seeing. A neural network might be trained to correctly use the outputs from each of the 52 neuronal models in order to differentiate the 16 different self-motion, and it will be interesting to compare the speed and accuracy of such system with other machine vision systems with similar functionalities.

8. References

[1]. Adelson, E.H., and Bergen, J.R., “Spatiotemporal energy models for the perception of motion.” Journal of Optical Society of America, Vol. 2, No. 2, pp. 284-299, February 1985.

[2]. Beardsley, S.A., Ward, R.L, and Vaina, L.M., “A neural network model of spiral-planar motion tuning in MSTd.” Vision Research, Vol. 43, pp. 577-595, 2003.

[3]. Crist, C. F., Yamasaki, D. S., Komatsu, H., and Wurtz, R. H., “A grid system and microsyringe for single cell recordings.” Journal of Neuroscience Methods, Vol. 26, pp. 117-122, 1988.

[4]. Duffy, C. J., and Wurtz, R. H., “Sensitivity of MST Neurons to Optic Flow Stimuli. I. A Continuum of Response Selectivity to Large-Field Stimuli.” Journal of Neurophysiology, Vol. 65, No. 6, pp. 1329-1345, 1991.

[5]. Duffy, C. J., and Wurtz, R. H., “Sensitivity of MST Neurons to Optic Flow Stimuli. II. Mechanisms of Response Selectivity Revealed by Small-Field Stimuli.” Journal of Neurophysiology, Vol. 65, No. 6, pp. 1346-1359. 1991.

[6]. Enroth-Cugell, C., and Robson, J., “The Contrast Sensitivity of Retinal Ganglion Cells of the Cat.” Journal of Physiology, Vol. 187, pp. 517-552, 1966.

[7]. Gaborski, R., Vaingankar, A, Chaoji, V., and Teredesai, A., "VENUS: A System for Novelty Detection in Video Streams with Learning," FLAIRS, 2004.

[8]. Grossberg, S., Mingolla, E., and Pack, C., “A Neural Model of Motion Processing and Visual Navigation by Cortical Area MST.” Cerebral Cortex, Vol. 9, No. 8, pp. 878-895, December 1999.

[9] Hays, A. V., Richmond, B. J., and Optican, L. M., “A UNIX-based multiple process system for real-time data acquisition and control.” WESCON Conf. Pro., Vol. 2, pp. 1-10, 1982.

[10]. Huang, X., Albright, T.D., and Stonger, G.R., “Adaptive Surround Modulation in Cortical Area MT.” Neuron, Vol. 53, pp. 761-770, March 1 2007.

[11]. Hubel, D.H., “Eye, Brain and Vision.” Scientific American Library, No 22, 1995.

[12]. Hubel, D., and Wiesel, T., “Receptive fields, binocular interaction, and functional architecture in the cat’s visual cortex.” Journal of Physiology, 1962.

[13] Judge, S. J., Richmond, B. J., and Chu, F. C., “Implantation of magnetic search coils for measurement of eye position: and improved method.” Vision Res, Vol. 20, pp. 535-538, 1980.

[14]. Kuffler, S.W., “Discharge patterns and functional organization of mammalian retina.” Journal of Neurophysiology, Vol. 16, pp. 37-68, 1995.

[15]. Lappe, M., “A model of the combination of optic flow and extraretinal eye movement signals in primate extrastriate visual cortex Neuronal model of self-motion from optic flow and extraretinal cues.” Neural Networks, Vol. 11, pp. 397-414, 1998.

[16]. Robinson, D. A., “A method of measuring eye movement using a scleral search coil in magnetic field.” IEEE Trans. Bio.-Med. Eng, Vol. 10, pp. 137-145, 1963.

[17]. Rolls, E. T., and Milward, T., “A Model of Invariant Object Recognition in the Visual System: Learning Rules, Activation Functions, Lateral Inhibition, and Information-Based Performance Measures.” Oxford: Oxford University Press.

[18]. Rolls, E. T., and Stringer, S., “Invariant object recognition with trace learning and multiple stimuli present during training.” Department of Experimental Psychology, Oxford University, 2007.

[19]. Rust, N. C., Mante, V., Simoncelli, E. P., and Movshon, J. A., “How MT cells analyze the motion of visual patterns.” Nature Neuroscience, Vol. 9, No. 11, pp. 1421-1431, 2006.

[20]. Serre, T., and Poggio, T., “Object Recognition with Features Inspired by Visual Cortex.” Massachusetts Institute of Technology, 2005.

[21]. Tadin, D., Lappin, J.S., Gilroy, L.A., and Blake, R., “Perceptual consequences of centre-surround antagonism in visual motion processing.” Nature, Vol. 424, pp. 312-315, July 17 2003.

[22]. Young, R.A., and Lesperance, R.M. “The Gaussian Derivative model for spatial-temporal vision: I. Cortical model” Spatial Vision, Vol. 14, No. 3,4, pp. 261-319, 2001.

[23]. Young, R.A., and Lesperance, R.M. “The Gaussian Derivative model for spatial-temporal vision: II. Cortical data” Spatial Vision, Vol. 14, No. 3,4, pp. 321-389, 2001.

[24]. Yu, C.P., Page, W., Gaborski, R. and Duffy, C., “Modelling the Receptive Field Organization of Optic Flow Selective MST Neurons,” accepted: Neuroscience 2007, San Diego, CA.